MICRODEBONDING TEST FOR MEASURING SHEAR STRENGTH OF THE FIBER/MATRIX INTERFACE IN COMPOSITE MATERIALS

by

DODD HARRISON GRANDE

B.S.M.E. Seattle University
(1980)

Submitted in Partial Fulfillment of the Requirements
for the Degree of

Master of Science

at the

MASSACHUSETTS INSTITUTE OF TECHNOLOGY

June 1983

Signature of Author _____
Department of Materials Science and
Engineering, May 6 1983

Certified by _____
Frederick J. McGarry
Thesis Supervisor

Accepted by _____
Robert W. Balluffi
Chairman, Departmental Committee on Graduate Students

MICRODEBONDING TEST FOR MEASURING SHEAR STRENGTH OF THE FIBER/MATRIX INTERFACE IN COMPOSITE MATERIALS

by

DODD HARRISON GRANDE

Submitted to the Department of Materials Science and Engineering on May 6, 1983 in Partial Fulfillment of the Requirements for the Degree on Master of Science

ABSTRACT

A microdebonding test for the measurement of the shear strength of the fiber/matrix interface in composite materials was developed. This technique provides a quantitative measure of the interfacial shear strength for typical composite specimens, in-situ. Results of tests which were performed on two S-glass/Epoxy systems and one Graphite/Epoxy system are presented. The results of these tests were used to study the effects of the system variables on the microdebonding test results and to develop test procedures and data reduction methods for use with the microdebonding test.

The microdebonding test is based upon the application of a load to the end of a fiber located in a composite specimen which has been sectioned perpendicular to the fiber direction and polished metallographically. The load is applied using a probe mechanism which has been developed, and debonding is detected optically using a research quality microscope. The loading is applied incrementally, with optical inspection between each increment of loading to detect the initiation of debonding. A finite element analysis which was developed in another study is used to calculate interfacial shear strength from the experimental measurements.

The failure which results from the application of a microdebonding load is confined to the interfacial region. The results of the finite element analysis indicate that the test results should be relatively insensitive to the loading conditions, provided that the necessary accuracy in location of the probe during loading can be achieved. The results of the finite element analysis also indicate that the details of the specimen's surface preparation should not have a significant effect on test results, which has been confirmed experimentally.

The ability of this test to use selected individual fibers for testing makes it especially attractive for use in degradative studies of composites.

Thesis Supervisor: F.J. McGarry

Title: Professor of Materials Science

ACKNOWLEDGEMENTS

I would like to thank Professor F.J. McGarry for support he has given me and for knowledge he has imparted, and Dr. John Mandell for the tremendous amount of technical insight which he has provided and the opportunity to learn from his experience in the field of composites. Credit should also be given to him for his patience in working with me and my fellow students in the lab.

Additionally, it is to Dr. Mandell that the credit for the basic concept and development of the microdebonding test goes. Anyone can design a machine if they know it's going to work, but Dr. Mandell is the one who knew this one would work in the first place.

Of course, I owe a great debt to my parents for the tremendous support they've given me throughout my college education. Without this support, achievements such as this would be impossible.

Finally, I give mention last to those who make the biggest difference in making my day enjoyable, namely all my friends who have helped make my time here enjoyable. To Ann Kraft for her kindness, understanding and patience goes my deepest affection. To those people who I play soccer with goes the thanks for an opportunity to play.

TABLE OF CONTENTS

LIST OF FIGURES

LIST OF TABLES

NOMENCLATURE

A_f	Cross sectional area of fiber
A_σ	Area of load application
D_f	Fiber diameter
D_σ	Diameter of area of load application
E_f	Young's modulus of fiber
G_m	Shear modulus of matrix
P	Microdebonding load
σ_A	Average axial stress applied to fiber (= P/A_f)
$\bar{\sigma}$	Average axial stress applied to fiber at initiation of debonding
$\bar{\sigma}_{.40}$	Value of $\bar{\sigma}$ corresponding to $T_m/D_f = 0.40$
T_m	Thickness of matrix layer surrounding fiber
T_{m-exp}	Distance separating test fiber from nearest neighboring fiber, measured from fiber/matrix interface
τ	Shear stress at fiber/matrix interface
τ_{max}	Maximum shear stress at fiber/matrix interface
$\bar{\tau}$	Shear strength of fiber/matrix interface
Y	Distance from surface of specimen measured along fiber axis

"MICRODEBONDING TEST FOR MEASURING SHEAR STRENGTH OF THE FIBER/MATRIX INTERFACE IN COMPOSITE MATERIALS"

1.0 INTRODUCTION

The objective of this work was to develop a test method capable of quantitatively measuring the strength of the fiber/matrix interface in composite materials. It was also desired that the test method be easily utilized to study the degradation of interfacial bond strength in composite specimens subjected to environmental degradation. The microdebonding test which has been developed can accurately measure the shear strength of the fiber/matrix interface in composite specimens. Measurements can be made in localized regions of a specimen, allowing degradative processes to be monitored throughout a laminate.

Many of the impressive mechanical properties exhibited by fiber reinforced composite materials are influenced by the strength of the fiber/matrix interface. Efficient transfer of shear stress through the interface and matrix between the fibers of a composite material is largely responsible for these materials' ability to exhibit the high strength properties of the reinforcing fibers without the brittle behavior characteristic of these materials in bulk (1,2,3,4). Additionally, many of the strength

characteristics of composite laminates have some dependence upon the strength of the fiber/matrix interface (5,6,7). Studies of fracture surface morphologies indicate that the integrity of the interfacial bond has an effect on the failure mechanisms of composite materials (6,7).

The study of the environmental degradation of composite materials has usually been divided into studies of the three major constituents of the material: Fiber, matrix and interface. Examinations of the fractured surfaces of failed composite specimens which have been subjected to environmental degradation show changes in failure modes involving the interfacial regions (8). Other studies have reported disruption of the interfacial bond due to water exposure (9,10).

The influence of the interface on composite properties has generated a need for the characterization of the interfacial regions of composite materials. Characterization of the interface includes many considerations such as fiber surface chemistry and fiber surface morphology as well as interfacial bond strength. However, it is the strength of the interfacial bond that is usually the parameter of primary interest for considerations related to mechanical properties of composite materials.

Therefore, it would be very useful if a test method were available which could measure the strength of the fiber/matrix interface. It would be desireable that the

test be capable of;

1) Quantitatively measuring the interfacial shear strength of typical fiber reinforced composite materials.
2) Producing failure of only the interface.
3) Selecting test sites in localized regions of a specimen in order to measure degradation effects or to avoid regions of physical damage.

The microdebonding test which has been developed can quantitatively measure the shear strength of the fiber/matrix interface in unidirectional composite specimens. The specimens are sectioned and polished perpendicular to the fibers. The test involves the application of a load to the end of a single fiber on the polished surface, using a diamond tipped probe (shown schematically in Figure 1). The load is applied incrementally, with microscopic inspection between loadings to detect the initiation of debonding. The use of a finite element analysis (11) allows the calculation of the maximum interfacial shear stress from the experimentally measured quantities. The microdebonding apparatus is shown schematically in Figure 2.

Experiments conducted to date indicate that interfacial shear strengths can be obtained through the use of the microdebonding test for common glass/epoxy and graphite/epoxy systems.

2. OVERVIEW OF METHODS USED FOR MEASURING INTERFACIAL BOND STRENGTH IN FIBER REINFORCED COMPOSITES

Although the strength of the fiber/matrix interface is an important parameter in the characterization of composite materials, the test methods which are available for the measurement of interfacial strength typically have limitations. Test methods which have commonly been used to measure the strength of the fiber/matrix interface have generally been either tests on model systems, in which the components of the system do not have the same arrangement as that found in actual composite materials (6,13), or tests measuring mechanical properties of composite specimens (12).

2.1 TESTS ON MODEL SYSTEMS

Standard adhesive tests (5,14) can be considered model systems if the appropriate adherend, adhesive and surface treatment are used, and can be useful in the comparison of different systems. However, because of the limited similarity between these systems and actual composite materials, results obtained using these tests must be considered as being qualitative in nature. In addition,

the use of such tests to study the effects of moisture and environment on the fiber/matrix interface of composite materials is severely limited for the same reason.

Other tests based on model systems have the advantage of being closer in configuration to actual composite materials.

Fiber pullout tests, which utilize single fibers or rods embedded in resin, have been used to measure the shear strength of the fiber/matrix interface (6,13,15,16). Performing such tests with the brittle fibers which are typically used as composite reinforcement can, however, be difficult, especially when reasonably high interfacial bond strengths are obtained.

Other model systems using fibers embedded in blocks of resin have been used to study the fiber/matrix bond strength (17,18). These tests utilize specimens which have geometries which are specially designed to produce a desired stress state at the fiber/matrix interface when the block of resin is loaded in compression.

Tests have also been developed which utilize the breakdown in length of a single fiber embedded in a strained resin coupon to determine interfacial shear strength (19,20 21,22). Several of these investigations also utilized photoelastic techniques tc obtain additional information about the stress fields in the resin surrounding the fibers (20,21,22).

Tests on the model systems which employ fibers or rods have the advantage of being closer in configuration to actual composite materials than the standard adhesive tests. However, these systems still only correspond in a limited way to actual composite materials. Results from such tests can yield qualitative information about interfacial strength of various systems, but are limited in their ability to yield quantitative values of interfacial bond strength applicable to actual composite materials. Limitations also exist concerning the use of these methods to study the effects of environmental exposure on interfacial bond strength due to the lack of similarity between the model systems and actual composite materials.

2.2 MECHANICAL TESTS ON COMPOSITE SPECIMENS

Mechanical tests are often used to infer the interfacial bond strength in fiber reinforced composites. Several types of shear characterization tests such as short beam shear, notched shear, torsion of thin walled cylinders and off-axis tension are commonly used for this purpose (12,23,24,25).

The short beam shear test is one of the more popular tests used as a measure of interfacial strength. Short

beam shear results have been used to study the effects of fiber surface treatments (26,27) as well as the effects of moisture and environmental exposure (28,29) on interfacial strength. However, the shear stress distribution at the midplane of such specimens is not constant over the width of the beam, and is strongly influenced by specimen geometry. Additionally, the mode of failure may vary depending upon the geometry of the specimen and the material characteristics of the system being tested (30,31). These considerations make interpretation of short beam shear results difficult.

Notched shear specimens have been used to study surface treatment and environmental effects on the interface (32,33,34). However, the stress fields imposed on the test section by such tests have been reported to deviate from that of pure shear (35).

Transverse tension (36,37) and off-axis tension (38) have been used to study the effect of environmental aging on the interface. However, interpretation of such results, with respect to the contribution of the interface, is difficult.

Although the mechanical strength tests have the advantage of providing data on actual composites, and can be useful in the determination of engineering design properties, the use of such tests to determine the strength of the interface is questionable. The results of mechanical

tests may be influenced by the interfacial bond strength, but composite failure is complex and may be dominated by other factors.

Composite materials subjected to hygrothermal exposure have been noted to contain discrete regions of cracking (39,40). The presence of these cracks may have a dominant effect on the results of mechanical tests resulting in a lack of sensitivity to the strength of the interfaces. Although the formation of such cracks may be influenced by the strength of the interface, their presence makes the interpretation of mechanical strength tests difficult.

3.0 EXPERIMENTAL METHOD

The microdebonding test has, through all of its modifications, been based upon the application of a load to the end of a fiber located in a specimen which has been sectioned normal to the fibers and metallographically polished, as shown in Figure 1. The load is increased incrementally until interfacial failure is detected. Interfacial failure is detected through inspection using an optical microscope after each increment of loading. The load which results in the failure of the fiber/matrix interface is then related to the strength of the interfacial bond through the use of the finite element analysis.

The microdebonding apparatus in its current configuration is shown in Figure 2 and consists of the following major components:

1. Research quality optical microscope (Reichert Zetopan, model 323 474) used for probe location and detection of interfacial debonding. Magnification of 900X.

2. Probe mechanism utilizing extensometer (Instron Model 2620-526) for load measurement. Instrument quality ball bushings and precision ground shaft to provide linear probe travel, with linkage to

transfer load to extensometer. Diamond tipped probe (radii 6 μm or 13 μm) for application of load to fiber.

3. X-Y axis micrometer drive stage for location of specimen in relation to probe position.

4. Turntable with magnetic stops for reproducible movement of specimen between probe location and optical axis of microscope.

5. Bridge amplifier and meter (Vishay Instruments BAM-1) for load indication.

6. Camera used for taking calibrated photomicrographs of test points which are used to measure fiber diameter and spacing.

7. Vibration Isolation table.

The test procedure consists of selecting a desired test point (fiber) on the polished surface of the specimen and locating it on the cross hair in the ocular of the microscope by using the micrometer drive stage. The specimen is then positioned under the probe by rotating the turntable,

and a load is applied by raising the specimen using the focus knob of the microscope. The load is read from the meter of the bridge amplifier. The specimen is then lowered to remove the load, repositioned under the optical axis of the microscope, and inspected for initiation of debonding. The applied load at initiation of debonding is recorded and a photomicrograph is taken of the tested fiber in order to obtain fiber diameter and spacing values. The value of the interfacial shear strength is obtained from the experimental data through the use of a finite element model which has been developed (11).

Evolution of an apparatus capable of obtaining a quantitative measurement of the shear strength of the fiber/matrix interface, based upon the procedures outlined above, involved numerous developmental phases which will be briefly outlined.

3.1 DEVELOPMENT OF MICRODEBONDING APPARATUS

PHASE I

The earliest prototypes of the microdebonding test apparatus centered around the use of a modified Vickers microhardness testing machine to apply a debonding load. The microhardness tester was modified to allow loads of 0-50

grams to be applied in one gram increments. It was also modified to accept steel probes which were used to apply the debonding load to the composite specimen. This work is reported in reference (41).

In this earlier work, the feasibility of producing interfacial debonding through the application of a load to the polished surface of a composite specimen was demonstrated. It was also determined that detection of interfacial debonding by inspection using an optical microscope was possible.

A variety of probe designs were investigated using the modified Vickers apparatus. The probes were designed to apply a load to either single fibers, or small groups of fibers. Probes were produced by machining and/or polishing either conventional sewing needles or drill rod stock.

It was observed that different debonding patterns resulted from loadings applied by the various probe geometries. Typical probe geometries and the debonding patterns they produced are shown in Figure 3. Results indicated that debonding loads could be determined with acceptable scatter using several of the probe geometries shown. Results obtained using probe geometries producing multiple and single fiber debonding are shown in Figure 4.

The modified Vickers apparatus was also used to study the degradation of the interfacial bond in composite specimens which had been subjected to environmental degradation. The reduction of debonding load was obtained for glass rein-

forced epoxy specimens which had been immersed in water at elevated temperatures. Results showing the reduction of debonding load as a function of the time of immersion and as a function of fiber location in the thickness direction of a laminate were obtained and are shown in Figure 5-7. Further details of these tests are given in reference (41).

Although the modified Vickers apparatus provided valuable information regarding the feasibility of the microdebonding test, results were not reproducible following realignment or adjustment of the probe apparatus, as shown in Figure 8. Additionally, the positioning and loading of the probe proved to be very demanding and tedious.

Another consideration was the desire to reduce the experimental data to a quantitative value of the interfacial bond strength. The prospect of using a finite element model to reduce the experimentally measured quantities into the stress components at the interface of a single fiber favored the development of an apparatus with the accuracy necessary to perform the microdebonding test on single fibers.

PHASE II

Further development of the microdebonding apparatus was based on the use of a strain gage extensometer (Instron model 2620-526) as a load cell, as reported in reference (42). The compliance of this extensometer is approximately 0.03

mm/gram which is soft enough to minimize high transient forces as the probe contacts the fiber surface during loading. The accuracy of load application using this extensometer as a load cell is 0.1 gram.

The probes used for load application were mounted directly to the moveable arm of the extensometer using an adapter. Probes consisted of ground diamond tips (radii 6 μm and 13 μm) mounted on 1/8" diameter steel drill stock. A schematic of the probe mechanism is shown in Figure 9.

The microdebonding apparatus was arranged around a research quality optical microscope (Reichert Zetopan model 323 474) which was used to select the desired point of load application and to detect debonding. Location of the point to be loaded on the specimen was accomplished through the use of a cross hair in one ocular of the microscope which was aligned to correspond with the point of probe contact.

The polished specimen was placed on a standard X-Y axis micrometer drive stage to facilitate positioning of the probe contact point on the specimen. This stage was placed on a turntable, similar to those used in birefringence studies, which was located with its axis of rotation offset from the optical axis of the microscope such that rotation of the turntable moved the specimen between the optical axis of the microscope and the location of the probe. The turntable was equiped with internal positioning stops which were used to index the specimen at the two locations.

Loading was accomplished by raising the specimen until it nearly contacted the probe using the coarse focus knob of the microscope. The fine adjustment knob was then used to apply the load, and increase it to the desired value. The magnitude of the load was read from the meter on a standard bridge amplifier (Vishay Instruments BAM-1).

The subsequent use of a finite element model to reduce the experimental measurements to values of interfacial shear strength required the measurement of fiber diameter. This was accomplished through the use of calibrated photomicrographs. A schematic of the microdebonding apparatus in this phase of its development is shown in Figure 10.

The design and fabrication of a new, more stable, mounting fixture for the probe mechanism was also required before single fiber loadings with the microdebonding apparatus could be attempted.

Tests conducted with this apparatus indicated that the positioning mechanisms were adequate for location of the probe to within approximately 1 μm. However, it was noted that the reproducibility of the probe contact location was marginal for repeated loadings which required several rotations of the turntable between the inspection and loading positions. This was determined

to be caused by a slight shift of the internal positioning stops of the turntable over the course of several rotations. This deficiency was corrected in later versions of the apparatus.

The most significant problem associated with this configuration was the sliding of the probe on the fiber surface during load application. This sliding was associated with the hinged motion of the moveable arm of the extensometer, which caused the tip of the probe to trace an arc during load application. This resulted in the sliding of the probe along the fiber surface during loading. The nature of this motion is illustrated in Figure 11. The magnitude of the probe sliding was found to be proportional to the distance that the specimen was raised during application of the load, which supported this hypothesis.

Subsequent modifications of the geometry of the probe mechanism reduced the magnitude of the sliding such that debonding could be obtained in some cases without the probe's sliding off the fiber surface. However, in most cases, the probe had slid to within a small distance of the interface when debonding occurred. In such cases, it is likely that debonding occurred due to the localized stresses generated by the probe in its immediate vicinity. This was substantiated by noting that most debonds initiated preferentially at the point on the interface closest to the termination

of the track made by the probe as it slid across the fiber surface. Due to this complication, the idea of attaching the probe directly to the arm of the extensometer was discarded.

An additional problem which was encountered when the accuracy of the microdebonding test was extended to the single fiber range was that of vibration noise. Evidence of excessive vibration consisted of surface damage to the specimen from bouncing or "plowing" of the loaded probe along the specimen surface. This damage sometimes extended for distances of several fiber diameters from the intended point of load application.

The vibrations which were encountered were determined to be inherent to all locations of the main buildings at MIT, but were of a lower amplitude in some basement locations. In locations other than basement rooms, vibrations caused by pedestrian traffic and the closing of doors in the vicinity of the test apparatus were very deleterious to the test operation. The use of heavy base plates and rubber absorbers beneath the microdebonding apparatus did little to alleviate the problem.

Further investigations revealed that the natural frequency of the cantilevered portion of the specimen stage was lowered by the addition of the turntable

and micrometer stage to a value very near that of the natural frequency of the building (approximately 30 hz). Therefore, vibration isolation is necessary for use of the microdebonding apparatus in most locations.

3.2 CURRENT APPARATUS - LINEAR PROBE MECHANISM

Based upon the previous work, the general requirements for a single fiber microdebonding apparatus were considered to include:

1. Accurate and reproducible location of the probe within the inner 20% of the fiber diameter. Most fibers tested are approximately 10 μm in diameter, so this translates to positioning within 1 μm.

2. Accurate load application and measurement, with the ability to apply a load in increments of approximately 0.2 grams, without the generation of high transient forces as the probe contacts the fiber surface.

3. Probe geometry and loading mechanism capable of confining load application to a region no closer than one quarter of a fiber diameter from the interface.

4. Optics capable of detecting failure of the fiber/matrix interface.

5. A method for measuring fiber diameters and spacings.

6. Vibration isolation.

Further improvements which were made to the earlier prototypes of the microdebonding apparatus focused primarily on the development of a probe mechanism in which the probe travel was linear, in order to eliminate sliding of the probe on the fiber surface. This was accomplished by the use of instrument quality ball bushings along with a precision ground shaft to provide the linear travel of the probe. Use of the extensometer as a load cell was retained. A simple linkage was constructed to transfer the linear motion of the shaft to the moveable arm of the extensometer. The weight of the shaft was made great enough (13 grams) to prevent slack from occuring in the linkage over the normal range of loadings. Additional weights could be attached to extend this range. The linear probe mechanism is shown in Figure 12.

Reproducibility of probe location during repeated loadings was improved through the use of magnetic stops for the turntable which replaced the original internal stops.

Problems due to vibrations were first eliminated by locating a basement room in a building unconnected with the main MIT building which had low vibration levels. A vibration isolation table was obtained for use in later work which eliminated the vibration problem associated

with operation in the main building of MIT. A schematic of the current microdebonding apparatus is shown in Figure 2.

Sliding of the probe along the fiber surface during loading has been eliminated by the use of the linear probe mechanism. Some sliding of the probe during loading, due to moments generated by misalignment of the linkage, has been noted in several instances. Proper alignment of the linkage was found to eliminate this.

The specifications of the current microdebonding apparatus are given in Table 1.

3.3 EXPERIMENTAL PROCEDURE

3.3.1 SPECIMEN PREPARATION

Specimens for the microdebonding test consist of composite laminates which have been sectioned perpendicular to the reinforcing fibers. Specimens may be either unidirectional laminates or multidirectional laminates which have been sectioned perpendicular to the fibers in a particular lamina. Specimens are then potted in a polyester mounting compound and polished using standard metallographic techniques. Specimen preparation typically consists of the following steps:

1. Section specimen perpendicular to fibers.
2. Pot specimens in polyester compound.
3. Polish specimens using standard metallographic techniques.
4. Store in desiccator jar until time of test.

Sectioning of the specimens is performed with a water cooled diamond tipped saw. Special care must be used when sectioning angle plied or off-axis unidirectional specimens to section perpendicular to the fibers.

Specimens are potted in a polyester compound in plastic casting cups. Sample mounting clips made of stainless steel are used to insure that the specimens are positioned perpendicular to the bottom face of the casting cup.

Polishing procedes through several stages using emmery paper followed by several stages using polishing compound. The normal progression of emery paper grit sizes is: 60,120,320,600. Approximately 1/16"-1/8" is removed from the specimen using the 60 grit emery paper to remove any of the specimen which may have been damaged during sectioning. The normal progression of polishing compounds used is: 1μ,0.3μ,0.05μ. Polishing is continued until virtually no scratches are visible on the surface of the specimen when observed with the optical microscope at the magnification used for testing (900X) and the interfaces appear continuous from fiber to matrix.

Alumina polishing compound is normally used. Diamond compounds were tried in several cases, but any increases in performance were too small to justify the increased cost. Polishing cloths used are rayon bonded to a cotton backing. Silk cloths were used in conjunction with the diamond compounds.

Specimens are stored in a desiccator jar for at least a week prior to testing.

3.3.2 TEST PROCEDURE

The various steps involved in performing the micro-debonding test will be outlined.

I. Apparatus Calibration and Alignment

1. Calibrate bridge amplifier and load cell using analytical weights.
2. Align the cross hair of the ocular lens to correspond with the location of probe contact on the specimen. This is most easily done by scratching a X on the polished surface of the potting compound surrounding the specimen and trying to locate the probe near the intersection of the lines. This is accomplished through a combination of adjusting the probe position, adjusting the objective lens, and rotating the ocular lens containing the cross hair. It has been found that using the tip of a single crosshair as opposed to the intersection of two crosshairs is easiest. This also allows adjustment of the reference point location by rotation of the ocular lens.

II. Debonding Test Procedure

1. Mount the specimen on the stage using plasticene. Use a press to level the plasticene on the specimen base prior to mounting on the test stage to insure a level surface. Loading on a surface which is not level has been noted to cause the probe to slide along the specimen surface.
2. Locate the region of interest on the specimen using the micrometer drive stage.
3. On a nearby area, realign the optics similar to in step I.2 (the scratching of an aligning mark should be unnecessary in this case). This is necessary due to shifts in the optics of the microscope when shifting to the photo mode, as well as chromatic aberrations of the optics which shifts the position of the image for different wavelengths of light.
4. Align the crosshair with the center of the fiber of interest.
5. Rotate the turntable until the magnetic stop engages in the probe position.
6. Slowly raise the specimen using the microscope coarse focus knob until the probe nearly contacts the specimen.
7. Using the fine adjustment knob, raise the specimen until the desired load is indicated by the strain gage meter. Hold the load for approximately 5 seconds. Lower the specimen to release the load.

II. Debonding Test Procedure (continued)

8. Rotate the turntable until the magnetic stop engages with the specimen under the optical axis of the microscope.
9. Inspect the specimen for initiation of debonding or evidence of off-centered loading or probe sliding. In the event of an off-centered loading the test point should be discarded. If evidence of the probe's sliding is observed, the linkage of the probe mechanism should be realigned and levelness of the specimen surface checked.
10. Repeat steps 5-9 until interfacial debonding is detected.
11. Record the load at initiation of debonding and photograph the tested fiber for measurement of the fiber diameter and spacing. Label photo and mark test fiber on photo.
12. For environmentally degraded specimens, record distances from test fiber to the edges of the specimen.

4.0 ANALYSIS OF MICRODEBONDING TEST

The primary objective of this work was to develop a test method capable of determining a quantitative value of the shear strength of the interfacial bond. In order to accomplish this, it was necessary to determine the state of stress at the interface due to the applied microdebonding load. Therefore, an analysis was required through which the state of stress at the interface could be calculated using the experimental measurements and the elastic constants of the system.

The quantities which are measured experimentally include the microdebonding load at the initiation of interfacial failure, the diameter of the test fiber and the spacing between the test fiber and the nearest adjacent fiber. The elastic constants of the fiber, matrix and composite system are generally known. Hence, from these parameters the state of stress at the interface must be determined.

In performing the microdebonding test, a load is applied to a fiber or group of fibers by a probe which transmits the load to the polished surface of the specimen. In general, problems involving contact stresses are very complex and involve the deformation of both the probe and specimen. Additionally, such problems often involve singularities near the edge of the contact area (43). Since it is necessary to determine the stress state at the interface in order to obtain a value of the interfacial shear strength, the region of loading should be kept far removed from the interface in order

to avoid complication in the analysis. This precludes the use of multifiber loadings, in which the interfacial regions are involved in the contact problem. It also suggests that the application of the microdebonding load to single fibers should be restricted to regions of the fiber which are far enough removed from the interface such that contact stress problems remain confined to regions which do not affect the stress state at the interface.

It is expected that if the complications mentioned above can be eliminated through careful and accurate loading of a single fiber, a finite element analysis might be used to determine the stress state at the interface due to an applied microdebonding load. From these results, the shear strength of the interface may be determined through the use of an appropriate failure criterion.

4.1 FINITE ELEMENT ANALYSIS

Several finite element models have been developed which give the stress distribution at the fiber/matrix interface for single fibers subjected to a microdebonding load (11).

The finite element models which have been developed use either two dimensional or axi-symmetric geometries to model the microdebonding test. In both cases, the model consists of a fiber which is surrounded by a layer of matrix material having constant thickness, which in turn is surrounded by material which is assigned the anisotropic properties of the average composite material. The model geometry is shown in Figure 13. For the two dimensional, or plane strain case, the model consists of strips which extend normal to the plane of the diagram. The axi-symmetric model consists of cylindrical elements. All of the finite element results presented here are taken from Reference (11) and were obtained using the axi-symmetric model unless stated otherwise.

A hybrid stress anisotropic finite element analysis was used to determine the stress distributions. A typical finite element mesh is shown in Figure 14. The length of the fiber was modelled as being much longer than the fiber diameter to simulate the case of continuous fibers. The stress distributions obtained for the interfacial regions near the surface of the specimen have been shown to be insensitive to further changes in length.

The actual deformation behavior of the probe was not modelled. Instead, the extreme cases of imposed pressure and imposed displacement were considered.

The stress values presented are those at the center of the first element on the matrix side of the interface. This location appeared to be the most consistent for determination of the stress distribution values. The discontinuous variation of the modulus across the interface resulted in some discrepancies in the values of the shear stress in the fiber and matrix immediately on either side of the interface, which precluded the use of an average of the two values. Since interfacial failure would generally be expected to occur preferentially in the phase which is weakest, the use of the stress values obtained at this location would appear to be consistent with the prediction of failure.

A typical shear stress distribution is shown in Figure 15. The shear stress values are normalized to give the shear stress, τ, in terms of σ_A, which is the axial stress applied to the fiber, averaged over the entire fiber area. Note that the shear stress vanishes at the free surface as would be expected from simple equilibrium considerations. The important implication of this is that the microdebonding test should be relatively insensitive to minor surface imperfections associated with specimen preparation, since interfacial failure would be expected to initiate at some distance from the specimen surface, where the shear stress obtains its maximum value.

Figure 16 shows shear stress distributions for E-glass/Epoxy, for cases having different contact areas of load application. The maximum value of the shear stress is noted to occur at distances ranging from 0.25 to 0.55 of a fiber dia-

meter from the surface. It is important to note, however, that the magnitude of the maximum shear stress does not vary appreciably with the loading area.

The values of the maximum shear stress obtained for the two extreme loading cases of imposed displacement and imposed pressure are shown as a function of the contact area of loading in Figure 17. The values of maximum shear stress are nearly constant for the range of loading conditions shown. This suggests that the microdebonding test should be rather insensitive to variations in probe contact characteristics involving the area of loading and the deformation of the probe and fiber surface.

The results presented in Figures 16 and 17 were obtained using the two dimensional model geometry and plane strain analysis.

In contrast to the lack of sensitivity shown by the maximum shear stress values to the various loading conditions, there is a strong dependence on the elastic and geometric properties of the composite.

Figure 18 shows the variation of the maximum shear stress as a function of the parameter $(G_m/E_f)^{1/2}$, where G_m is the shear modulus of the matrix and E_f is the Young's modulus of the fiber. Existing micromechanics solutions predict a similar dependence (6,16,44). The distance from the free surface at which the maximum shear stress occurs is also influenced by the parameter $(G_m/E_f)^{1/2}$ as can be seen in Figure 19. However,

it is not expected that this will have any appreciable influence on the microdebonding results.

The thickness of the matrix layer surrounding the fiber is also expected to influence the stresses at the interface. Figure 20 shows the shear stress distributions obtained for S-glass/Epoxy for several values of T_m/D_f, where T_m is the thickness of the matrix layer surrounding the fiber and D_f is the fiber diameter. It can be noted that the basic shape of the shear stress distribution is not greatly influenced by the thickness of the matrix layer, but that the magnitudes are strongly influenced.

The variation of the maximum shear stress as a function of the ratio T_m/D_f is shown in Figures 21, 22, and 23 for E-glass/Epoxy, S-glass/Epoxy and Graphite/Epoxy systems. Micromechanics solutions predict a 1/2 power relationship between the magnitude of the shear stress and the ratio T_m/D_f (16), and the results of a micromechanics solution based on a shear lag method are presented along with the finite element results for comparision in Figures 21, 22 and 23. It should be noted that the nature of the approximations involved in the micromechanics solution cause the results obtained for large values of matrix thickness, and values of matrix thickness approaching zero, to be in error.

Numerical values of the shear stress distributions obtained from the finite element analysis are given in Tables 2, 3, and 4 for E-glass/Epoxy, S-glass/Epoxy and Graphite/

Epoxy. The elastic constants used for these determinations are also presented in Tables 2, 3 and 4.

For purposes of comparison, the shear stress distribution predicted by the shear lag micromechanics analysis is presented with that obtained using the finite element analysis for S-glass/Epoxy in Figure 24.

4.2 DEFINITION OF FAILURE CRITERION

The finite element analysis which has been developed allows the calculation of the maximum shear stress at the interface based on quantities which can be measured experimentally using the microdebonding test. In order to obtain a value of interfacial shear strength, an appropriate failure criterion must be used. Since the values of the stress components other than τ are relatively small and compressive for the microdebonding case, it is expected that use of a maximum shear stress failure criterion is reasonable. Based on this assumption, the shear strength of the interface will be defined by the maximum value of the interfacial shear stress when initiation of interfacial debonding occurs.

4.3 DEFINITION OF EXPERIMENTAL PARAMETER CORRESPONDING WITH T_m.

From the determined value of the microdebonding load at initiation of debonding and given the values of the elastic constants of the composite and the parameter T_m, the maximum interfacial shear stress can be calculated and the shear strength of the interface can be determined. The results of the finite element analysis indicate that the thickness of the matrix layer surrounding the fiber, T_m, has a strong influence on the stresses which result from the microdebonding load. Therefore, it is necessary that a measure of the specimen geometry which corresponds with this parameter be chosen in order to relate the local fiber spacing of the test specimen to the geometry of the finite element model.

However, a complication arises in the application of the finite element analysis to the microdebonding results due to the dissimilarity between the geometry used for the finite element model and the actual local geometry surrounding the fibers in composite materials. In order to apply the results of the finite element analysis to the microdebonding test, it is necessary to specify some value of fiber spacing or a thickness of the matrix material surrounding the fiber, which corresponds to the thickness of the layer of matrix material, T_m, which is used in the finite element model. However, the layer of matrix material surrounding a fiber in actual composite materials varies in thickness around the circumference

of the fiber, and the distances between fibers usually varies significantly. Therefore, the finite element model used can only approximate the actual geometries encounted.

Analyses have been developed in which the influence of neighboring fibers are considered (16,45). However, due to the countless number of spatial arrangements which are possible between neighboring fibers, consideration of the exact local geometry would be extremely impractical, even if an appropriate analysis were available. It is likely, due to the complex and highly variable nature of the local geometries encounted experimentally, that the more sophisticated models would still merely approximate the actual stress states involved.

Of course, it is possible to avoid the complications discussed above by testing only fibers which are far removed from other fibers. However, composite materials containing the fiber volume fractions necessary for use as structural materials contain very few fibers which are far enough removed from neighboring fibers for this to be a practical alternative. Therefore, the effects of fiber spacing must be considered if tests are to be performed on normal composite systems.

The measure of specimen geometry chosen to correspond with T_m was the distance of separation between the fiber being tested and the nearest adjacent fiber which is designated $T_{m\text{-}exp}$. This was based upon the assumption that the nearest fiber would be the most dominant for considerations related to the transfer of stress. This assumption appears to be

valid based on the observation that the point of debonding initiation tends to occur at locations on the interface in the proximity of the nearest neighboring fiber. Therefore, the trends of the microdebonding results as a function of T_{m-exp} were examined.

5.0 APPLICATION OF THE MICRODEBONDING TEST TO TYPICAL GLASS/EPOXY AND GRAPHITE/EPOXY SYSTEMS.

Extensive tests were performed on three typical composite systems to evaluate the performance of the microdebonding test. The results of these tests were used to develop a suitable data reduction procedure for the calculation of interfacial shear strength and to characterize the influence of the various parameters on the results obtained from typical systems.

In order to determine the influence of the fiber spacing, T_{m-exp}, on the average axial stress applied to the fiber at interfacial failure, tests were performed on fibers having a wide range of values of T_{m-exp}. Tests were performed on two glass/epoxy systems and one graphite/epoxy system.

The glass/epoxy systems were both S-glass epoxy prepregs manufactured by the 3-M Company. The two systems were identical except for the silane based coupling agents applied to the fibers. These were proprietary coupling agents produced by Owens Corning Fiberglass and are designated as 463 and 449, the 449 coupling agent being a newer formulation developed to enhance the hygrothermal performance of the material. Specimens were in the form of unidirectional and cross ply laminates having fiber volume fractions of approximately 50%. These specimens are designated SP 250 S2 463 and SP 250 S2 449. For further details on these two systems see Table 5.

The Graphite/Epoxy system which was tested was reinforced with Celion 6000 graphite fibers produced by the Celanese Corporation and used an epoxy resin formulation produced by Celanese. The fibers were unsized. This specimen is designated C-CK-U. Further details of the Graphite/Epoxy system are given in Table 5.

Results from the microdebonding test were obtained for a wide range of fiber spacings. From the results of these tests, the trends of the microdebonding data as a function of the fiber spacing were determined. Based on these results, data reduction procedures for the calculation of the interfacial shear strength were developed.

Several factors were considered in order to develop a reasonable data collection and reduction procedure for the microdebonding test.

Typical fibers in a composite specimen have a wide range of distances separating them from the surrounding fibers. In order to allow the collection of a reasonable number of data points in a practical manner, it is desirable to utilize the results obtained from tests on individual fibers having different values of the spacing parameter T_{m-exp}. The ability to utilize fibers having different spacing values greatly enhances the ease with which the data points can be obtained.

Another factor of importance in the development of a data reduction procedure was the application of the finite element analysis to the data obtained experimentally. In order to avoid inconsistencies which may arise from differing

trends of the experimental and analytical results, over a range of values of T_m, it was decided that the finite element analysis should be applied to the experimental data at a consistent value of T_m.

This value needs to be chosen in a range where it is likely to be the most valid. The value should also be chosen in a range which includes large numbers of test fibers in typical composite systems in order to avoid excessive extrapolation of the experimental data.

Based on the considerations outlined above, the value $T_m = 0.40\ D_f$ was chosen for the application of the finite element analysis to the experimental data. It was felt that as the values of T_m approached zero, the accuracy of the analysis was likely to become more critical. Inspection of Figure 21,22, and 23 shows that the rate of change of τ_{max}/σ_A with respect to T_m/D_f becomes larger in magnitude as $T_m/D_f=0$ is approached. Based on these considerations, the use of small values of T_m for application of the analysis was avoided.

On the other hand, practical considerations were against the use of large spacing values for analysis of results. Only small numbers of fibers having spacings greater than ~$0.50\ D_f$ are present in typical composite specimens. The use of test points with spacings over $0.50\ D_f$ would be extremely impratical.

Although most fibers in the specimens which were tested had spacings of less than $0.30\ D_f$, a reasonable amount were available in the range through $0.40\ D_f$. This allows test points with similar spacing values to be located with reasonable ease.

The test results obtained from the three systems were analyzed in order to develop a consistent procedure for the application of the finite element analysis to the experimental results in order to calculate the value of the interfacial shear strength.

5.1 REDUCTION OF MICRODEBONDING DATA

The results of the microdebonding test are shown in Figures 25,26, and 27 for the SP 250 463, SP 250 449 and C-CK-U specimens respectively. The average applied axial stress at the initiation of debonding, designated $\bar{\sigma}$, is shown plotted as a function of the ratio $T_{m\text{-}exp}/D_f$. These results indicate that the value of $T_{m\text{-}exp}/D_f$ has an effect on the microdebonding data which is in qualitative agreement with that which would be expected based on the results of the analysis. The data obtained were curve fit using a least squares method for a power curve of the form $Y = AX^B$ and the curves which were obtained are shown along with the experimental data in Figures 25-27. The coefficients obtained from the curve fits and the values of $\bar{\sigma}$ obtained from the results of the curve fit for $T_m/D_f = 0.40$ are presented in Table 7. The curve fit was applied to the data at values of T_m/D_f greater than 0.10 in order to avoid problems involving the validity of a power curve relation at values of T_m/D_f approaching zero.

In order to compare the experimental results to the behavior which would be expected based on the finite element analysis, it is useful to compare the experimental results to the parameter σ_A/τ_{max} obtained from the finite element analysis, normalized to the experimental results at $T_m/D_f = 0.40$. This indicates the trend which would be predicted by the finite element analysis, and is shown along with the results

of the curve fits in Figures 28,29 and 30 for the three systems studied.

It is also interesting to compare these results to those predicted by the shear lag micromechanics analysis (16). The trends of the two analyses and typical experimental results are shown in Figure 34, with the results normalized to unity at $T_m/D_f = 0.40$. It can be seen that the finite element analysis predicts a lesser influence of T_m/D_f on the results than does the shear lag analysis. The experimental data shows less dependence on T_m/D_f than do either of the analyses.

Although it is difficult to apply an analysis with confidence to the fibers having very small values of T_{m-exp}, it is valuable to consider the data obtained from these points. Typical composite specimens contain many such fibers, and an ability to relate the experimental results obtained for these fibers to the analysis would be very useful. The data obtained at $T_{m-exp}/D_f \cong 0$ are shown plotted as the mean and standard deviation values of the individual data points. The mean value of $\bar{\sigma}$ obtained at $T_{m-exp}/D_f \cong 0$ is designated $\bar{\sigma}_o$. $\bar{\sigma}_o$ values determined for the three systems are given in Table 7. The values of the ratio of $\bar{\sigma}_o$ divided by the value of $\bar{\sigma}_{.40}$ obtained from the curve fit are also given in Table 7, where $\bar{\sigma}_{.40}$ is the average axial stress applied at the initiation of debonding for fibers having $T_m/D_f = 0.40$.

In order to reduce the quantity of data required for the testing of other systems, it would be desireable if the necessity to obtain a curve fit of the experimental data for

each individual system could be eliminated. In order to accomplish this, a procedure for adjusting the experimental results to the common value of $T_m/D_f = 0.40$ was investigated. This involved adjusting the experimentally determined values of $\bar{\sigma}$ through multiplication by the ratio of the $\bar{\sigma}_{.40}$ value obtained from the curve fit, divided by the curve fit value of $\bar{\sigma}$ obtained for the T_{m-exp}/D_f value of the test point in question. It was hoped that through this procedure, the data could be adjusted to the single value of $T_m/D_f = 0.40$, and that a mean value of $\bar{\sigma}_{.40}$ obtained in this manner might be determined. A power curve having a power value of 0.10 was used for this procedure, since this closely approximates the values obtained using the curve fit for two of the three systems (SP250 463 and C-CK-U).

In this manner, data points obtained from fibers having different values of T_{m-exp}/D_f could be used to obtain a value of $\bar{\sigma}_{.40}$. Values of $\bar{\sigma}_{.40}$ obtained using this procedure are given in Table 8.

In order to determine whether the proposed method of adjusting the data was consistent over the range of T_m/D_f values of interest, the values of $\bar{\sigma}_{.40}$ obtained using this procedure were plotted as a function of the value of T_{m-exp}/D_f at which the data were obtained. These results are shown in Figures 31-33 for the three systems tested.

The values of $\bar{\sigma}_0/\bar{\sigma}_{.40}$ calculated from the above results are given in Table 8. The average value determined for the three systems was 0.75. Based on this, values of $\bar{\sigma}_{.40}$ were calculated for the three systems by dividing the

mean values of $\bar{\sigma}_0$ by 0.75.

Having obtained values of $\bar{\sigma}_{.40}$ by the procedures outlined above, the determination of the interfacial shear strength was accomplished in a straightforward manner by applying the results of the finite element analysis obtained at $T_m/D_f = 0.40$ to the experimental data. The values of the interfacial shear strength $\bar{\tau}$ which were determined by the methods outlined above are presented in Table 9.

6.0 DISCUSSION

6.1 DISCUSSION OF RESULTS

Three possible procedures for obtaining microdebonding results corresponding to $T_m/D_f = 0.40$ have been presented. These methods include curve fitting the experimental data, adjusting the data to values corresponding to $T_m/D_f = 0.40$, and relating the data obtained for $T_{m-exp}/D_f \cong 0$ to the value at $T_{m-exp}/D_f = 0.40$. The results of the finite element analysis were then applied to these values in order to determine the interfacial shear strength. The results are given in Table 9.

From these results, it can be seen that the values obtained for the shear strengths of both S-glass systems are similar, with the value of the shear strength for the SP 250 449 system being approximately 2-3% lower than that obtained for the SP 250 463 system.

The similar values obtained for these two systems are reasonable based on composite test data for these materials. Studies conducted to determine the effects of environmental exposure on the mechanical properties of these systems showed that their properties were similar in the unexposed condition (46). The results of that study showed that the results of tensile tests performed at 0°, 10°, 30° and 45° from the fiber axis were an average of 4% lower for the SP 250 449

system as compared to the results obtained for the 463 system. More appreciable differences in performance were reported after exposure to hygrothermal aging. The results of these tests on unexposed specimens are presented in Table 10.

The values of interfacial shear strength obtained for the C-CK-U system displayed greater differences between the values determined by the different data reduction procedures. The values obtained do, however, all lie in a range which is reasonable for such a system. Studies have been done using the single fiber technique presented in references (21 and 22) on the C-CK-U system (47). The value of interfacial shear strength reported was $\tau = 9.7 \pm 1.77$ ksi. Differences between the two values should not be surprising based on the differences in the test methods, and especially the analyses, used.

The single fiber test bases its analysis on the average shear stress present at the interface at the time at which the breakdown of the fiber into segments of critical length occurs, without consideration of the nature of the stress distribution or the progression of debonding prior to the final breakdown of the fiber. Regardless of this fact, very valuable results have been obtained using this method. It is important that the significant approximations inherent in both analyses be understood before any attempt to correlate the results is made. It is felt that the shear strength reported in the reference (47) is of value in confirming that the microdebonding results obtained are in a reasonable range for this system.

The values of interfacial shear strengths obtained for the S-glass/Epoxy specimens show a variation of 1% or less between the values which were obtained by the different data reduction procedures. The values obtained for the Graphite/Epoxy system, however, show a maximum variation of 8% between the results obtained by the different methods.

From the results presented in Tables 7 and 8, it can be seen that the data obtained from the Graphite/Epoxy system displays more scatter than that obtained for the two S-glass/Epoxy systems.

The typical coefficients of variation for the Graphite/Epoxy system were 13-14%. This is clearly a greater amount than is desireable. The coefficient of variation of the SP 250 463 data was approximately 10% and the SP 250 449 data had values of 5-7%. This scatter in the data is reflected by the magnitudes of the variation in shear strength values obtained using the different data reduction methods.

An explanation for the greater scatter exhibited by the Graphite/Epoxy data can be made from the magnitudes of the experimentally measured quantities obtained from the Graphite/Epoxy system. The debonding loads applied to the fibers at failure for the Graphite/Epoxy system were typically on the order of 3 grams. The increment of loading used for all tests was 0.5 grams. Additionally, the values of the fiber diameters generally did not vary over as great a range for the graphite fibers, as did those of the glass fibers, for the systems which were tested. This resulted in the average

increment of applied axial stress for the Graphite/Epoxy system being quite large in relation to the value at failure. It is felt that this was the main cause of the greater amount of scatter exhibited by the Graphite/Epoxy system. Typical loads for failure of the S-glass systems were in the 4-6 gram range. Thus, the greater scatter displayed by the data obtained for the Graphite/Epoxy system is not surprising.

This limitation can be reduced by decreasing the increment of loading to a value of ~0.2-0.25 grams. This is still well within the capability of the apparatus, and would be expected to alleviate this problem to a major extent.

Improvement of the quality of photomicrographs obtained for use in determining the fiber diameter would also improve the results obtained.

However, it would be adviseable in any event to reduce the increment of loading from 0.5 grams, as was used in these tests, to approximately 0.25 grams, for both glass and graphite reinforced systems.

All three methods of data reduction which were investigated yielded results of interfacial shear strength which were essentially of the same magnitude, when consideration was given to the scatter of the data. Therefore, it seems reasonable that any of the methods could be used, and that the method most suited to the specific case in question should be chosen.

The major disadvantage involved with using a curve fitting procedure is that application of this method to a

small number of data points, or to data points gathered over a small range of T_{m-exp} values could easily result in an improper form for the curve which is obtained. Therefore, it is felt that a general form for the variation of $\bar{\sigma}$ with respect to T_m/D_f should be applied to the data, based on the results of more extensive tests than would normally be performed on each specimen.

Aside from this, either of the other two methods seem to yield acceptable results, and selection of the procedure for use in a given case should probably be based on practical considerations related to the specimen being studied.

A consideration of importance to the results obtained using the microdebonding test is that of the residual stress state which is present near the free surface of a specimen. Although these stresses undoubtedly contribute somewhat to the behavior which is observed, micromechanics analyses of similar problems indicate that the shear component of such stresses should be relatively small (6). The normal component of these stresses is not likely to have a great effect on the microdebonding results due to the compressive normal stresses generated at the interface by the microdebonding load. Therefore, it is not expected that the residual stresses will have an appreciable affect on the microdebonding results.

It is important, when comparing the results obtained using the microdebonding test with those obtained using other methods, that the nature of the analysis and failure crite-

rion which are used be considered. Although there is limited similarity between the model used for the finite element analysis and the local geometries found in actual composites, which may lead to discrepancies in the predicted stress state at the interface, this problem will be common to all test methods in which the test is applied to an actual composite specimen.

The microdebonding test has the advantage of confining the failure to the phase of the material for which the strength is desired. This is a major advantage over most other measures of interfacial adhesion which are obtained from tests on actual composite specimens. Additionally, the results of the microdebonding test are not overly sensitive to the details of the loading conditions, which is in contrast to most test methods.

6.2 DISCUSSION OF EXPERIMENTAL METHOD - POSSIBILITIES FOR FURTHER DEVELOPMENT.

The development of the microdebonding test apparatus has resulted in a mechanism which can meet all of the requirements associated with application of the microdebonding test to typical composite materials.

However, the question often arises as to the possibility of alternate methods for the detection of debonding. A detection method by some means other than optical inspection would be favorable for several reasons. A method which eliminated the need for inspection after each increment of loading would allow the microdebonding load to be increased continuously until the point of failure, which would reduce the time necessary for testing. Such a method would also eliminate the possibility of subjective differences in results due to differences in operator judgement concerning the initiation of debonding.

Several alternatives have been considered, although no experimental investigations into their feasibility have been conducted. However, most of the alternate methods seem to have serious problems associated with them.

The deflection which results from the debonding of the fiber, and the associated change in stiffness, are of magnitudes well below the measuring capability of any standard method of detection. It is also questionable whether the initiation of debonding releases enough elastic energy to be detectable by accoustic methods compared with contact

noise. Electrical detection techniques would have to address the problems associated with the contact resistance of whatever probe arrangement was used, which would likely be a significant problem.

The optical detection method does, however, have some advantages associated with its use which are not immediately apparent. The optical inspection of the test site prior to loading allows regions of macroscopic damage or microcracking to be avoided for use as test points. More importantly, it allows the operator to monitor the loading such that improperly loaded cases can be easily detected and rejected. In addition to this consideration, the use of photomicrographs for the determination of geometric parameters has the advantage of allowing the entire nature of the geometry surrounding a fiber to be recorded, in addition to the single spacing parameter which is normally used for the purposes of data reduction.

In connection with tests which are performed on specimens which have been subjected to environmental degradation, a measure of the degree of microcracking which is present in the materials might be gained through the optical inspection and from the photomicrographs, which could be useful for considerations related to mechanical test results obtained for the degraded laminate. Therefore, the optical detection method has some advantages, which are not immediately evident.

The major disadvantage of the current optical detection method is the practical consideration of the eye fatigue of

the operator. However, it is questionable whether the advantages associated with the inherent simplicity of this technique can be outweighed by the capabilities of any other technique which has been considered.

7.0 CONCLUSIONS

1) The microdebonding test which has been developed can produce consistent failures which are confined to the interfacial region surrounding a fiber through the application of an axial load to the end of a fiber at the polished surface of a composite specimen. The area of probe contact through which the load is applied can be confined to a central region of the fiber cross section which is well removed from the interface.

2) A finite element analysis developed in another study allows the determination of the shear stresses at the fiber/matrix interface from the experimentally measured parameters.

3) Based on the finite element analysis, the results of the microdebonding test should be relatively insensitive to the loading conditions, provided that the load is centrally applied and the area of probe contact is confined to less than 75% of the fiber cross sectional area, such that the region of contact remains well removed from the interface.

4) Based on the shear stress distributions obtained from the finite element analysis, the results of the microdebonding test should be relatively insensitive to the details of the surface preparation of the specimen.

5) A data reduction procedure has been developed through which the results obtained from the microdebonding test can be related to the finite element results in a consistent manner. This allows the calculation of a quantitative value of the shear strength of the fiber/matrix interface based on a maximum shear stress criterion.

6) The microdebonding test can be applied to actual composite materials to measure the strength of the fiber/matrix interface of individual fibers, in-situ. This makes the test very valuable for purposes of studying the interfacial shear strength in composite materials which have been subjected to degradative environments.

7) Values of interfacial shear strength have been determined using the microdebonding test for two S-glass/Epoxy systems and one Graphite/Epoxy system. The results obtained for the Graphite/Epoxy system are consistent with reported values of interfacial shear strength which were obtained using a single fiber technique. The results obtained for the two S-glass/Epoxy systems are consistent with the reported results of mechanical tests performed on both systems.

8) The coefficients of variation of the data obtained for the S-glass/Epoxy specimens were 5-10%. This is considered marginally acceptable. The coefficient of variation of the Graphite/Epoxy data was 13-15%. This is considered to be

unacceptable. This is believed to be due largely to the magnitude of the loading increments used. The microdebonding apparatus has the capability of applying loads in significantly smaller increments, which should alleviate this deficiency.

8.0 RECOMMENDATIONS

Based on the observations of the microdebonding tests, it is felt that consideration of the following topics would be of interest or of value.

1. It would be beneficial to reduce the increment of loading which is presently being used. The present value of the increment in load is too large in relation to the normal range of loads which produce interfacial debonding. It is likely that this contributes significantly to the scatter which has been observed in the experimental results. Decreasing the increment by a factor of two (from 0.5 to 0.25) would still result in an increment which is well within the capabilities of the mechanism and should reduce the amount of scatter, especially for systems which tend to debond at relatively low values of the microdebonding load.

2. It would be helpful to construct a new linkage member for the probe mechanism. The present linkage has some eccentricities inherent in its configuration which have been noted to induce sliding of the probe if not properly adjusted. It is felt that a linkage which would suspend the shaft and probe from a pair of knife-edge contact points would be superior to the present version.

3. Improving the resolution or magnification of the photomicrographs would be very beneficial. Increased magnification would naturally improve the accuracy of the measurements made from the photomicrographs. However, the reduction in eye strain which would result from this improvement would also manifest itself in the form of additional increases in accuracy and reliability of measurement.

4. Based on the quantity of information which is presently available in the form of single fiber tests which measure interfacial shear strength, and the wide range of mechanical test results available which are often used to infer interfacial strength, it would be interesting to use the microdebonding test to do comparative studies of these various test methods.

5. It would be valuable to study the effects of residual stresses on the results of the microdebonding test. By combining a finite element study of the stress states which result from the combined effects of the residual stresses and the stresses imposed due to the microdebonding loading, with an experimental study to determine the effects that annealing the residual stresses has on the microdebonding results, it is possible that some insight into this problem could be gained.

REFERENCES

REFERENCES

1. Rosen, B.W., in Modern Composite Materials, L.J. Broutman and R.H. Krock, eds.,Addison-Wesley, Reading Mass.(1967), p. 106.

2. Harlow, D.G. and S.L. Phoenix, "The Chain-of-Bundles Probability Model for the Strength of Fibrous Materials I: Analysis and Conjectures," J.Composite Materials, Vol. 12, April 1978, p. 195.

3. Zweben, C. and B.W. Rosen, "A Statistical Theory of Material Strength with Application to Composite Materials," J. Mech. Phys. Solids, Vol. 18, 1970,p. 189.

4. Rosen, B.W., "Tensile Failure of Fibrous Composites," AIAA Jour., Vol. 2, No. 11, Nov. 1964, p. 1985.

5. Broutman, L.J., in Modern Composite Materials, L.J. Broutman and R.H. Krock, eds., Addison-Wesley, Reading Mass. (1967), p. 337.

6. Chamis, C.C.,in Composite Materials, Vol. 6, E.P. Plueddemann ed., Academic Press, New York (1974), p. 32.

7. Cooper, G.A. and A. Kelly, "Role of the Interface in the Fracture of Fiber-Composite Materials," Interfaces in Composites, ASTM STP 452, ASTM, 1969, p. 90.

8. Miller, A.G. and A.L. Wingert, "Fracture Surface Characterization of Commercial Graphite/Epoxy Systems," Nondestructive Evaluation and Flaw Criticality for Composite Materials, ASTM STP 696, R.B. Pipes ed., ASTM, 1977, p. 223.

9. Wyatt, R.C. and K.H.G. Ashbee, "Debonding in Carbon Fibre/Polyester Resin Composites Exposed to Water: Comparison with E-Glass Fibre Composites," Fibre Science and Technology, Vol. 2, 1969, p. 29.

10. Walter, E. and K.H.G. Ashbee, "Osmosis in Composite Materials," Composites, Oct. 1982, p. 365.

11. Tsiang, T.-H., "Damage Development in Fiber Composites Due to Bearing," Sc.D. Thesis, Massachusetts Institute of Technology, Feb. 1983.

12. Hanna, G.L., and S. Steingiser, "Defining the Adhesion Characteristics in Advanced Composites," Composite Materials: Testing and Design, ASTM STP 460, ASTM, 1969, p. 182.

13. Broutman, L.J., "Measurement of the Fiber-Polymer Matrix Interfacial Strength," Interfaces in Composites, ASTM STP 452, ASTM, 1969, p. 27.

14. Anderson, G.P. et.al., Analysis and Testing of Adhesive Bonds, Academic Press, London, 1977, pp. 1-21.

15. McGarry, F.J. and D.W. Marshall, "Research on Wire-Wound Composite Materials," Symposium on Standards for Filament-Wound Reinforced Plastics, ASTM STP 327, ASTM, Philadelphia, 1963, p. 133.

16. Greszczuk, L.B., "Theoretical Studies of the Mechanics of the Fiber-Matrix Interface in Composites," Interfaces in Composites, ASTM STP 452, ASTM, 1969, p. 42.

17. Mooney, R.D. and F.J. McGarry, "Resin-Glass Bond Study," Proc. 14th Reinforced Plastics\Composites Institute, Society of the Plastics Industry, Section 12-E, (1959).

18. Outwater, J.O., and M.C. Murphy, "The Influences of Environment and Glass Finishes on the Fracture Energy of Glass-Epoxy Joints," J. Adhesion, Vol. 2, Oct. 1970, p.242.

19. Fraser, W.A., F.H. Achker and A.T. DiBenedetto, "A Computer Modeled, Single Filament Technique for Measuring Coupling and Sizing Agent Effects In Fiber Reinforced Composites," Proc. 30th Ann. Tech. Conf., Reinforced Plastics/Composites Institute, Society of the Plastics Industry, Section 22-A, 1975.

20. Wadsworth, N.J., and I. Spilling, "Load Transfer From Broken Fibres in Composite Materials," Brit. J. Appl. Phys. (J. Phys. D.), Ser. 2, Vol. 1, 1968, p. 1049.

21. Drzal, L.T., M.J. Rich, J.D. Camping and W.J. Park, "Interfacial Shear Strength and Failure Mechanisms in Graphite Fiber Composites," Proc. 35th Ann. Tech. Conf., Reinforced Plastics/Composites Institute, Society of the Plastics Industry, Section 20-C, 1980.

22. Drzal, L.T., "Surface Characterization of Graphite Fibers," Proc. of DOD/TTCP Critical Review: Techniques for the Characterization of Composite Materials, Cambridge Mass., June 8-10, 1981.

12. Chamis, C.C., in Composite Materials, Vol. 6, E.P. Plueddemann ed., Academic Press, New York,(1974), pp. 43-50.

13. Broutman, L.J., "Measurement of the Fiber-Polymer Matrix Interfacial Strength," Interfaces in Composites, ASTM STP 452, ASTM, 1969, pp. 27-41.

14. Anderson, G.P. et.al., Analysis and Testing of Adhesive Bonds, Academic Press, London, 1977, pp. 1-21.

15. McGarry, F.J. and D.W. Marshall, "Research on Wire-Wound Composite Materials," Symposium on Standards for Filament-Wound Reinforced Plastics, ASTM STP 327, ASTM, Philadelphia, 1963, pp. 133-145.

16. Greszczuk, L.B., "Theoretical Studies of the Mechanics of the Fiber-Matrix Interface in Composites," Interfaces in Composites, ASTM STP 452, ASTM, 1969, pp. 42-58.

17. Mooney, R.D. and F.J. McGarry, "Resin-Glass Bond Study," Proc. 14th Reinforced Plastics\Composites Institute, Society of the Plastics Industry, Section 12-E, (1959).

18. Outwater, J.O., and M.C. Murphy, "The Influences of Environment and Glass Finishes on the Fracture Energy of Glass-Epoxy Joints," J. Adhesion, Vol. 2, Oct. 1970, p.242.

19. Fraser, W.A., F.H. Achker and A.T. DiBenedetto, "A Computer Modeled, Single Filament Technique for Measuring Coupling and Sizing Agent Effects In Fiber Reinforced Composites," Proc. 30th Ann. Tech. Conf., Reinforced Plastics/Composites Institute, Society of the Plastics Industry, Section 22-A, 1975.

20. Wadsworth, N.J., and I. Spilling, "Load Transfer From Broken Fibres in Composite Materials," Brit. J. Appl. Phys. (J. Phys. D.), Ser. 2, Vol. 1, 1968, p. 1049.

21. Drzal, L.T., M.J. Rich, J.D. Camping and W.J. Park, "Interfacial Shear Strength and Failure Mechanisms in Graphite Fiber Composites," Proc. 35th Ann. Tech. Conf., Reinforced Plastics/Composites Institute, Society of the Plastics Industry, Section 20-C, 1980.

22. Drzal, L.T., "Surface Characterization of Graphite Fibers," Proc. of DOD/TTCP Critical Review: Techniques for the Characterization of Composite Materials, Cambridge Mass., June 8-10, 1981.

23. Loveless, H.S. and J.H. Ellis, "A Comparison of Methods for Determining the Shear Properties of Glass/Resin Unidiredtional Composites," Jour. of Testing and Evaluation, Vol. 5, No. 5, Sept. 1977, p. 369.

24. Lyle, P.D., "Shear Testing of Continuous Fiber Reinforced Plastics," Proc. of 37th Ann. Conf., Reinforced Plastics/Composites Institute, Society of the Plastics Industry, Section 24-F, 1982.

25. Chiao, C.C., R.C. Moore and T.T. Chiao, "Measurement of Shear Properties of Fibre Composites, Part 1. Evaluation of Test Methods," Composites, July 1977, p. 161.

26. Goan, J.C., T.W. Martin and R. Prescott, "The Influence of Interfacial Bonding On the Properties of Carbon Fiber Composites," Proc. of 28th Ann. Tech. Conf., Reinforced Plastics/Composites Institute, Society of the Plastics Industry, Section 21-B, 1973.

27. Clark, D., N.J. Wadsworth and W. Watt, "The Surface Treatment of Carbon Fibers for Increasing the Interlaminar Shear Strength of CFRP," Proc. of Int. Conf. on Carbon Fibres, Their Place in Modern Technology, The Plastics Institute, 1974, p. 7/1.

28. McKague, E.L., J.D. Reynolds and J.E. Halkias, "Life Assurance of Composite Structures, Vol. 1 Moisture Effects," AFML-TR-75-51, Vol. 1, May 1975.

29. Mazor, A., L.J. Broutman and B.J. Eckstein, "Effect of Long Term Water Exposure on Properties of Carbon and Graphite Fiber Reinforced Epoxies," Polymer Eng. and Sci., Vol. 18, No. 5, Apr. 1978, p. 341.

30. Kedward, K.T., "On the Short Beam Test Method," Fibre Sci. and Tech., 5, 1972, p. 85.

31. Daniels, B.K., N.K. Harakas and R.C. Jackson, "Short Beam Shear Tests of Graphite Fiber Composites," Fibre Sci. and Tech., 3, 1971, p. 187.

32. Kaelble, D.H., P.J. Dynes and E.H. Cirlin, "Interfacial Bonding and Environmental Stability of Polymer Matrix Composites," J. Adhesion, 1974, Vol. 6, p. 22.

33. Kaelble, D.H. et. al., "Interfacial Mechanisms of Moisture Degradation in Graphite-Epoxy Composites," J. Adhesion, 1974, Vol 7, p.25.

34. Kaelble, D.H., P.J. Dynes and L. Maus, "Hydrothermal Aging of Composite Materials, Part 1: Interfacial Aspects," J. Adhesion, 1976, Vol. 8, p. 121.

35. Herakovich, C.T., H.W. Bergner and D.E. Bowles, "A Comparitive Study of Composite Shear Specimens Using the Finite-Element Method," Test Methods and Design Allowables for Fibrous Composites, ASTM STP 734, C.C Chamis ed., ASTM, 1981, p. 129.

36. Browning, C.E., G.E. Husman and J.M. Whitney, "Moisture Effects in Epoxy Matrix Composites," Composite Materials: Testing and Design (Fourth Conference) ASTM STP 617, ASTM, 1977, p. 481.

37. Ishai, O. and A. Mazor, "The Effect of Environmental Loading History on the Transverse Strength of GRP Laminate," Jour. Comp. Mat., Vol. 9, Oct. 1975, p.370.

38. Douglas, C.D. and E.R. Pattie, "Effects of Moisture on the Mechanical Properties of Glass/Epoxy Composites," Proc. DOD/TTCP Critical Review:Techniques for the Characterization of Composite Materials, Cambridge Mass., June 1981.

39. Browning, C.E. "The Mechanisms of Elevated Temperature Property Losses In High Performance Structural Epoxy Matrix Materials After Exposure to High Humidity Environments," Proc. of the 1978 Int. Conf. on Comp. Mat., Am. Inst. of Mining Metallurgical and Petroleum Engineers, 1978, p. 1527.

40. Kaelble, D.H., and P.J. Dynes, "Hydrothermal Aging of Composite Materials, Part 2: Matrix Aspects," J. Adhesion, 1977, Vol. 8, p.195.

41. Mandell, J.F., J.-H. Chen and F.J. McGarry, "A Microdebonding Test for In-Situ Fiber-Matrix Bond and Moisture Effects," Dept. of Materials Science and Engineering, Massachusetts Institute of Technology, Research Report R80-1, Feb. 1980.

42. Mandell, J.F. et. al., "Microdebonding Test for In-Situ Fiber/Matrix Bond Strength of Composites With Application to Moisture Degradation," Dept. of Materials Science and Engineering, Massachusetts Institute of Technology, Final Report Contract No. DAAG-46-77-C-0070, June 1981.

43. Muskhelishvilli, N.I., Some Basic Problems of the Mathematical Theory of Elasticity, Noordoff, Groningen, Holland (translated from Russian), (1953).

44. MacLaughlin, T.F., and R.M. Barker, "Effect of Modulus Ratio on Stress Near a Discontinuous Fiber," Experimental Mechanics, Vol. 12, 1972, p. 178.

45. Barker, R.M. and T.F. MacLaughlin, "Stress Concentrations Near a Discontinuity in Fibrous Composites," J. Composite Materials, Vol. 5, 1971, p. 492.

46. Douglas, C.D. and E.R. Pattie, "Effects of Moisture on the Mechanical Properties of Glass/Epoxy Composites," Proc. of DOD/TTCP Critical Review: Techniques for the Characterization of Composite Materials, Cambridge Mass., June 8-10, 1981.

47. Ying, L., "Role of Fiber/Matrix Interphase in Carbon Fiber-Epoxy Composite Impact Toughness," Proc. 38th Ann. Tech. Conf., Reinforced Plastics/Composites Institute, Society of the Plastics Industry, Section 12-F, 1983.

TABLES

TABLE 1

SPECIFICATIONS OF MICRODEBONDING APPARATUS

FUNCTION	TECHNIQUE	ACCURACY OR SENSITIVITY
Load Application	Linear Probe Mechanism	0.1 gram
Probe Location	X-Y Axis Micrometer Drive Stage	1 μm
Movement Between Loading and Inspection	Turntable	Indetectable
Measurement of Fiber Diameter and Spacing	Calibrated Photomicrograph	0.5 μm
Stickage of Probe Mechanism	_____	0.1 gram

TABLE 2

INTERFACIAL STRESS DISTRIBUTION IN E-GLASS/EPOXY

Material Properties: (psi)

	E_{11}	E_{22}	ν_{21}	ν_{12}	G_{12}
Composite	1.4×10^6	5.0×10^6	0.2	0.06	0.7×10^6
Matrix	0.4×10^6	0.4×10^6	0.3	0.3	1.538×10^5
Fiber	10×10^6	10×10^6	0.3	0.3	3.85×10^6

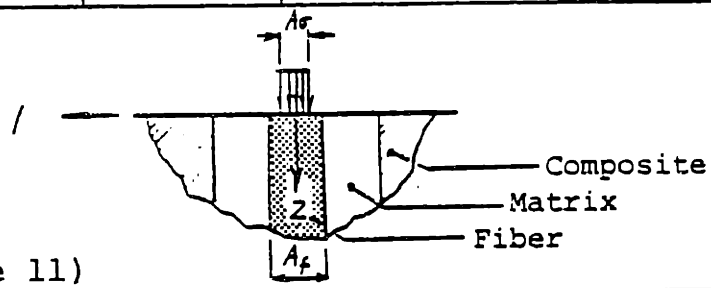

(From Reference 11)

$\frac{T_m}{D_f}$	1.0		0.4		0.1	
$\frac{A\sigma}{A_f}$	0.2500		0.2500		0.2500	
σ_{AV}	100 psi		100 psi		100 psi	
$\frac{Y}{d_f}$ (psi')	τ_{12}	$\frac{\tau_{12}/\sigma_{AV}}{A_\sigma/A_f}$ (10^{-2})	τ_{12}	$\frac{\tau_{12}/\sigma_{AV}}{A_\sigma/A_f}$ (10^{-2})	τ_{12}	$\frac{\tau_{12}/\sigma_{AV}}{A_\sigma/A_f}$ (10^{-2})
0.063	1.125	4.500	1.224	4.894	2.460	9.898
0.094	1.177	4.706	1.329	5.314	2.646	10.584
0.125	1.266	5.064	1.523	6.092	2.784	11.136
0.156	1.375	5.498	1.736	6.944	2.878	11.512
0.188	1.476	5.904	1.957	7.828	3.064	12.256
0.219	1.584	6.336	2.172	8.686	3.230	12.920
0.250	1.663	6.650	2.222	8.888	3.243	12.970
0.281	1.735	6.938	2.240	8.960	3.215	12.858
0.313	1.770	7.078	2.298	9.192	3.246	12.982
0.344	1.803	7.212	2.375	9.498	3.290	13.160
0.375	1.816	7.262	2.420	9.680	3.320	13.280
0.406	1.827*	7.308*	2.445*	9.780*	3.329*	13.314*
0.438	1.819	7.274	2.433	9.732	3.293	13.172
0.469	1.816	7.262	2.403	9.610	3.228	12.910
0.500	1.794	7.176	2.328	9.310	3.109	12.434
0.531	1.780	7.118	2.224	8.894	2.979	11.914
0.563	1.751	7.002	2.140	8.560	2.873	11.490
0.594	1.729	6.916	2.083	8.330	2.796	11.182

Note: "*" is the max. value; $(G_m/E_f)^{\frac{1}{3}} = 0.124$

TABLE 3

INTERFACIAL STRESS DISTRIBUTION IN S-GLASS/EPOXY

Material Properties: (psi)

	E_{11}	E_{22}	ν_{21}	ν_{12}	G_{12}
Composite	2.0×10^6	7.0×10^6	0.25	0.071	0.7×10^6
Matrix	0.4×10^6	0.4×10^6	0.3	0.3	1.538×10^5
Fiber	12.5×10^6	12.5×10^6	0.3	0.3	4.81×10^6

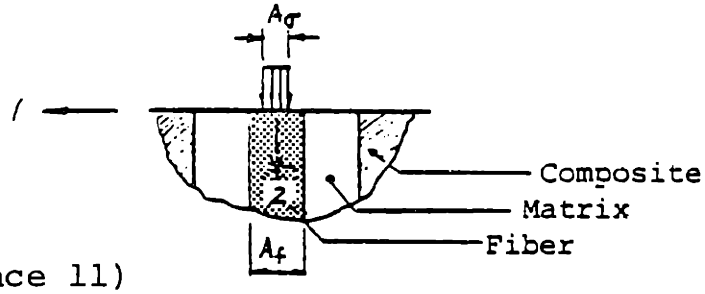

(From Reference 11)

$\frac{T_m}{D_f}$	1.0		0.4		0.1	
$\frac{A_\sigma}{A_f}$	0.2500		0.2500		0.2500	
σ_{AV}	100 psi		100 psi		100 psi	
$\frac{Y}{d_f}$ (psi')	τ_{12}	$\frac{\tau_{12}/\sigma_{AV}}{A_\sigma/A_f}$ (10^{-2})	τ_{12}	$\frac{\tau_{12}/\sigma_{AV}}{A_\sigma/A_f}$ (10^{-2})	τ_{12}	$\frac{\tau_{12}/\sigma_{AV}}{A_\sigma/A_f}$ (10^{-2})
0.063	1.050	4.198	1.160	4.640	2.383	9.530
0.094	1.109	4.436	1.237	4.948	2.534	10.130
0.125	1.235	4.940	1.406	5.622	2.656	10.620
0.156	1.309	5.234	1.590	6.358	2.722	10.890
0.188	1.377	5.508	1.783	7.130	2.884	11.540
0.219	1.467	5.868	1.970	7.878	3.027	12.110
0.250	1.534	6.134	2.016	8.062	3.022	12.130
0.281	1.595	6.378	2.034	8.136	3.001	12.000
0.313	1.625	6.500	2.089	8.354	3.026	12.100
0.344	1.705	6.820	2.159	8.636	3.064	12.260
0.375	1.718	6.870	2.204	8.816	3.092	12.370
0.406	1.755*	7.018*	2.230*	8.920*	3.101*	12.400*
0.438	1.731	6.922	2.223	8.892	3.073	12.290
0.469	1.715	6.860	2.198	8.790	3.016	12.060
0.500	1.700	6.800	2.131	8.524	2.913	11.650
0.531	1.681	6.724	2.040	8.158	2.798	11.190
0.563	1.628	6.512	1.967	7.868	2.707	10.830
0.594	1.612	6.448	1.918	7.672	2.640	10.560

Note: "*" is the max. value; $(G_m/E_f)^{\frac{1}{2}} = 0.1109$

TABLE 4

INTERFACIAL STRESS DISTRIBUTION IN GRAPHITE/EPOXY

Material Properties: (psi)

	E_{11}	E_{22}	V_{21}	V_{12}	G_{12}
Composite	1.0×10^6	19×10^6	0.25	0.013	0.7×10^6
Matrix	0.4×10^6	0.4×10^6	0.3	0.3	1.538×10^5
Fiber	40×10^6	40×10^6	0.20	0.01	2×10^6

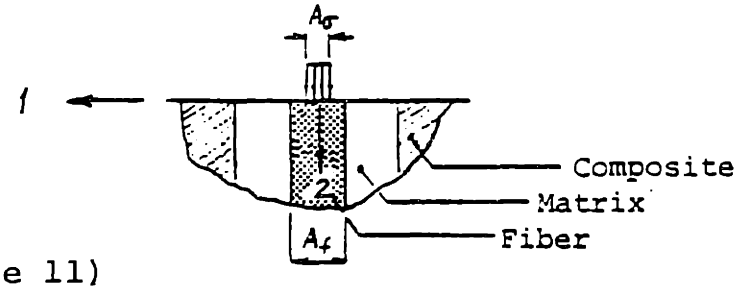

(From Reference 11)

$\frac{T_m}{D_f}$	1.0		0.4		0.1	
$\frac{A\sigma}{A_f}$	0.2500		0.2500		0.2500	
σ_{AV}	100 psi		100 psi		100 psi	
$\frac{y}{d_f}$ (psi')	τ_{12}	$\frac{\tau_{12}/\sigma_{AV}}{A_\sigma/A_f}$ (10^{-2})	τ_{12}	$\frac{\tau_{12}/\sigma_{AV}}{A_\sigma/A_f}$ (10^{-2})	τ_{12}	$\frac{\tau_{12}/\sigma_{AV}}{A_\sigma/A_f}$ (10^{-2})
0.063	0.3819	1.528	0.425	1.701	0.908	3.632
0.094	0.3990	1.596	0.461	1.845	1.033	4.130
0.125	0.4213	1.685	0.533	2.132	1.110	4.440
0.156	0.4593	1.837	0.613	2.451	1.163	4.650
0.188	0.5377	2.151	0.702	2.808	1.255	5.018
0.219	0.5858	2.343	0.789	3.155	1.333	5.330
0.250	0.6204	2.482	0.814	3.255	1.345	5.378
0.281	0.6555	2.622	0.840	3.360	1.345	5.380
0.313	0.6846	2.738	0.895	3.579	1.387	5.548
0.344	0.7165	2.866	0.958	3.832	1.431	5.726
0.375	0.7443	2.977	1.000	4.000	1.469	5.874
0.406	0.7717	3.087	1.044	4.176	1.495	5.980
0.438	0.7931	3.172	1.071	4.282	1.505*	6.020*
0.469	0.8166	3.266	1.083*	4.330*	1.491	5.966
0.500	0.8343*	3.337*	1.057	4.226	1.458	5.832
0.531	0.8226	3.290	1.021	4.082	1.411	5.642
0.563	0.7774	3.110	1.009	4.036	1.392	5.568
0.594	0.7635	3.054	1.014	4.054	1.391	5.564

note: "*" is the max. value; $(G_m/E_f)^{\frac{1}{3}} = 0.062$

TABLE 5

COMPONENTS OF GLASS/EPOXY SYSTEMS

SP250 S2 463 AND SP250 S2 449

Laminate Material: SP 250 Prepreg (3-M Company)

Fiber: S-2 (S-glass) (Owens Corning Fiberglass)

Matrix: SP250 Epoxy

Component	Wt %
ECN 1273 epoxy cresol novalac	45.8
EPON 828 DGEBA resin	38.1
Cardolite 513 flexibilizer and reactive diluent	4.7
Dicyanamide curing agent	7.5
Monuron accelerator	3.8

Coupling Agent: 463 and 449 respectively (OCF)

ELASTIC CONSTANTS

$E_f = 12.5 \times 10^6$ psi

$G_m = 1.538 \times 10^5$ psi

$(G_m/E_f)^{1/2} = 0.1109$

Specimens supplied by AMMRC.

TABLE 6

COMPONENTS OF GRAPHITE/EPOXY SYSTEM

Fiber: Celion 6000 (Celanese Corporation)

Matrix: "System F" - Epi-Res 508 (Celanese Corp.) 100 pts
Epi-Cure 841 " 22.5 pts

Coupling Agent: None

ELASTIC CONSTANTS

$E_f = 35 \times 10^6$ psi

$G_m = 1.75 \times 10^5$ psi

$(G_m/E_f)^{1/2} = 0.071$

Specimen supplied by Celanese Corporation.

TABLE 7

CURVE FIT PARAMETERS FOR MICRODEBONDING DATA AND VALUES OF $\bar{\sigma}$ AT $T_m/D_f=0$

Curve Fit Parameters

Power Curve Form: $Y=AX^B$

Parameter	SP250 463 (S-glass/Epoxy)	SP250 449 (S-glass/Epoxy)	C-CK-U (Graphite/Epoxy)
A	123,549 (psi)	115,007 (psi)	139,887 (psi)
B	0.104	0.061	0.096
R^2	0.248	0.105	0.231
(Note: R^2 is the coefficient of determination.)			
$\bar{\sigma}_{.40}$	112,367 (psi)	108,809 (psi)	128,088 (psi)
Mean Values at $T_m/D_f \simeq 0$			
$\bar{\sigma}_0$	84,836 (psi)	82,695 (psi)	100,856 (psi)
St. Dev.	9121 (psi)	5893 (psi)	14,866 (psi)
C.O.V.	10.8%	7.1%	14.9%
$\frac{\bar{\sigma}_0}{\bar{\sigma}_{.40}}$	0.755	0.760	0.787

TABLE 8

RESULTS OBTAINED BY SHIFTING MICRODEBONDING DATA TO $T_m/D_f=0.40$

	SP250 463 (S-glass/Epoxy)	SP250 449 (S-glass/Epoxy)	C-CK-U (Graphite/Epoxy)
$\bar{\sigma}_{.40}$	112,884 (psi)	110,210 (psi)	129,232 (psi)
St. Dev.	11,874 (psi)	5917 (psi)	17,136 (psi)
C.O.V.	10.5%	5.4%	13.3%
$\bar{\sigma}_0/\bar{\sigma}_{.40}$	0.751	0.750	0.780

TABLE 9

VALUES OF INTERFACIAL SHEAR STRENGTH CALCULATED FROM MICRODEBONDING RESULTS

	SP250 463	SP250 449	C-CK-U
$(\tau_{max}/\bar{\sigma})$ from finite element analysis for T_m/D_f= 0.40	8.92×10^{-2}	8.92×10^{-2}	4.980×10^{-2}
$\bar{\tau}$ calculated using $\bar{\sigma}_{.40}$ obtained from curve fit	10,023 psi	9706 psi	6966 psi
$\bar{\tau}$ calculated using $\bar{\sigma}_{.40}$ obtained by shifting results to T_m/D_f=0.40	10,069 psi	9831 psi	6436 psi
$\bar{\tau}$ calculated using $\bar{\sigma}_{.40}$ calculated from $\bar{\sigma}_{0.75}$	10,089 psi	9835 psi	6697 psi
Total % variation between values	1/2%	1%	8%

TABLE 10

MECHANICAL TEST DATA FOR SP250 463 AND SP250 449 SYSTEMS
(From Reference 46)

ANGLE OF AXIS	TENSILE STRENGTH	
	SP250 463	SP250 449
0°	1430 MPa	1400 MPa
10°	320 MPa	290 MPa
30°	115 MPa	110 MPa
45°	76 MPa	76 MPa
90°	50 MPa	--

FIGURES

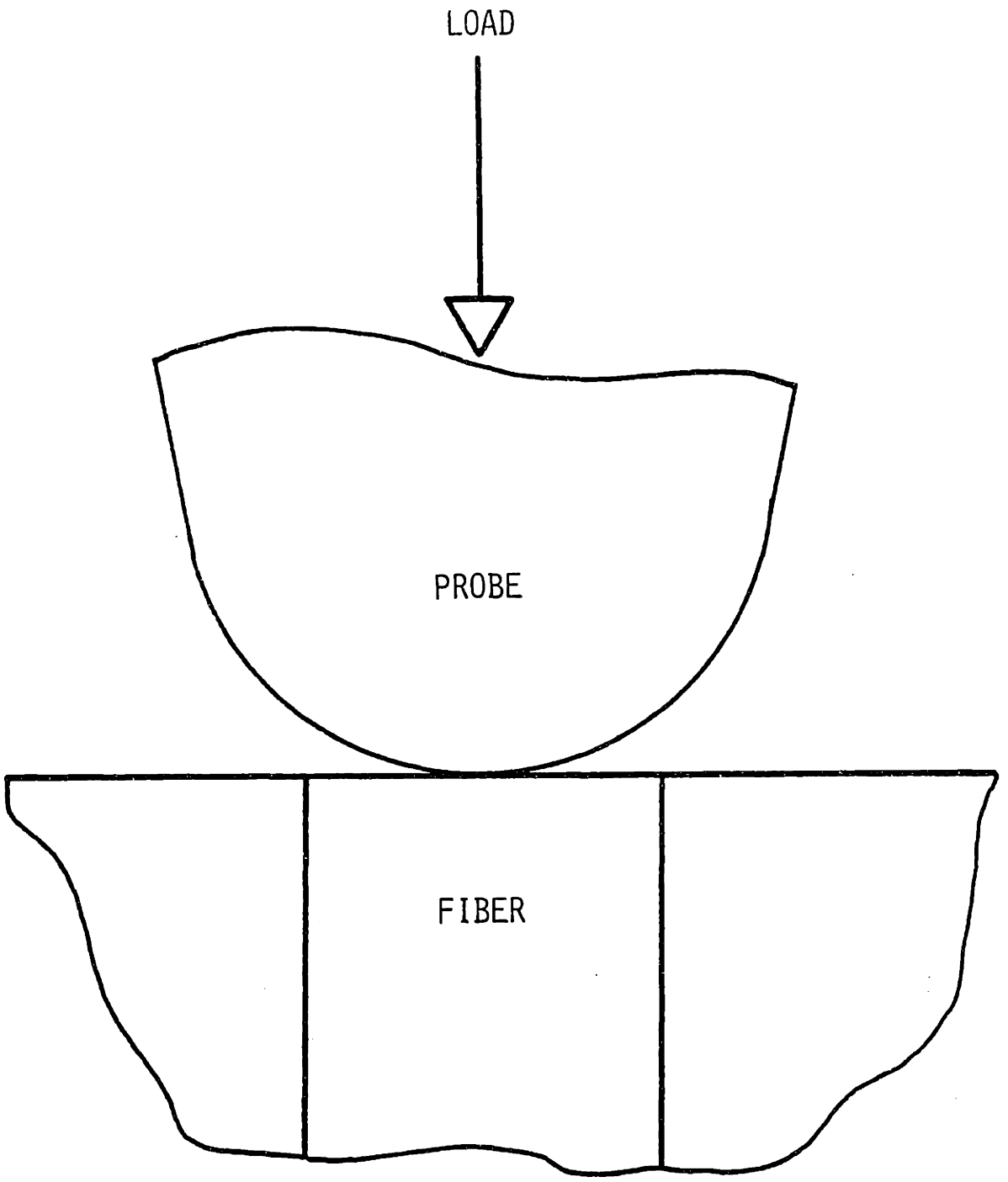

FIGURE 1

SCHEMATIC OF LOADING FOR MICRODEBONDING TEST

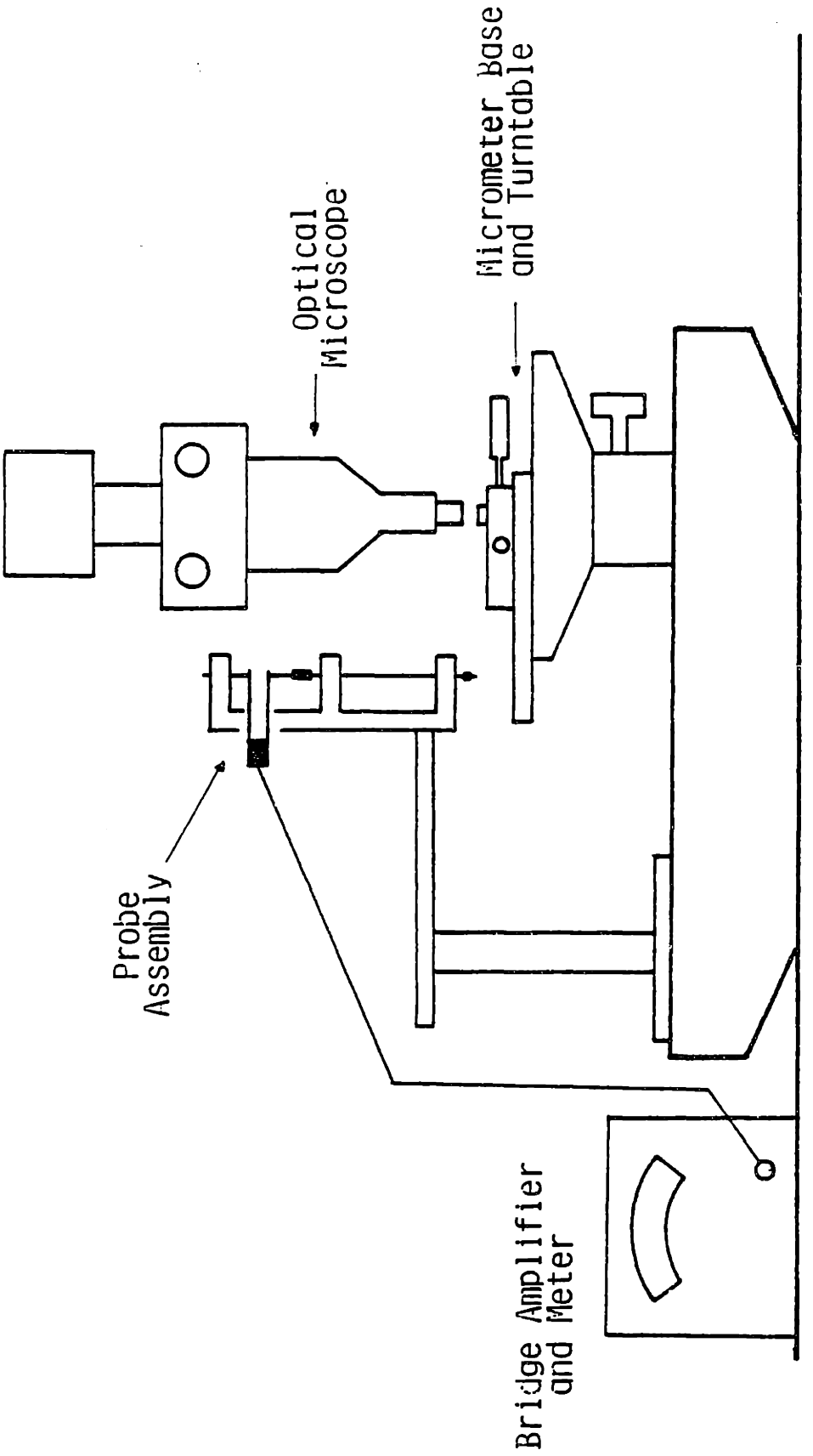

FIGURE 2

SCHEMATIC OF MICRODEBONDING APPARATUS

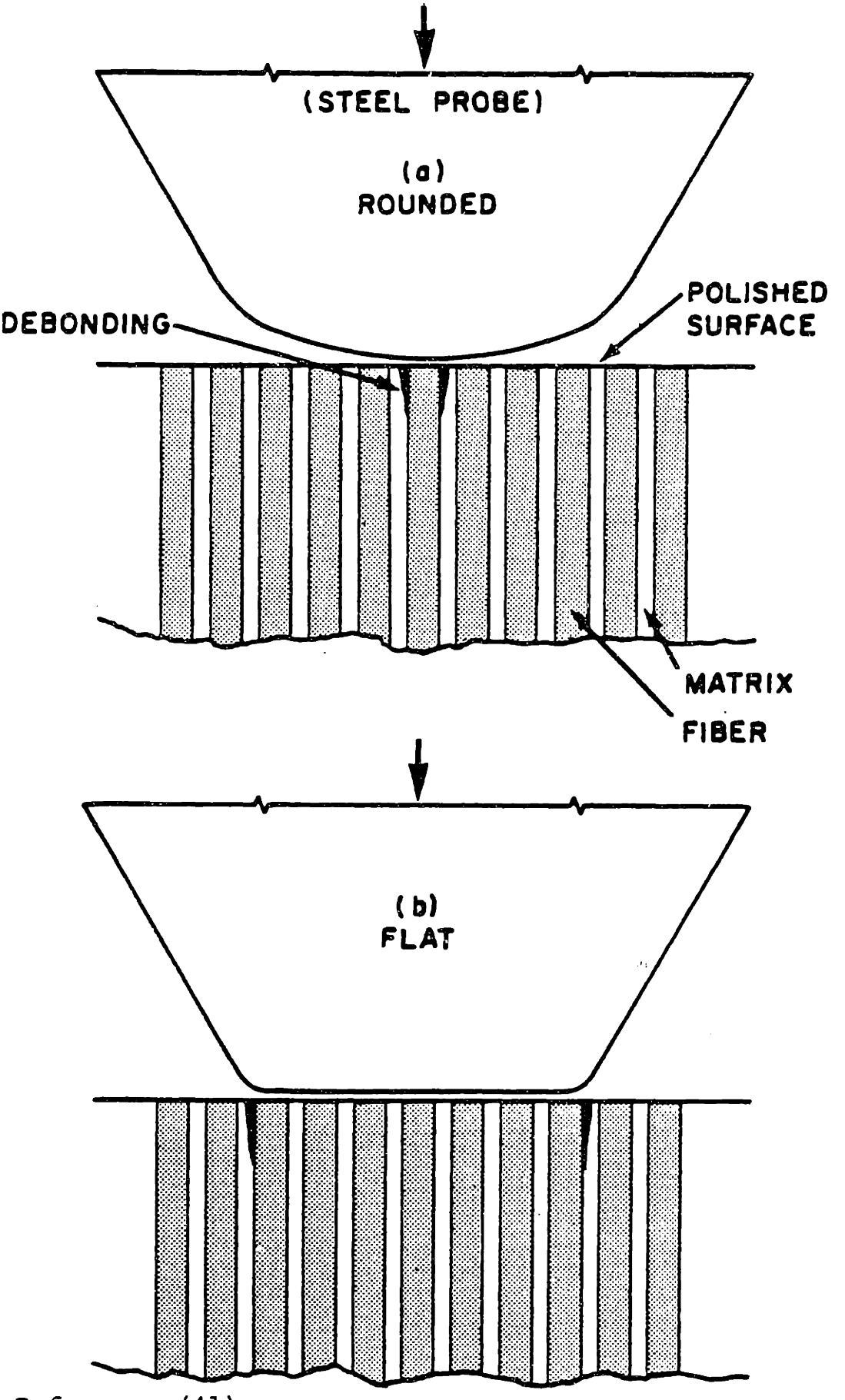

From Reference (41).

FIGURE 3

TYPICAL PROBE GEOMETRIES AND
ASSOCIATED DEBONDING PATTERNS
USED WITH MODIFIED VICKERS APPARATUS

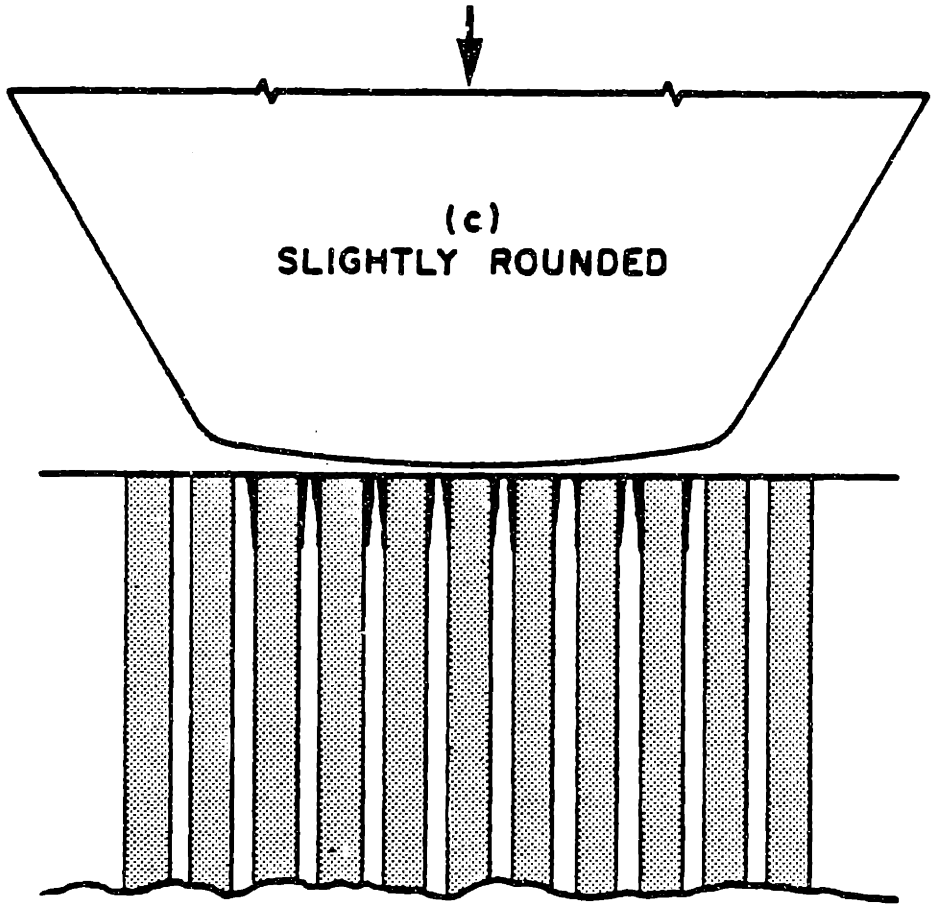

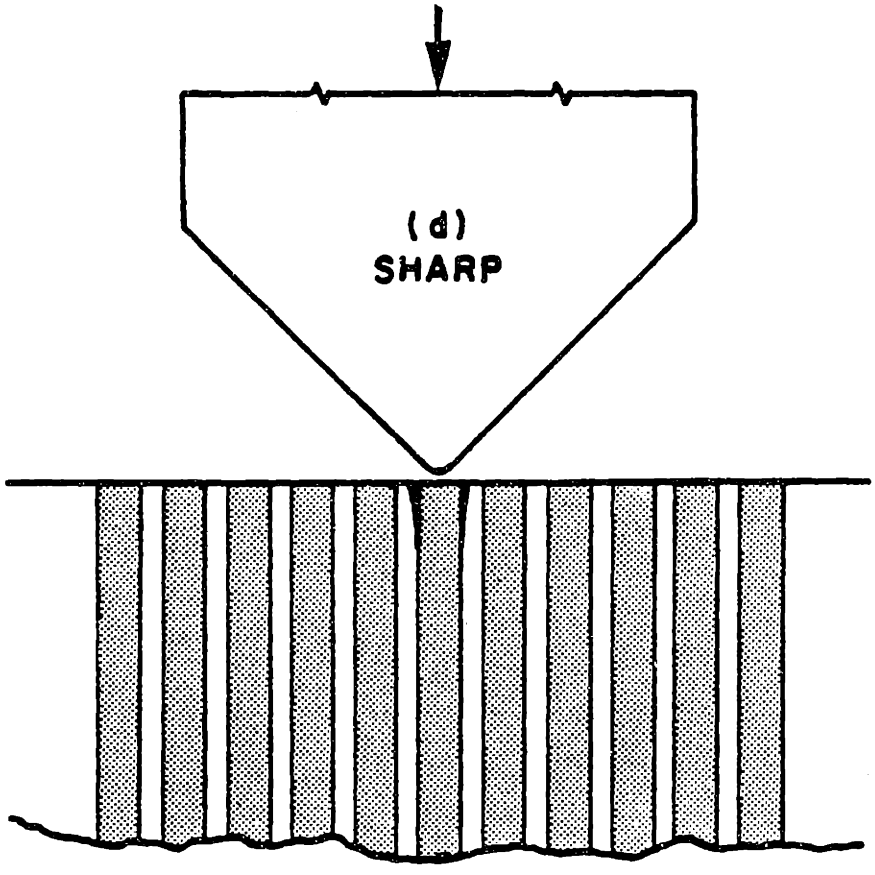

From Reference (41). FIGURE 3 (cont)

TYPICAL PROBE GEOMETRIES AND
ASSOCIATED DEBONDING PATTERNS
USED WITH MODIFIED VICKERS APPARATUS

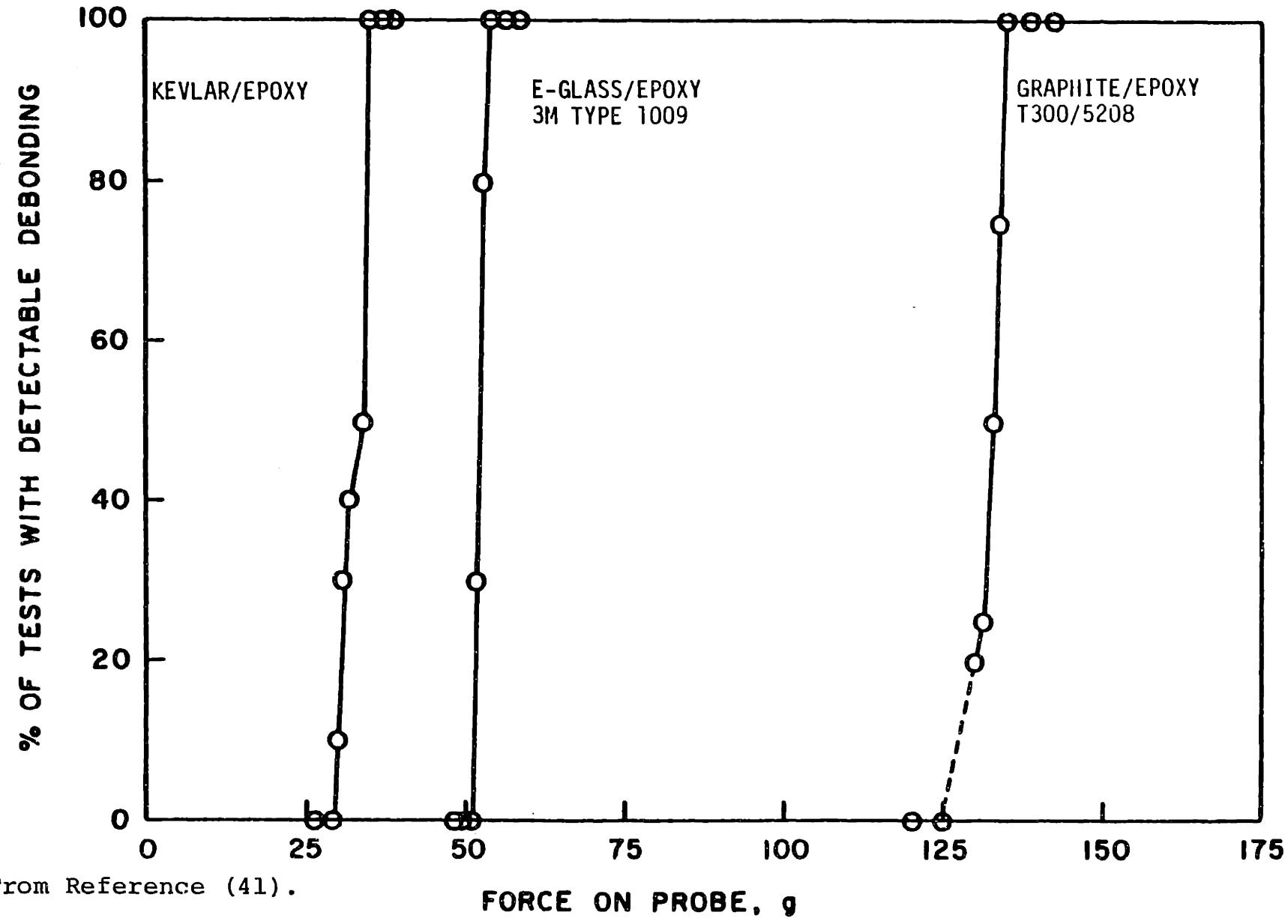

From Reference (41).

FIGURE 4.

MICRODEBONDING RESULTS FOR KEVLAR, E-GLASS, AND GRAPHITE FIBER/EPOXY USING SAME PROBE.
(Modified Vickers Apparatus)

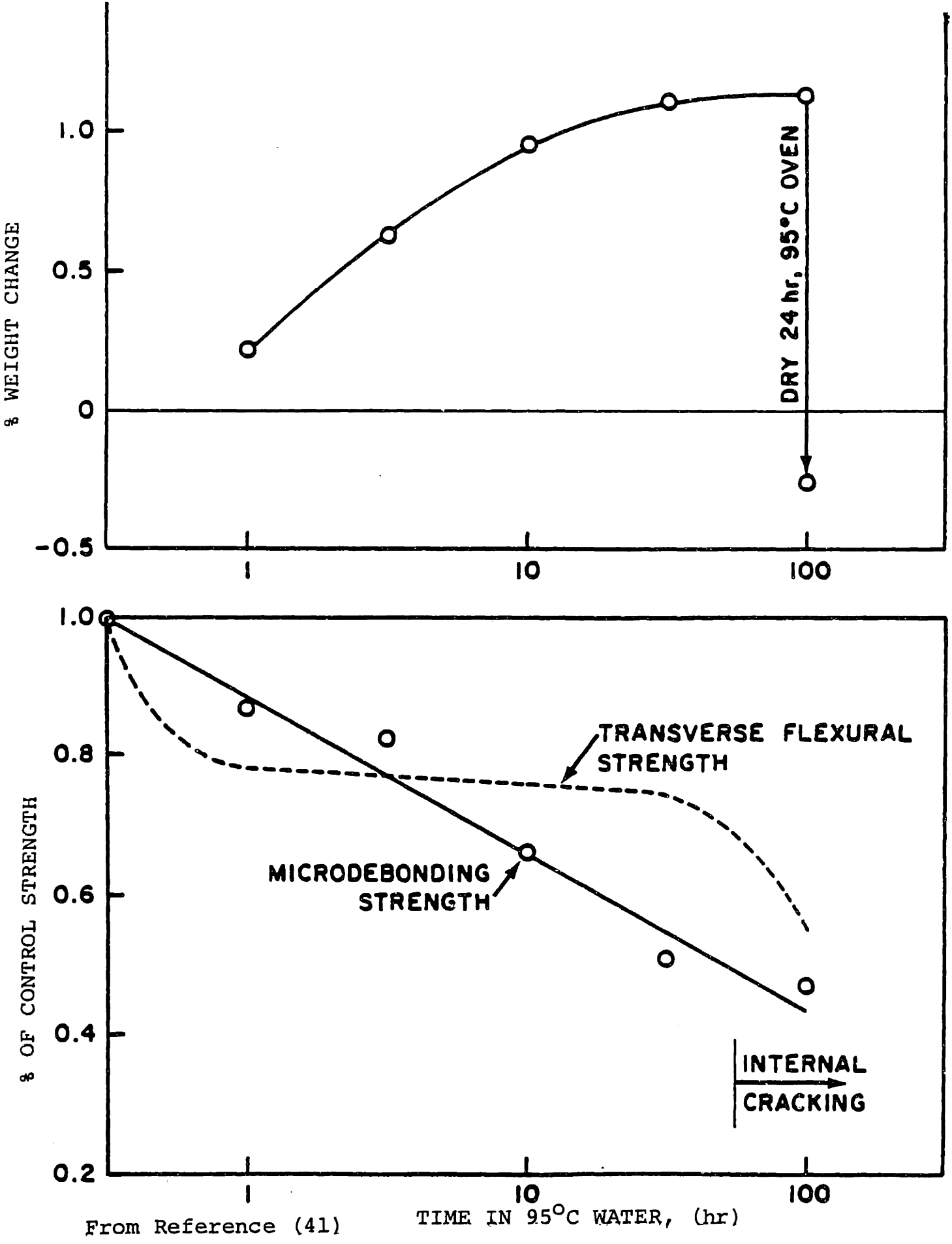

From Reference (41)

FIGURE 5

EFFECT OF 95°C WATER CONDITIONING ON THE MICRODEBONDING STRENGTH AND TRANSVERSE FLEXURAL STRENGTH OF GLASS/EPOXY. OBTAINED USING MODIFIED VICKERS APPARATUS.

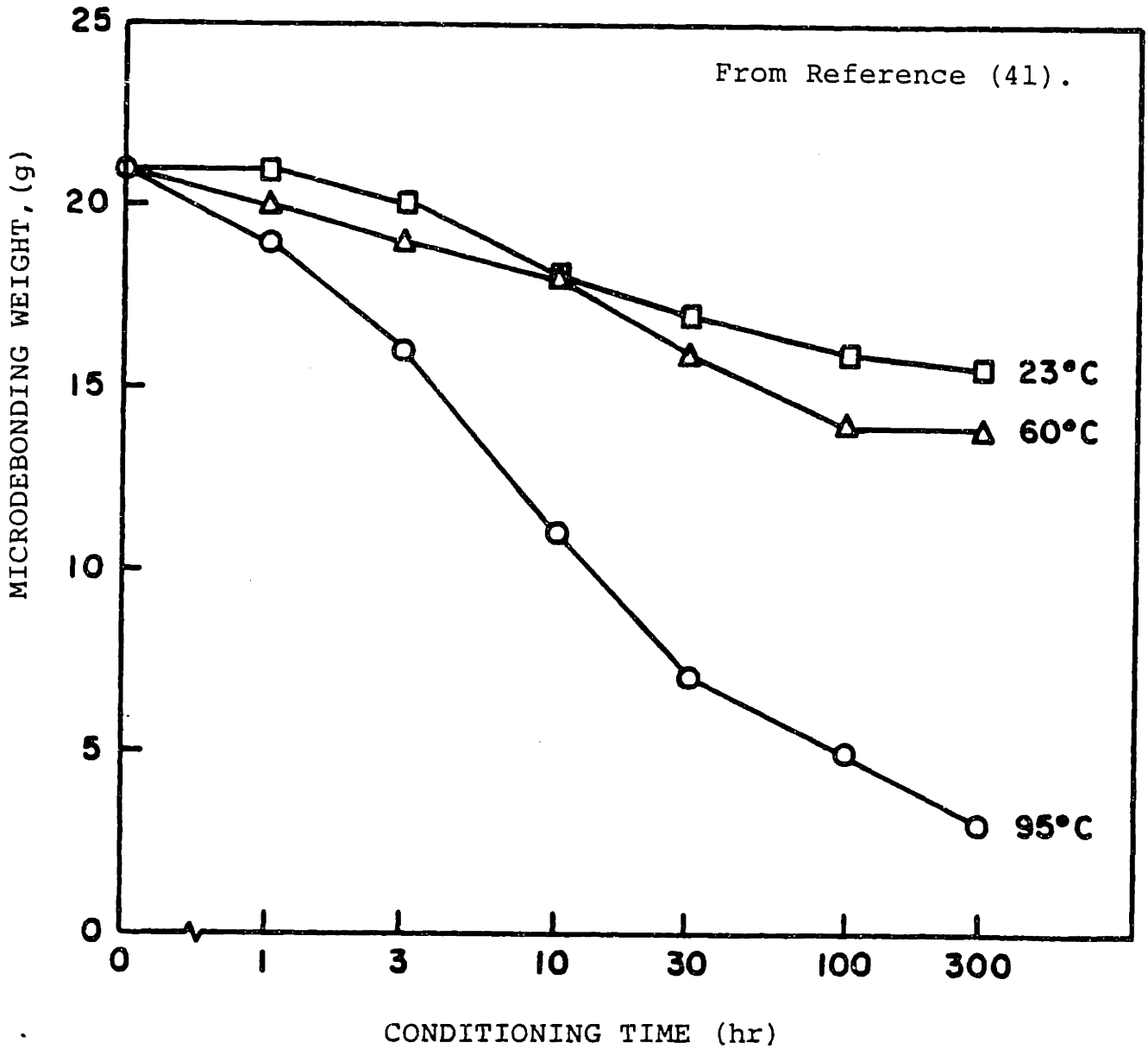

FIGURE 6 - MICRODEBONDING STRENGTH VS. CONDITIONING TIME IN WATER AT VARIOUS TEMPERATURES FOR GLASS/EPOXY, OBTAINED WITH SINGLE FIBER LOADINGS USING MODIFIED VICKERS APPARATUS.

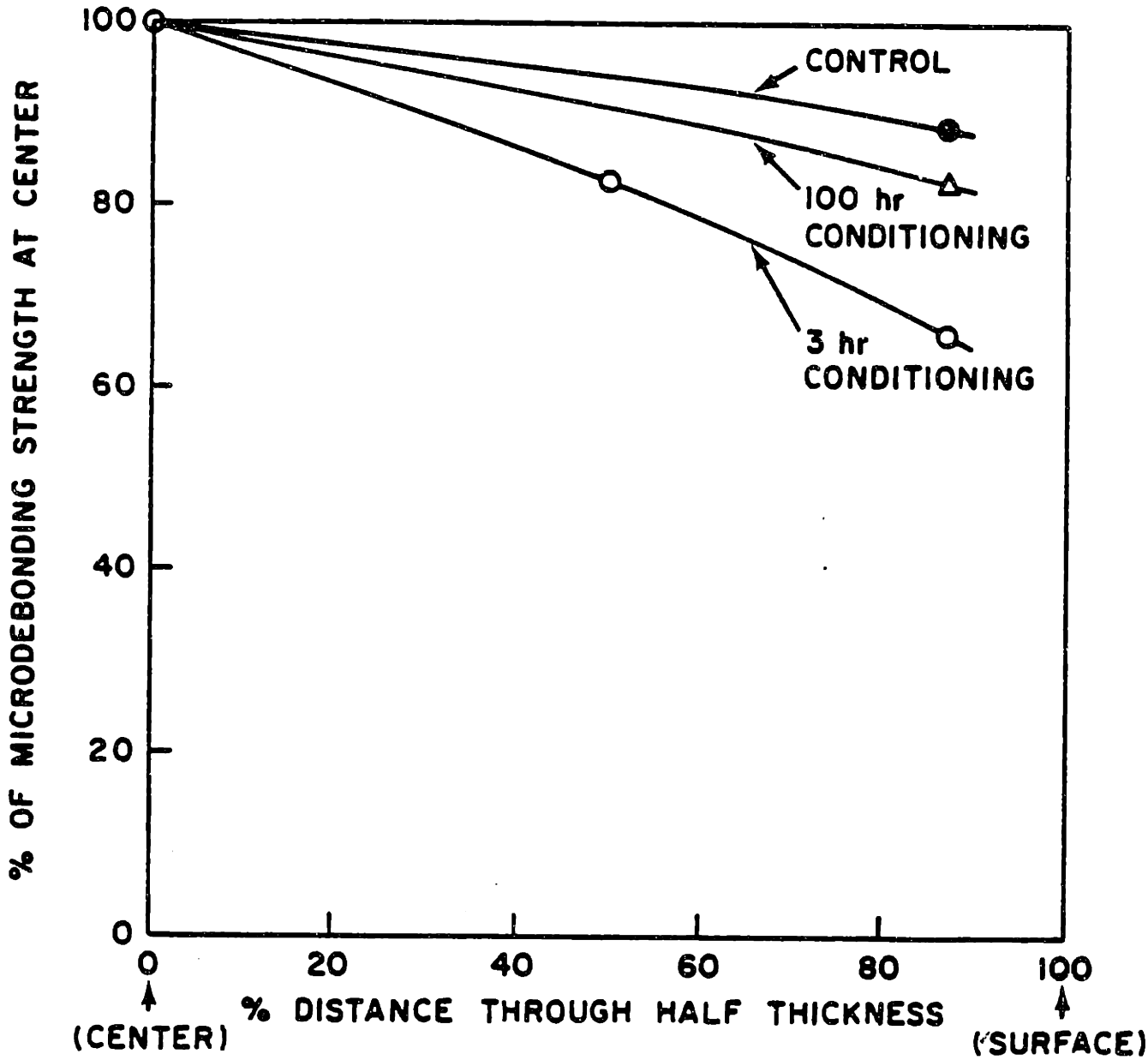

From Reference (41).

FIGURE 7.

MICRODEBONDING STRENGTH vs. DISTANCE THROUGH THICKNESS FOR CONDITIONING IN 95°C WATER.

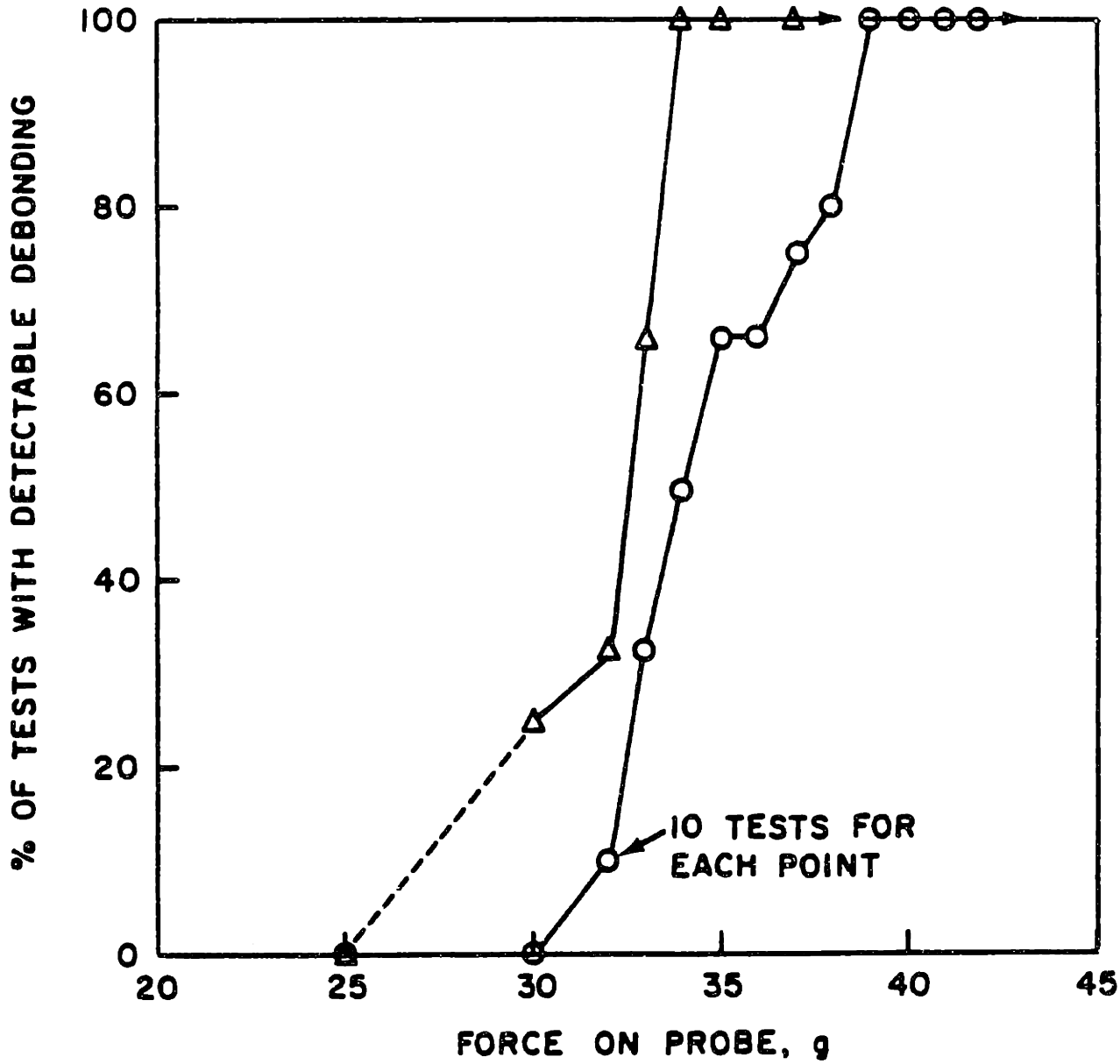

From Reference (41).

FIGURE 8

MICRODEBONDING DATA SHOWING INCONSISTENCIES IN RESULTS OBTAINED USING THE MODIFIED VICKERS APPARATUS DUE TO REPOSITIONING.

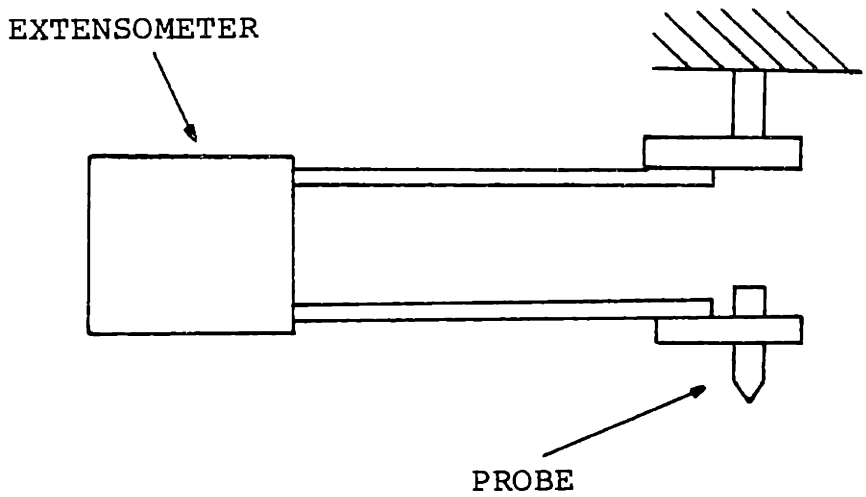

FIGURE 9

SCHEMATIC OF PROBE MECHANISM OF THE PHASE II APPARATUS - FIRST CONFIGURATION UTILIZING EXTENSOMETER

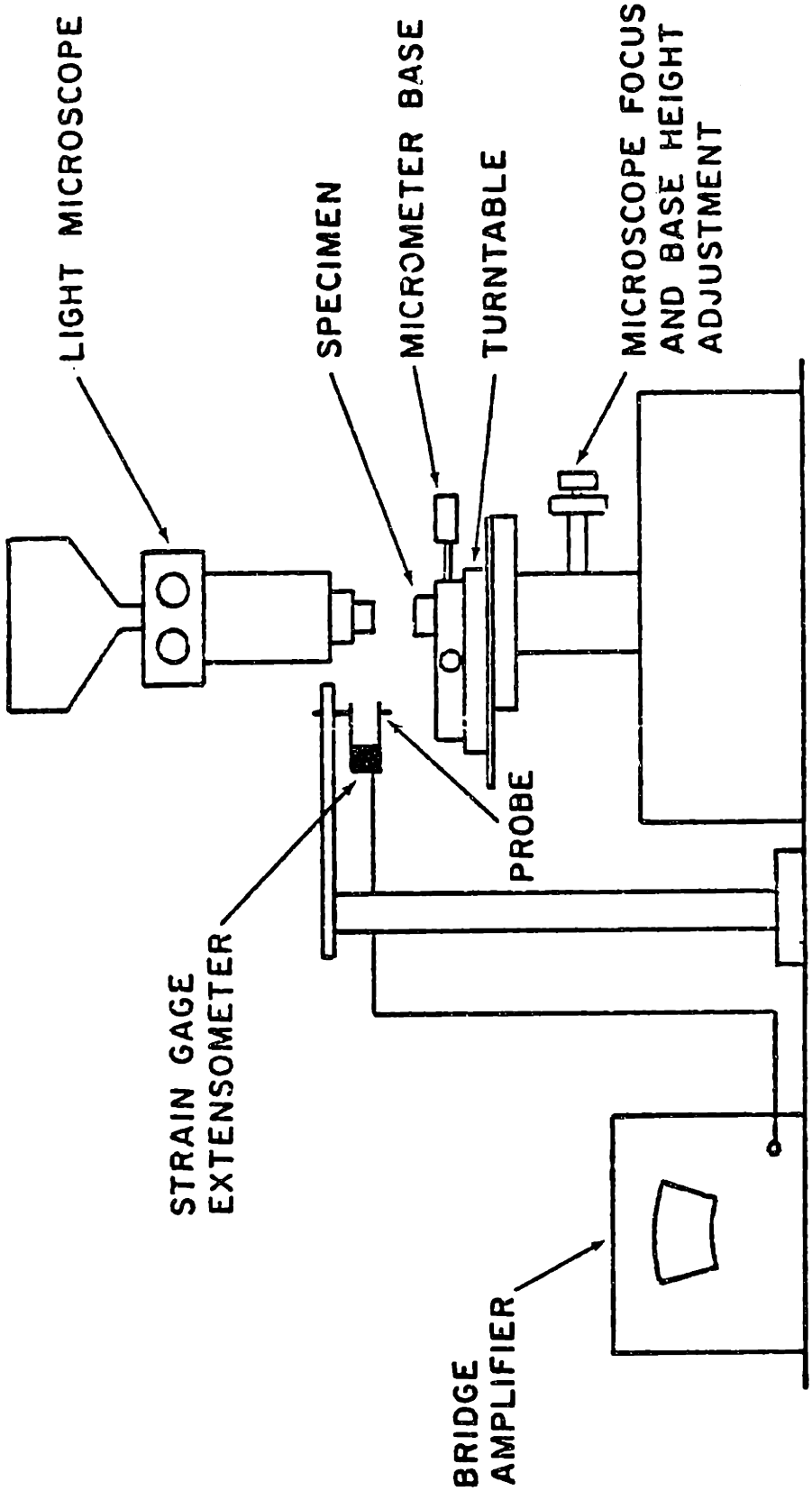

From Reference (42).

FIGURE 10

SCHEMATIC OF SINGLE FIBER MICRODEBONDING TEST APPARATUS.

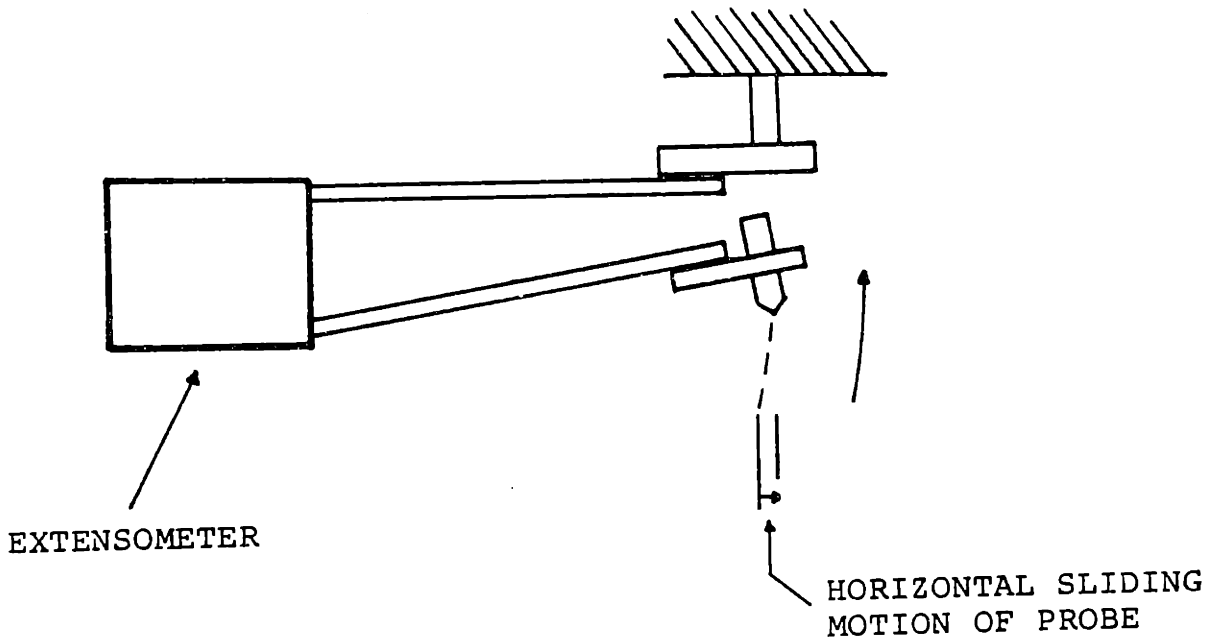

FIGURE 11

SCHEMATIC SHOWING PROBE MOTION RESPONSIBLE FOR HORIZONTAL SLIDING OF PROBE DURING LOADING WITH PHASE II PROBE MECHANISM

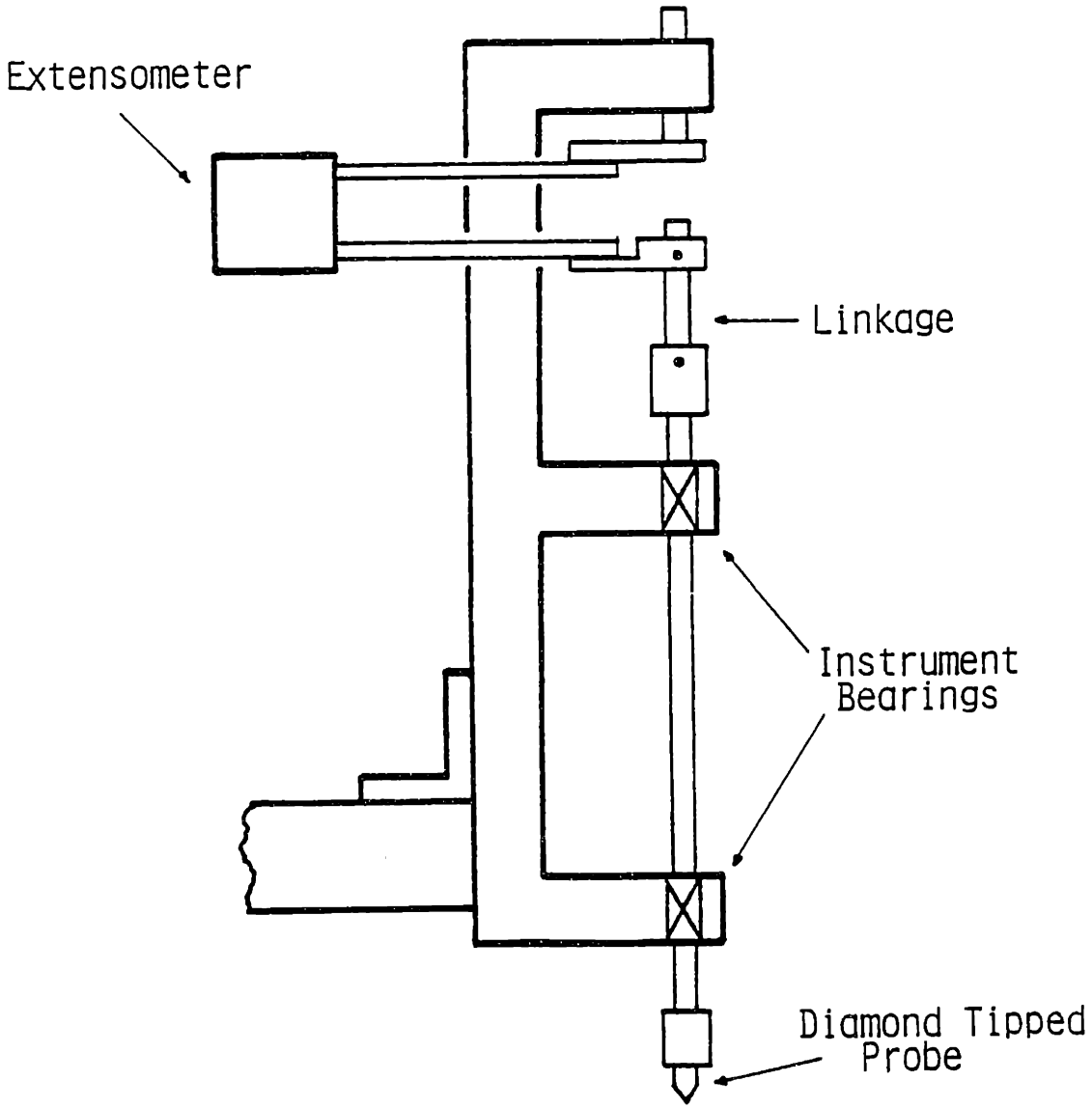

FIGURE 12

SCHEMATIC OF LINEAR TRAVEL PROBE MECHANISM

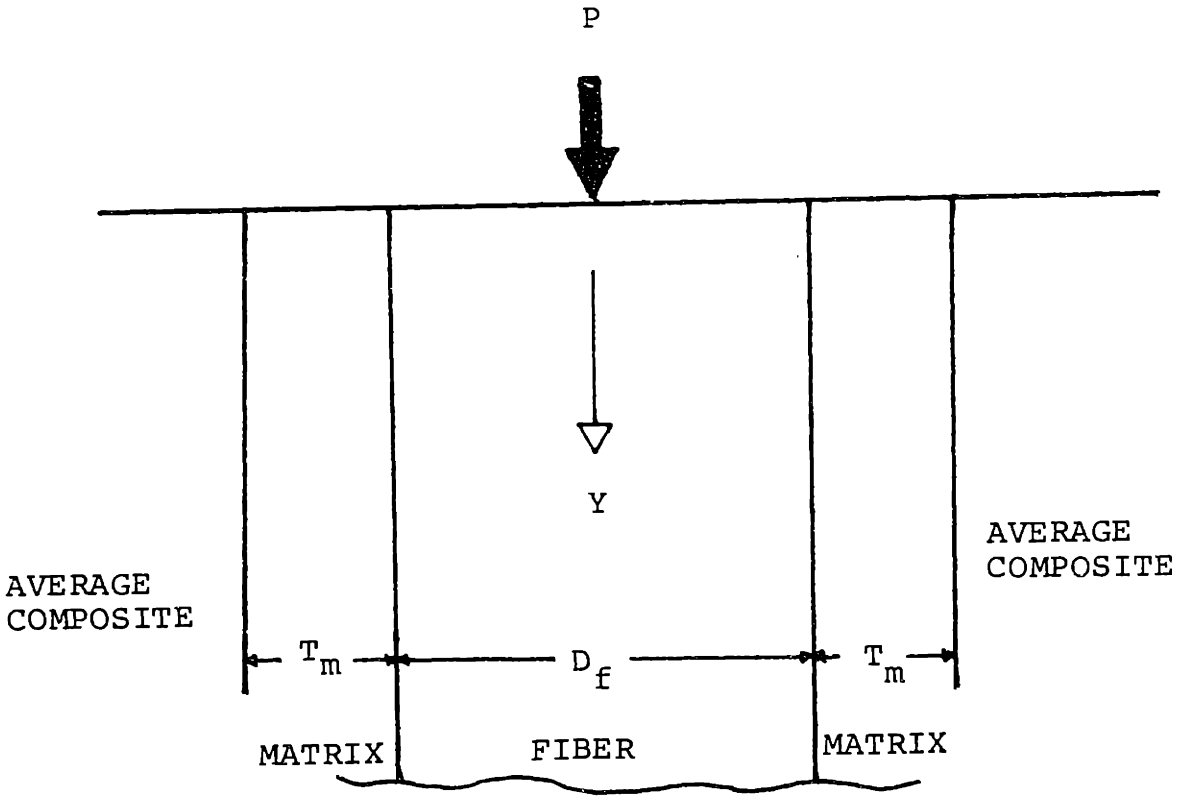

FIGURE 13

SCHEMATIC OF MICRODEBONDING GEOMETRY USED FOR FINITE ELEMENT MODEL.

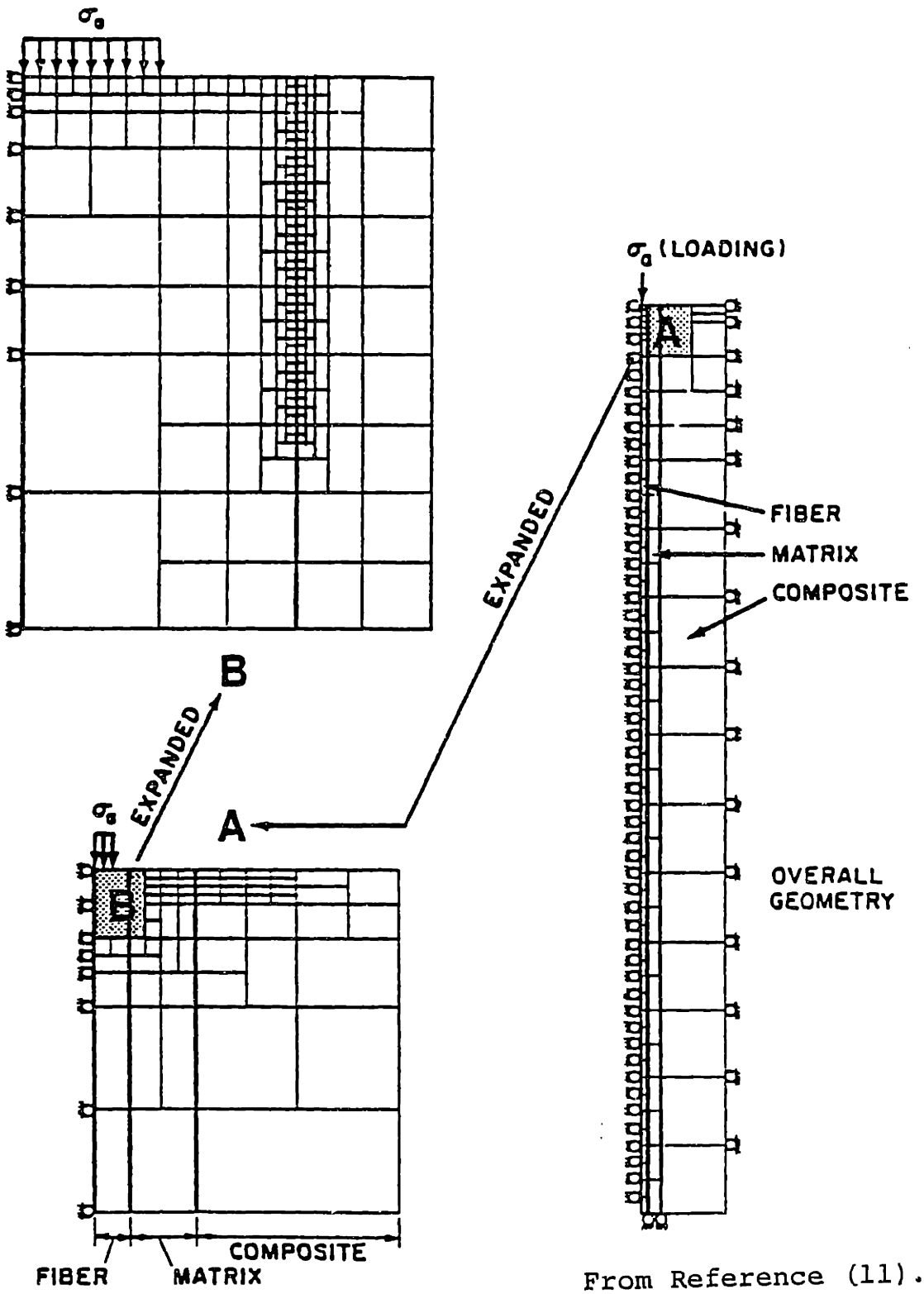

From Reference (11).

Fig.14 Finite Element Mesh of Single Fiber Model Subjected to Bearing Load.

S-GLASS/EPOXY
$(G_m/E_f)^{1/2} = 0.1109$
$T_m/D_f = 0.40$
$A_\sigma/A_f = 0.25$

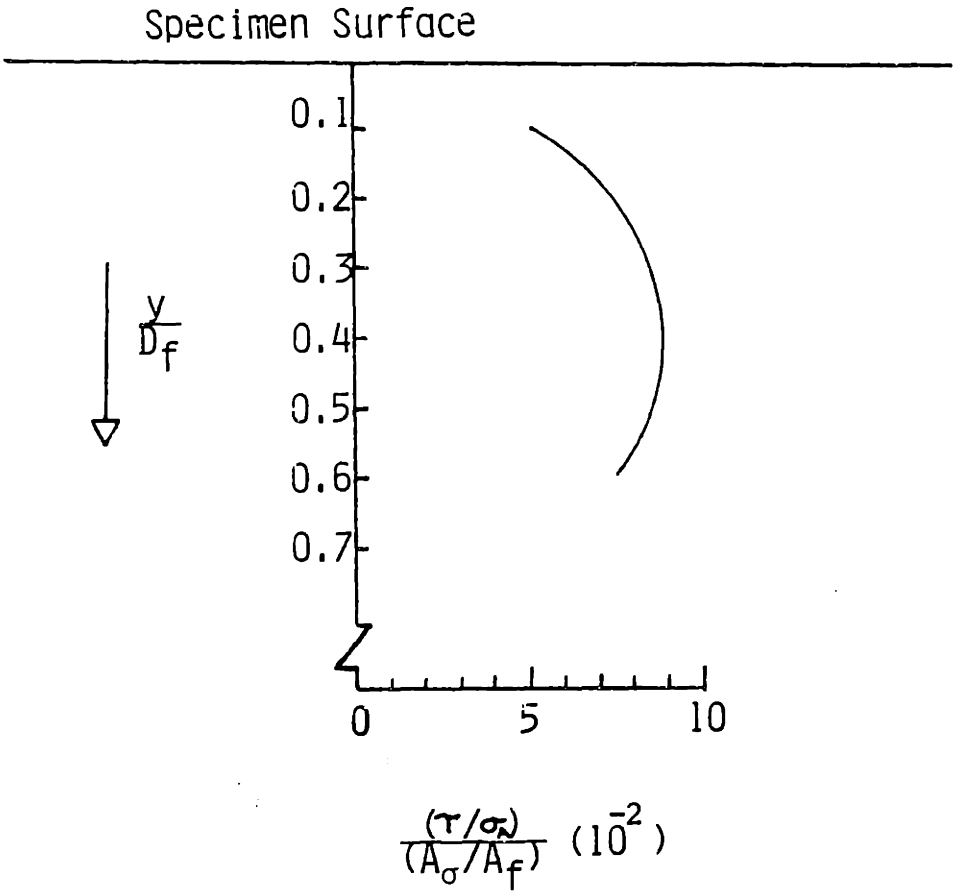

FIGURE 15 - TYPICAL SHEAR STRESS DISTRIBUTION OBTAINED FROM FINITE ELEMENT ANALYSIS.

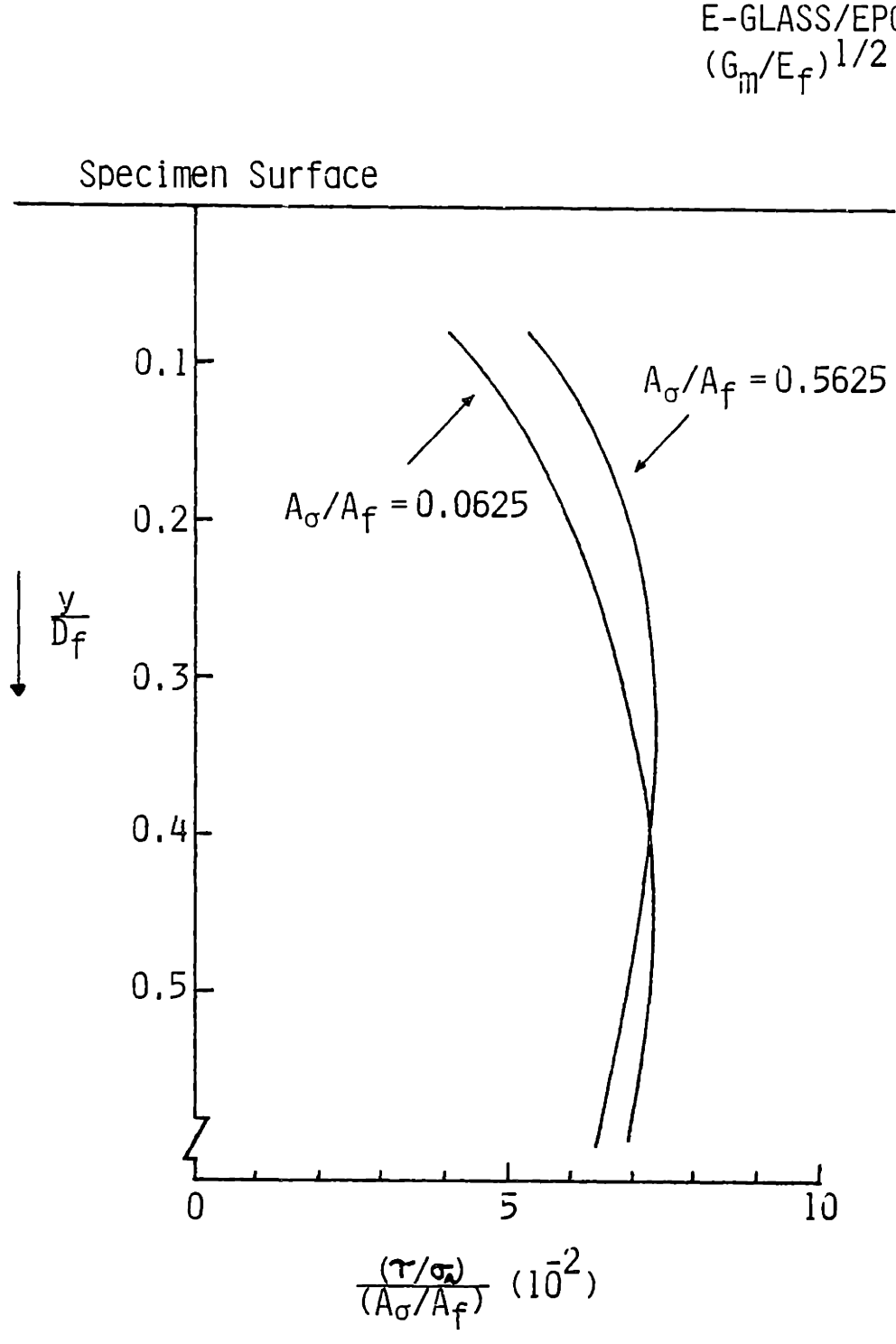

FIGURE 16

SHEAR STRESS DISTRIBUTIONS FOR E-GLASS/EPOXY
FOR DIFFERENT CONTACT AREAS OF LOADING

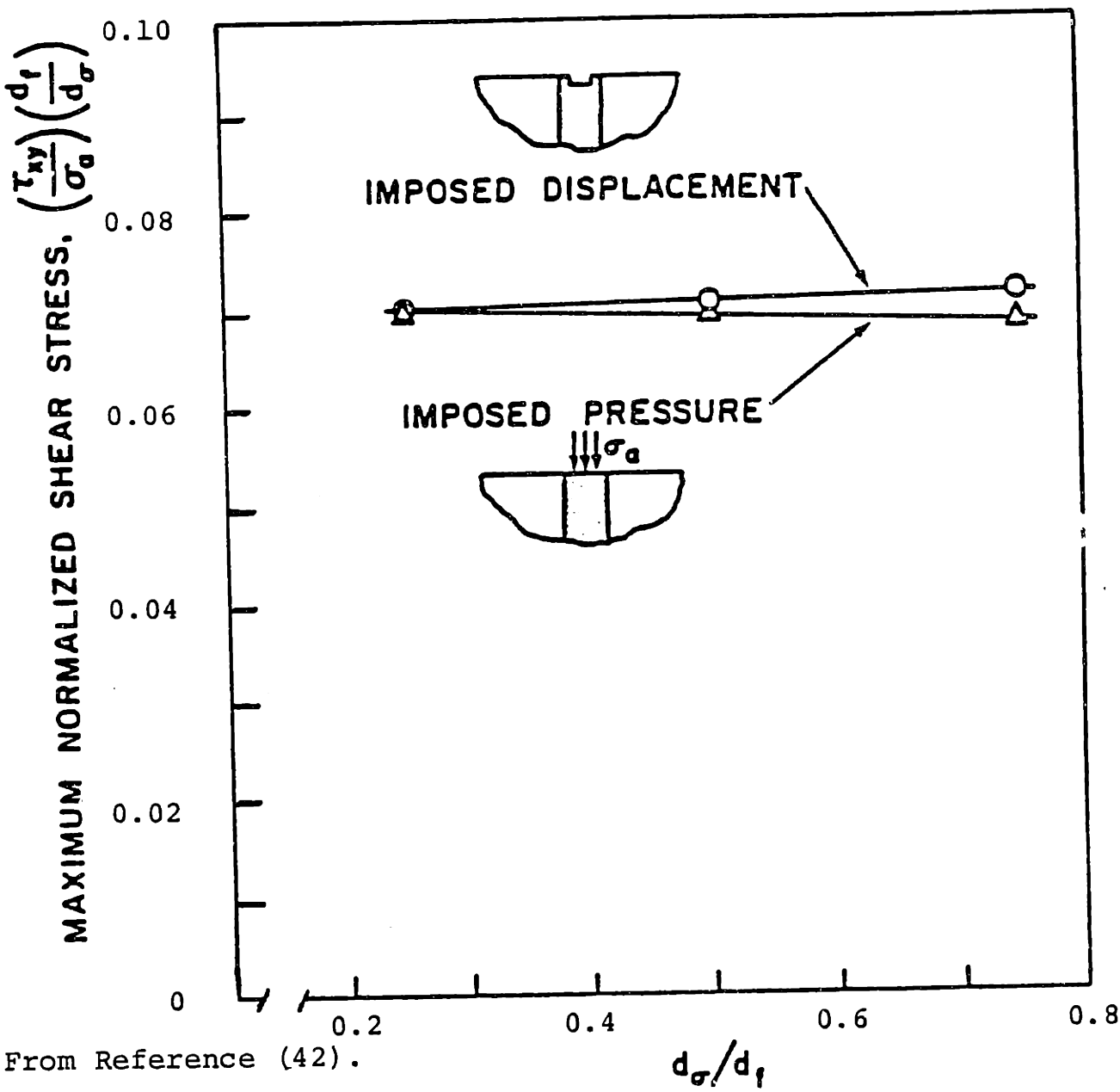

From Reference (42).

FIGURE 17

NORMALIZED MAXIMUM SHEAR STRESS AT INTERFACE vs. TYPE OF LOADING AND FRACTION OF FIBER LOADED, $(G_m/E_f)^{1/2}=0.124$.

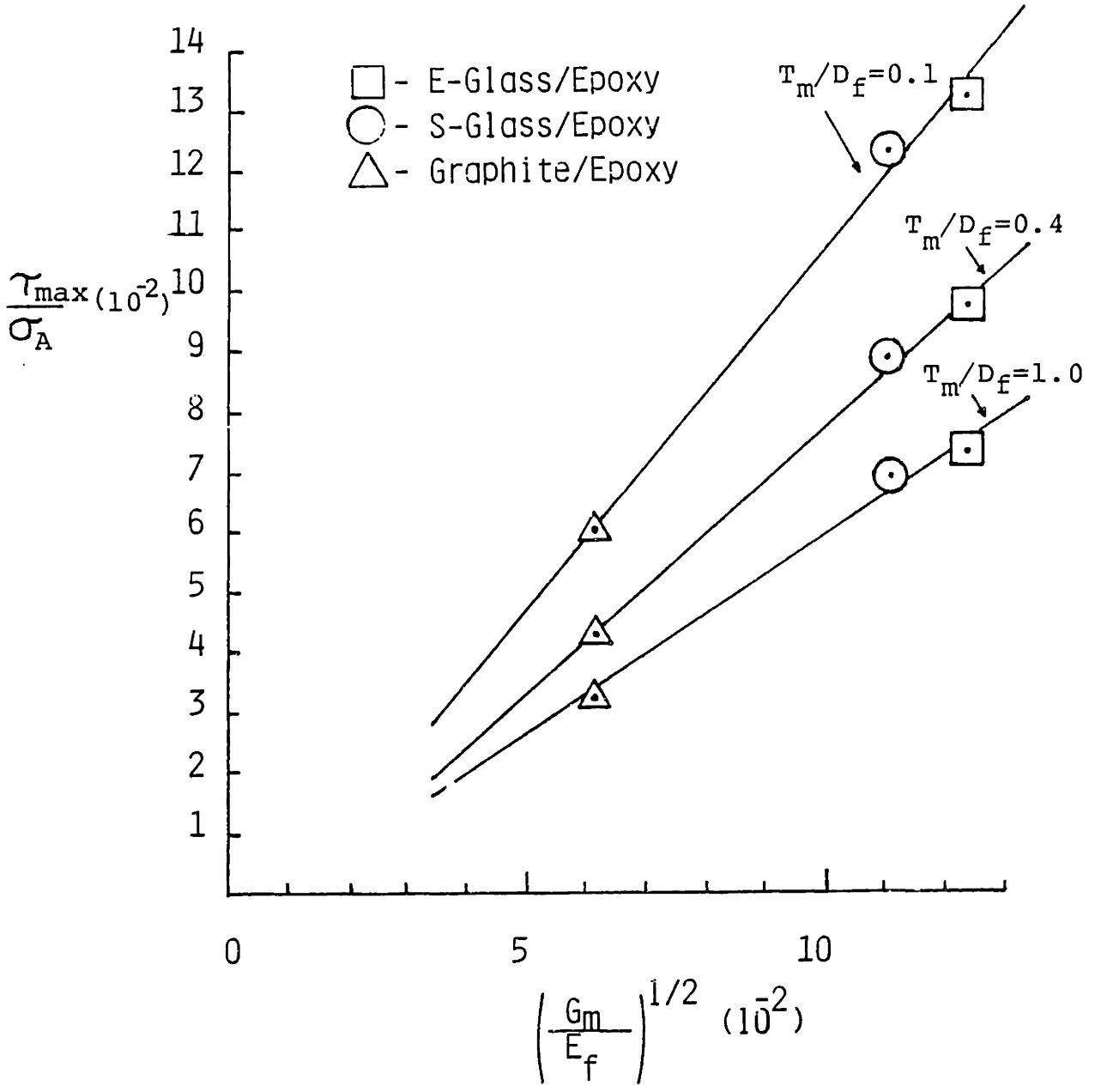

FIGURE 18

VARIATION OF NORMALIZED MAXIMUM SHEAR STRESS WITH $(G_m/E_f)^{1/2}$

$$\frac{T_m}{D_f} = 0.40$$

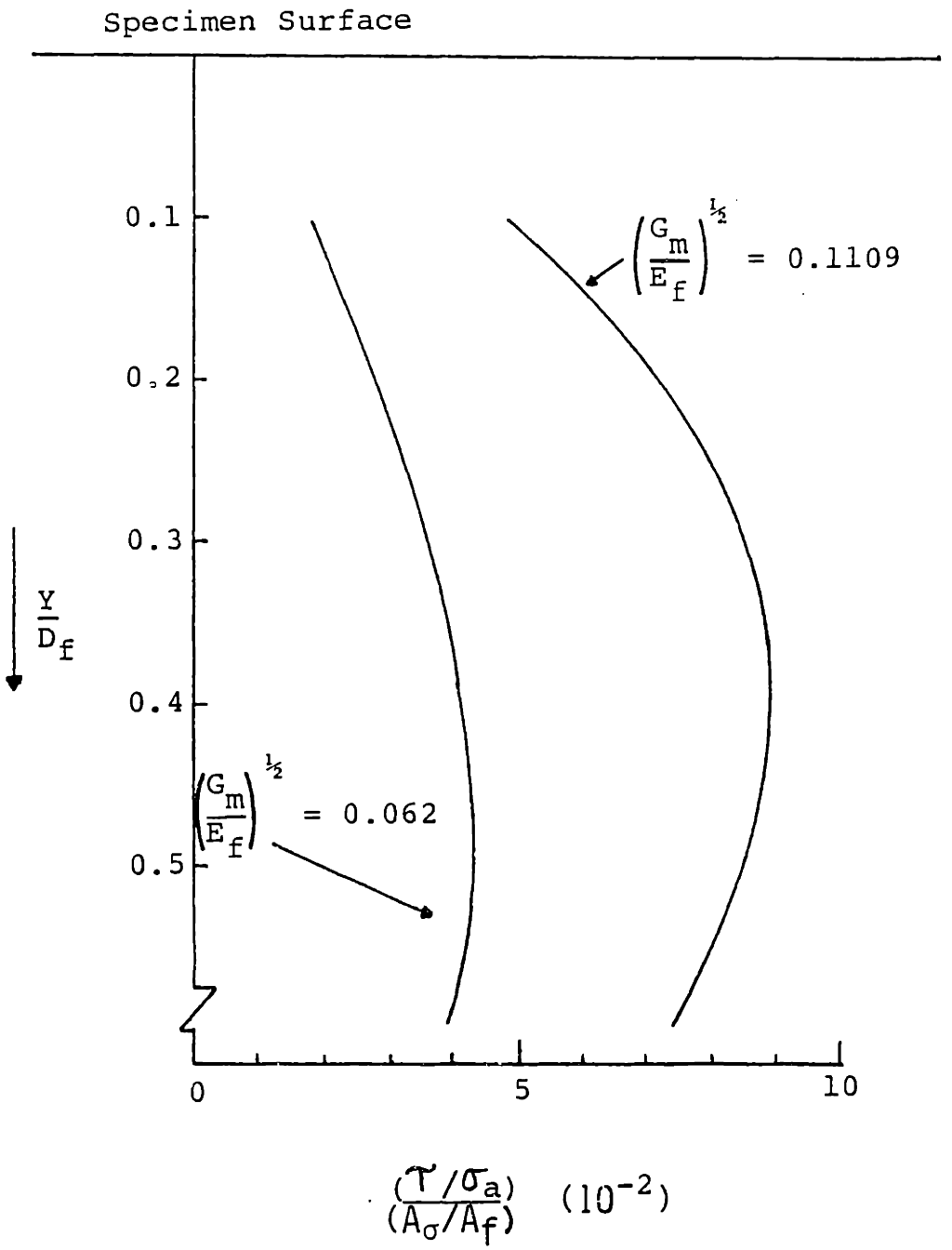

Figure 19. Variation of Normalized Shear Stress Distribution for Different Values of $(G_m/E_f)^{\frac{1}{2}}$.

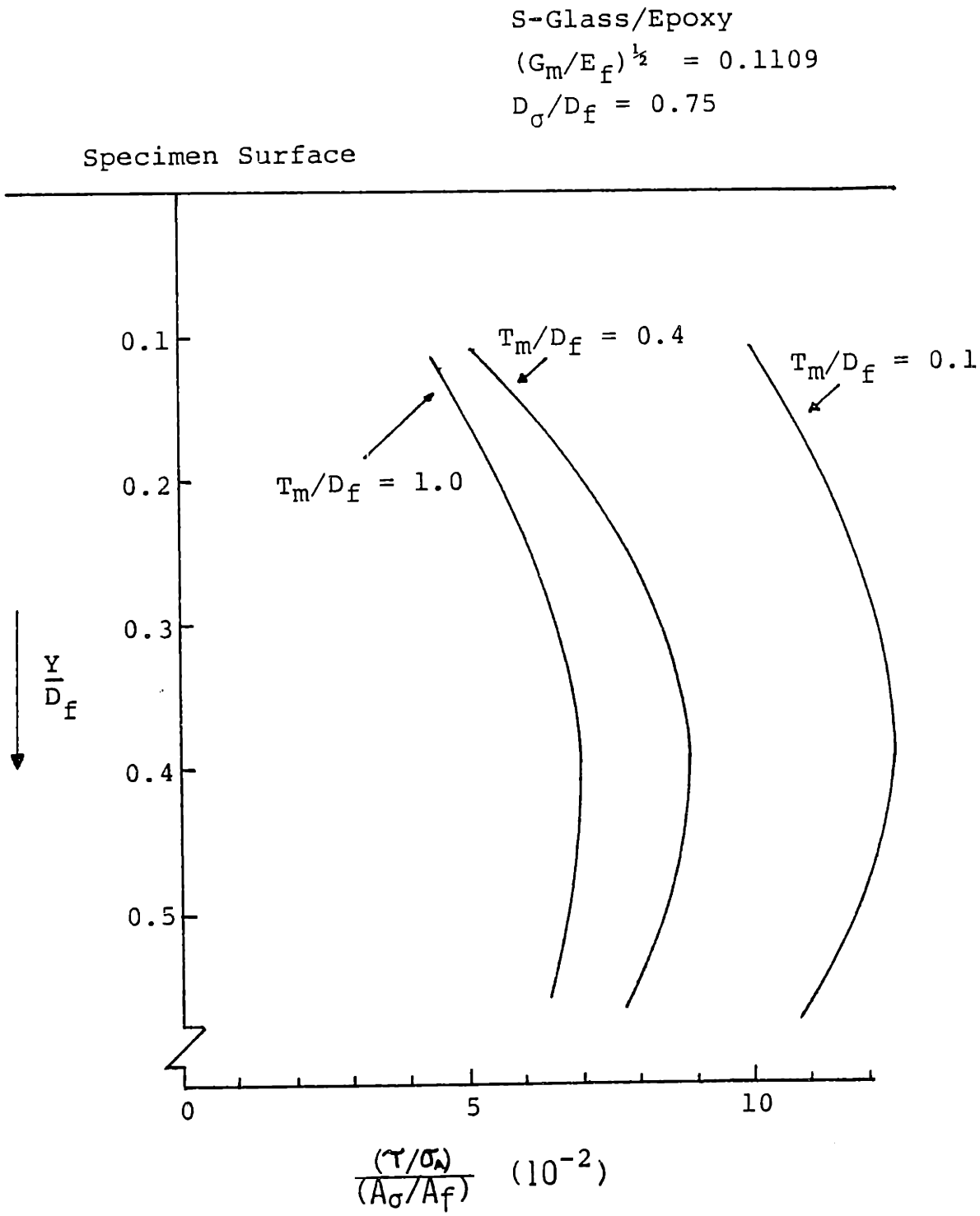

Figure 20. Normalized Shear Stress Distributions for Varying Fiber Spacing:Diameter Ratios, T_m/D_f.

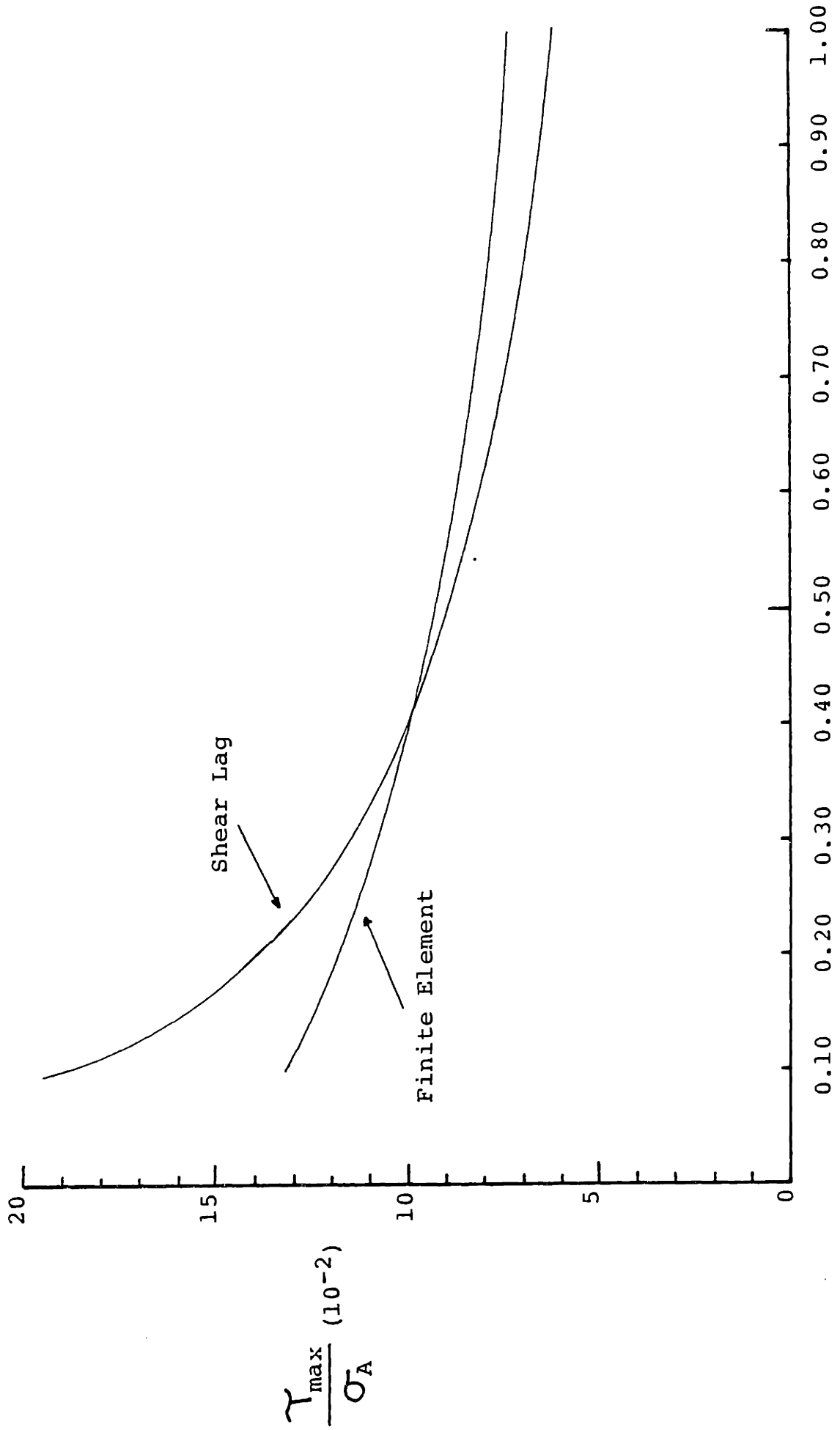

FIGURE 21 - NORMALIZED MAXIMUM SHEAR STRESS vs. T_m/D_f FOR E-GLASS/EPOXY.

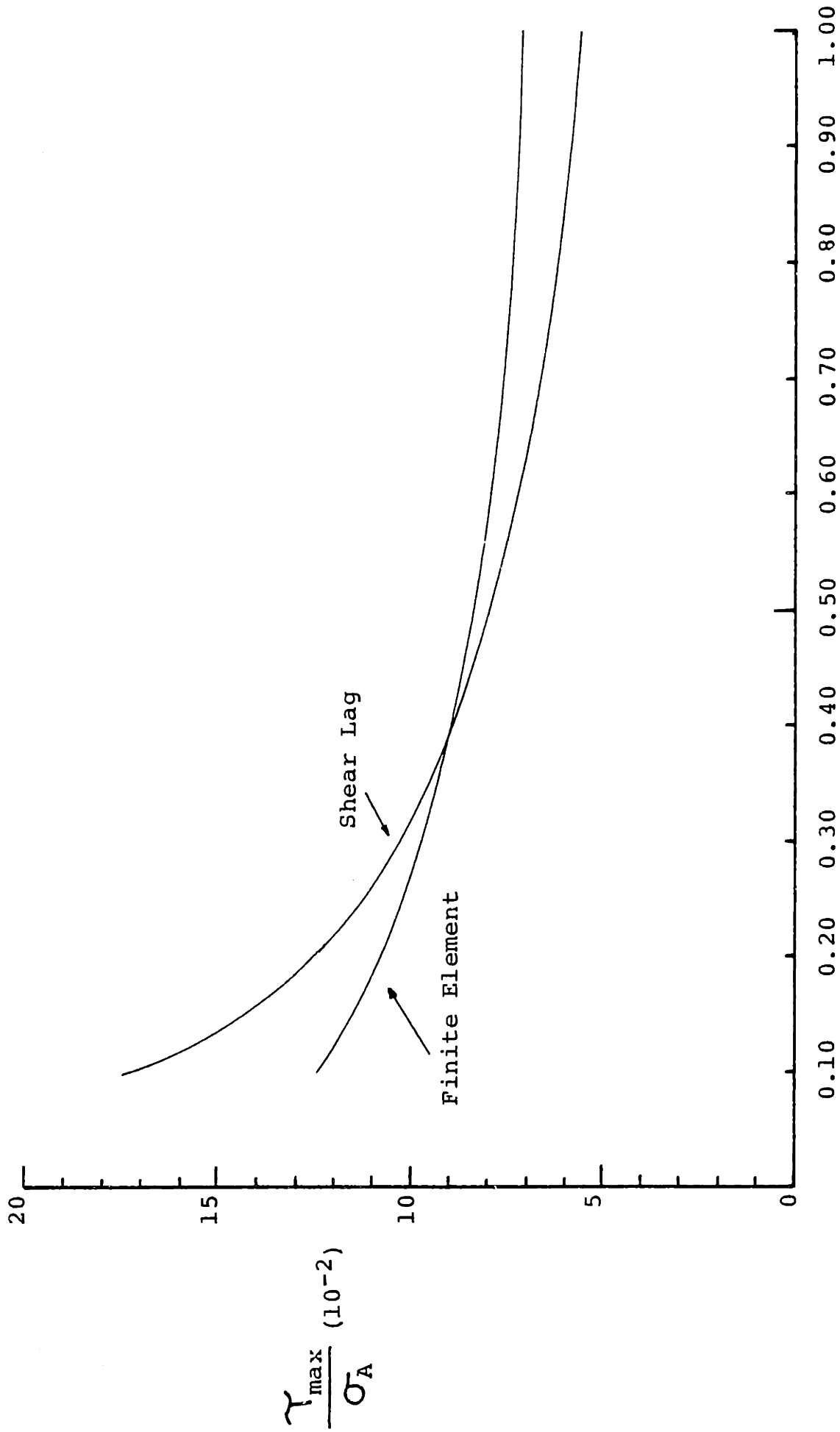

FIGURE 22 - NORMALIZED MAXIMUM SHEAR STRESS vs. T_m/D_f FOR S-GLASS/EPOXY.

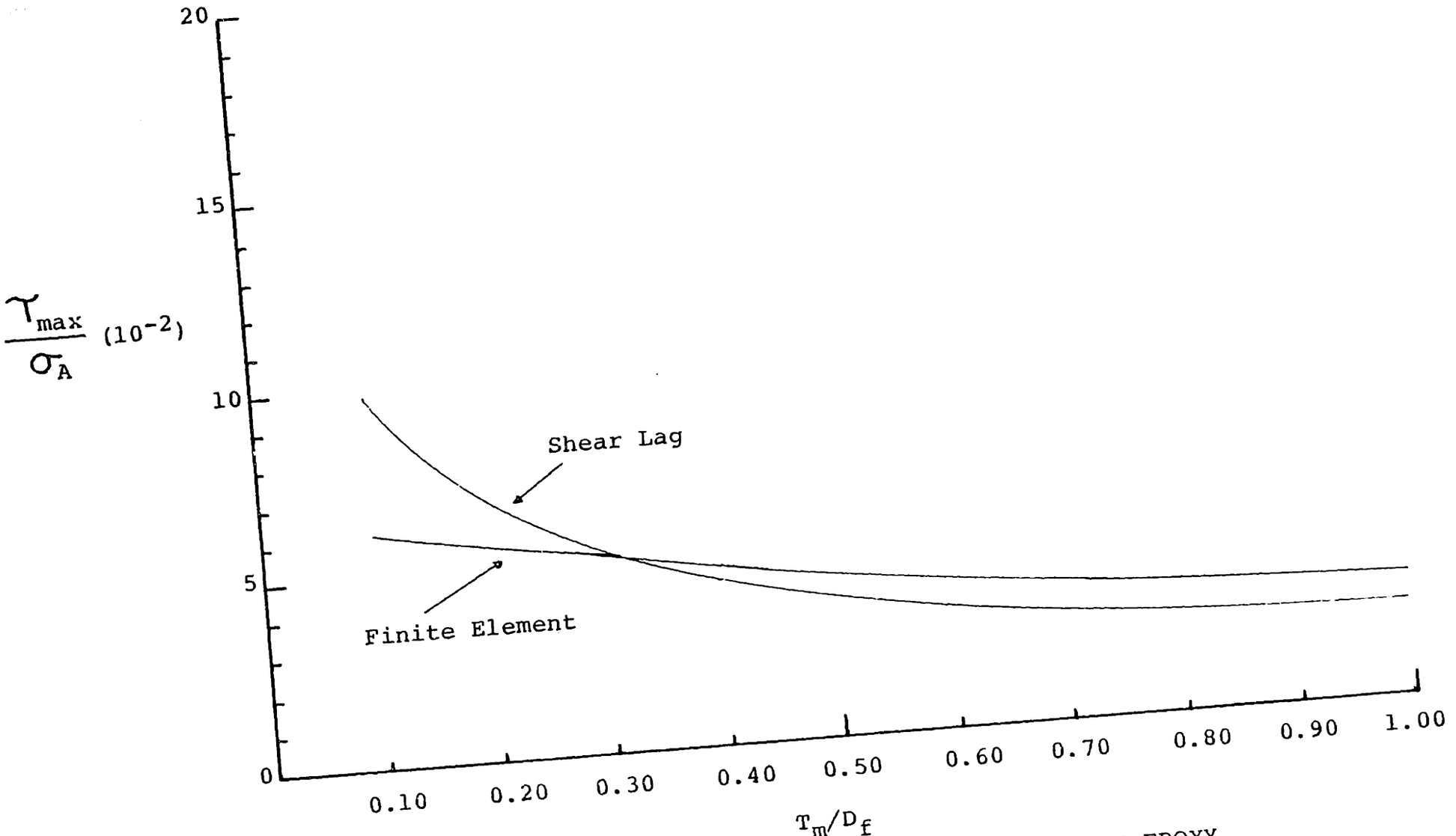

FIGURE 23 - NORMALIZED MAXIMUM SHEAR STRESS vs. T_m/D_f FOR GRAPHITE EPOXY.

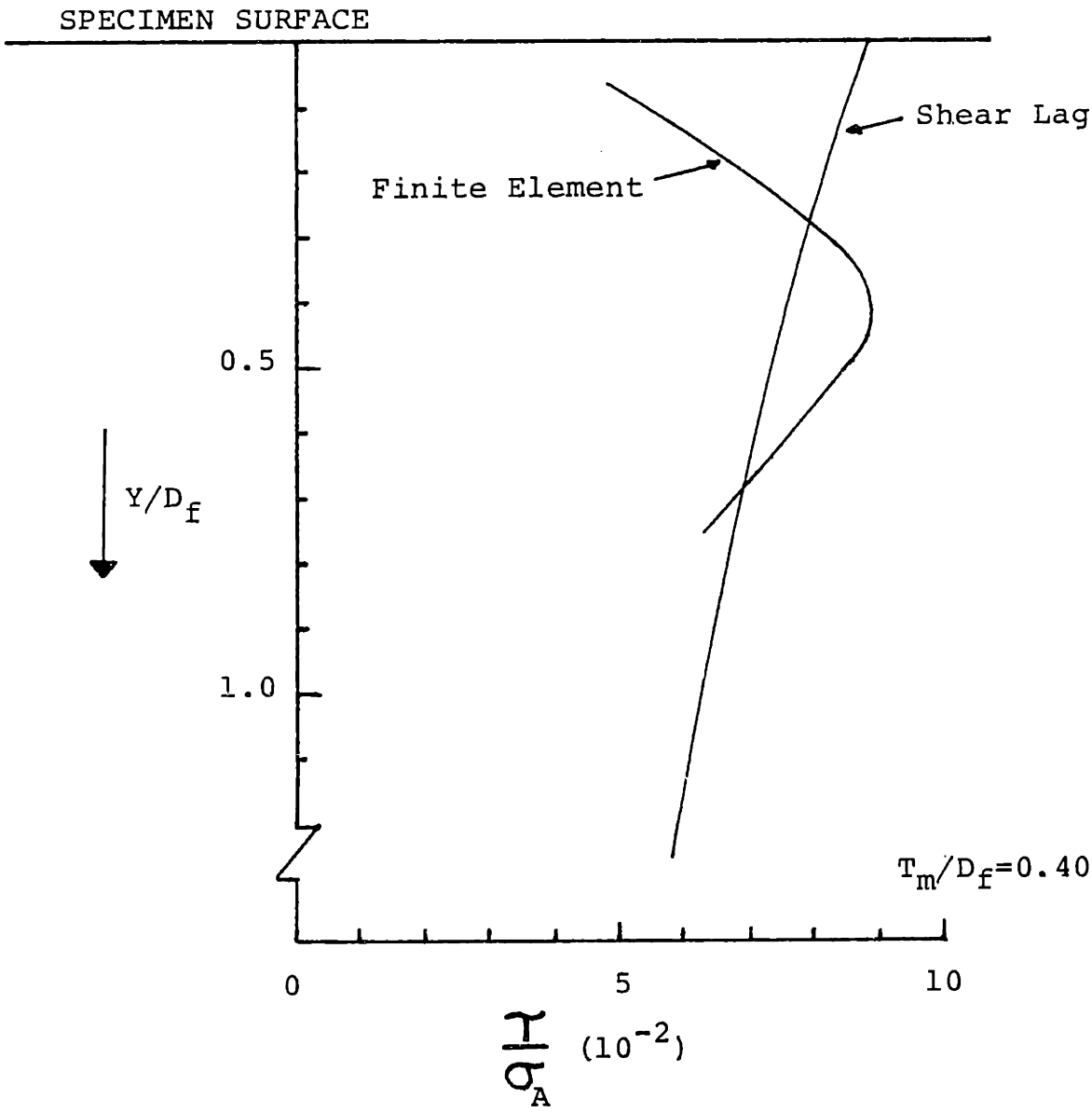

FIGURE 24 - COMPARISON BETWEEN SHEAR STRESS DISTRIBUTION PREDICTED BY FINITE ELEMENT ANALYSIS AND THAT PREDICTED BY SHEAR LAG MICROMECHANICS ANALYSIS FOR S-GLASS/EPOXY.

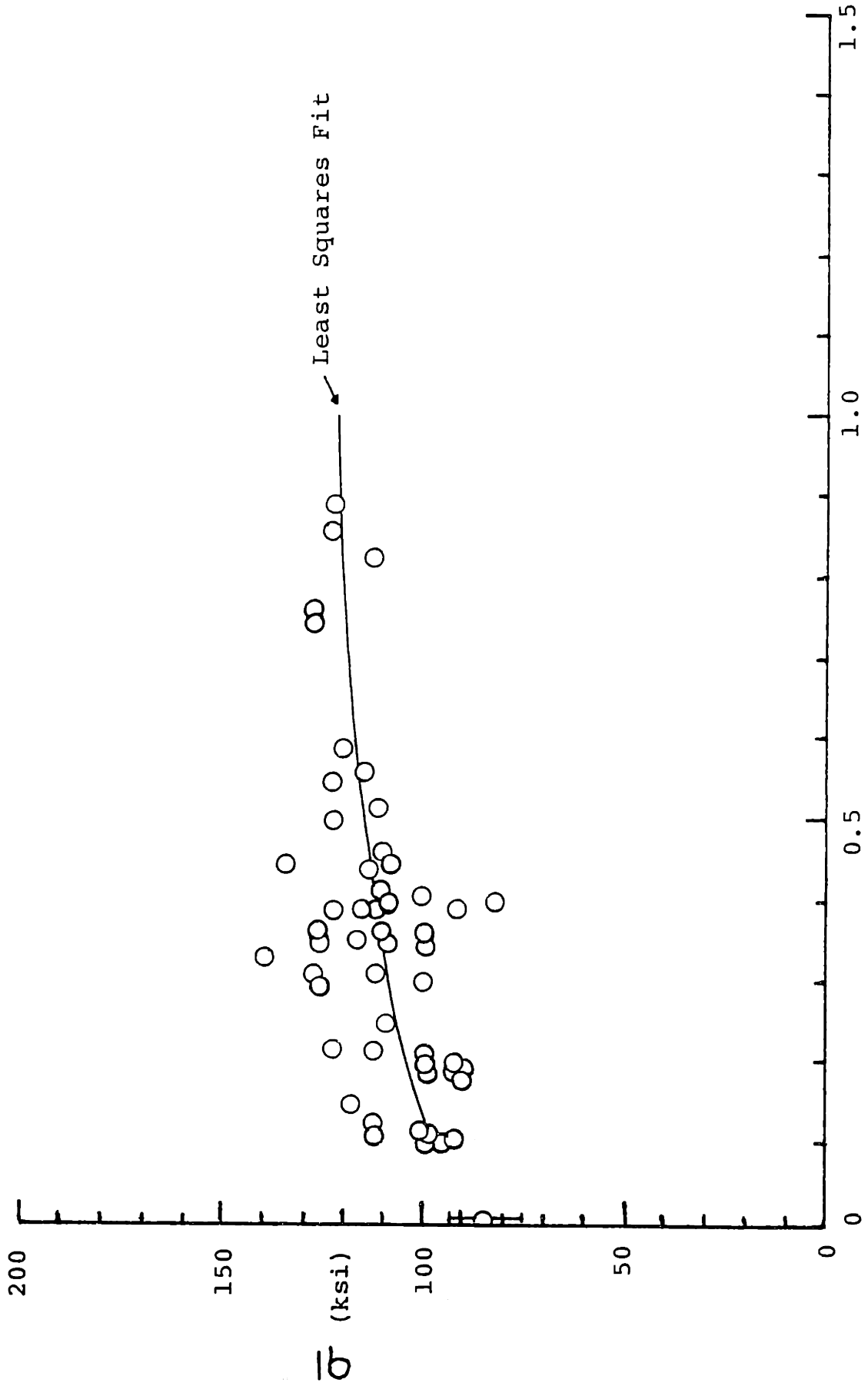

FIGURE 25 - MICRODEBONDING RESULTS AND LEAST SQUARES FIT OF DATA FOR SP250 463.

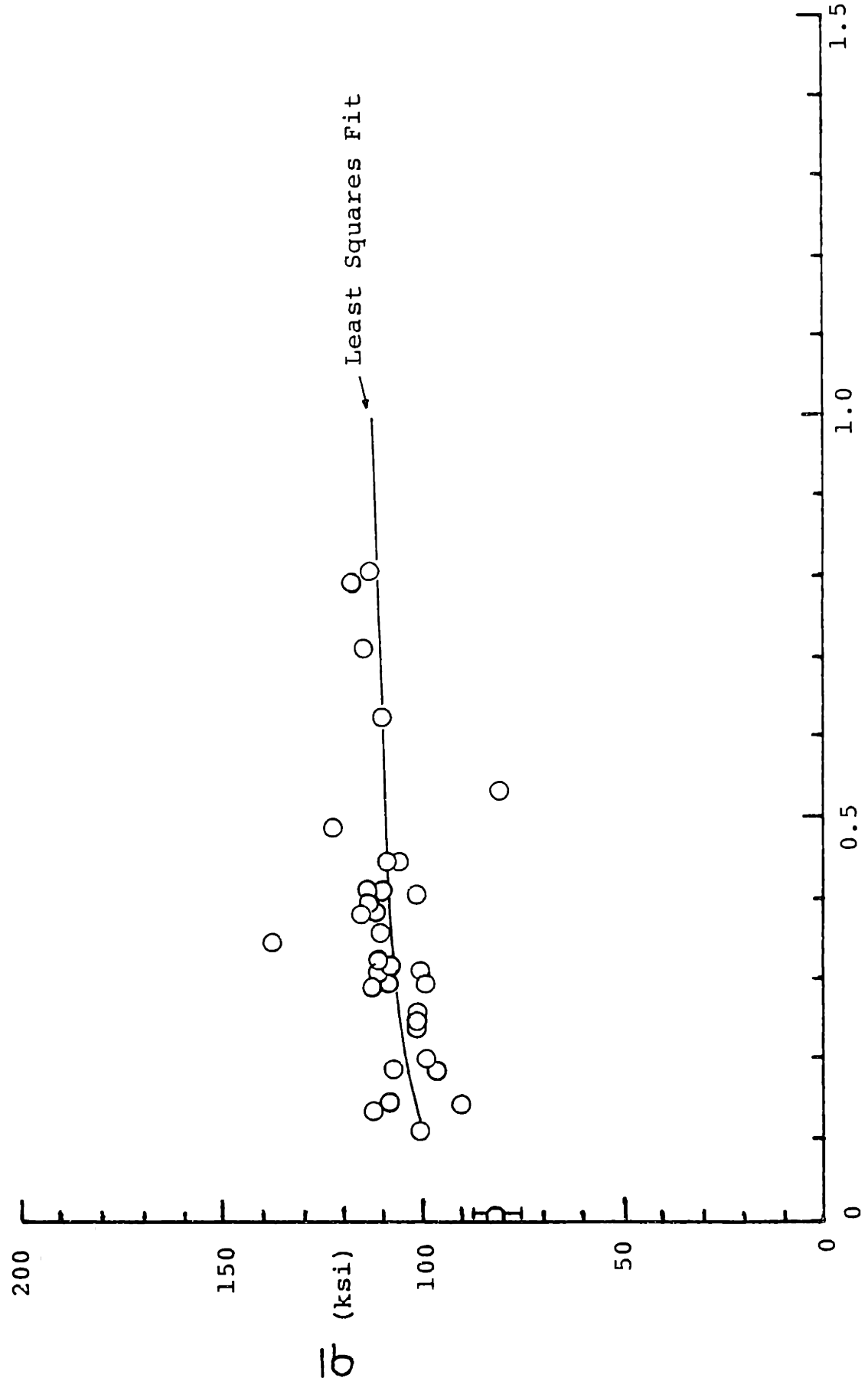

FIGURE 26 - MICRODEBONDING RESULTS AND LEAST SQUARES FIT OF DATA FOR SP250 449.

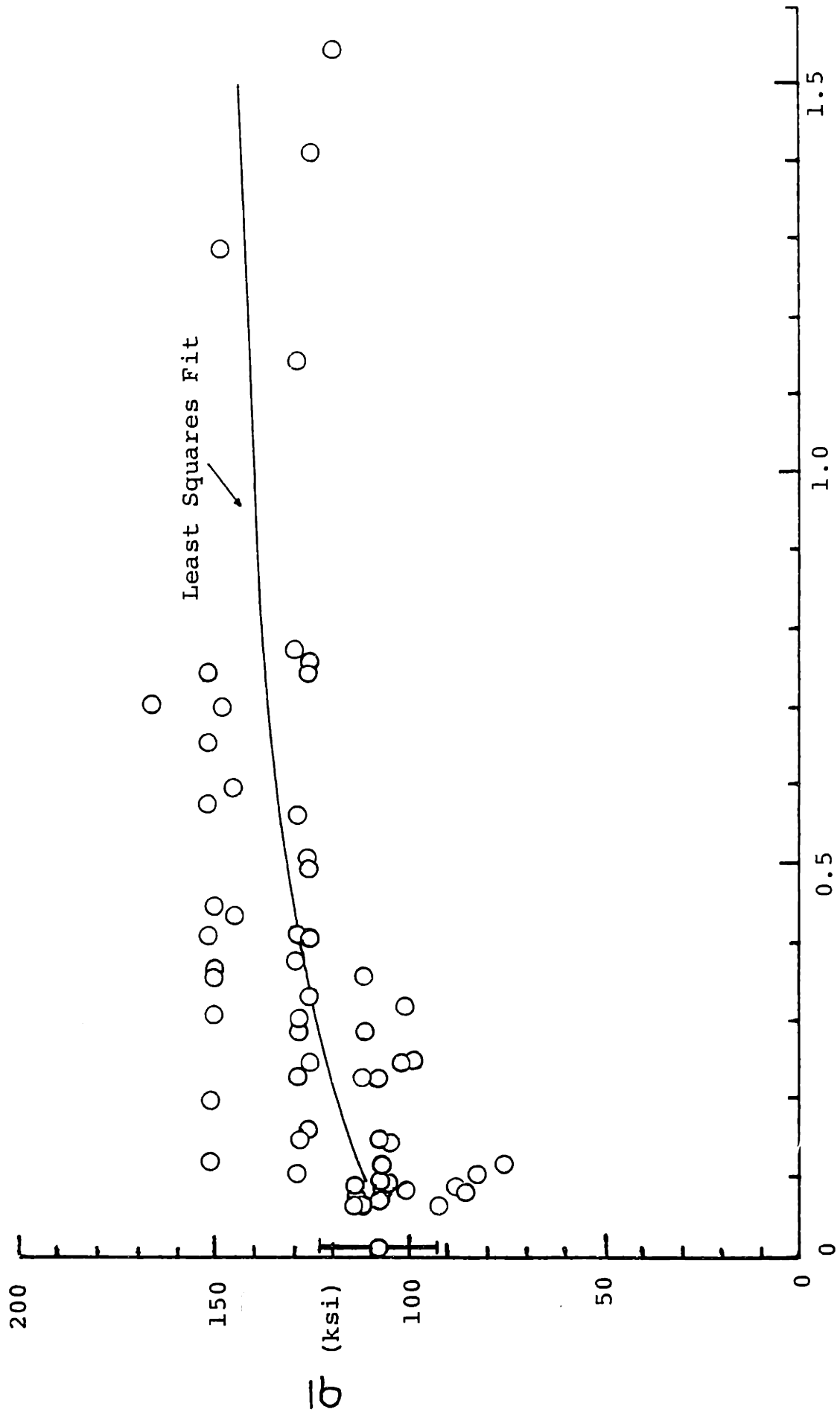

FIGURE 27 - MICRODEBONDING RESULTS AND LEAST SQUARES FIT OF DATA FOR C-CK-U.

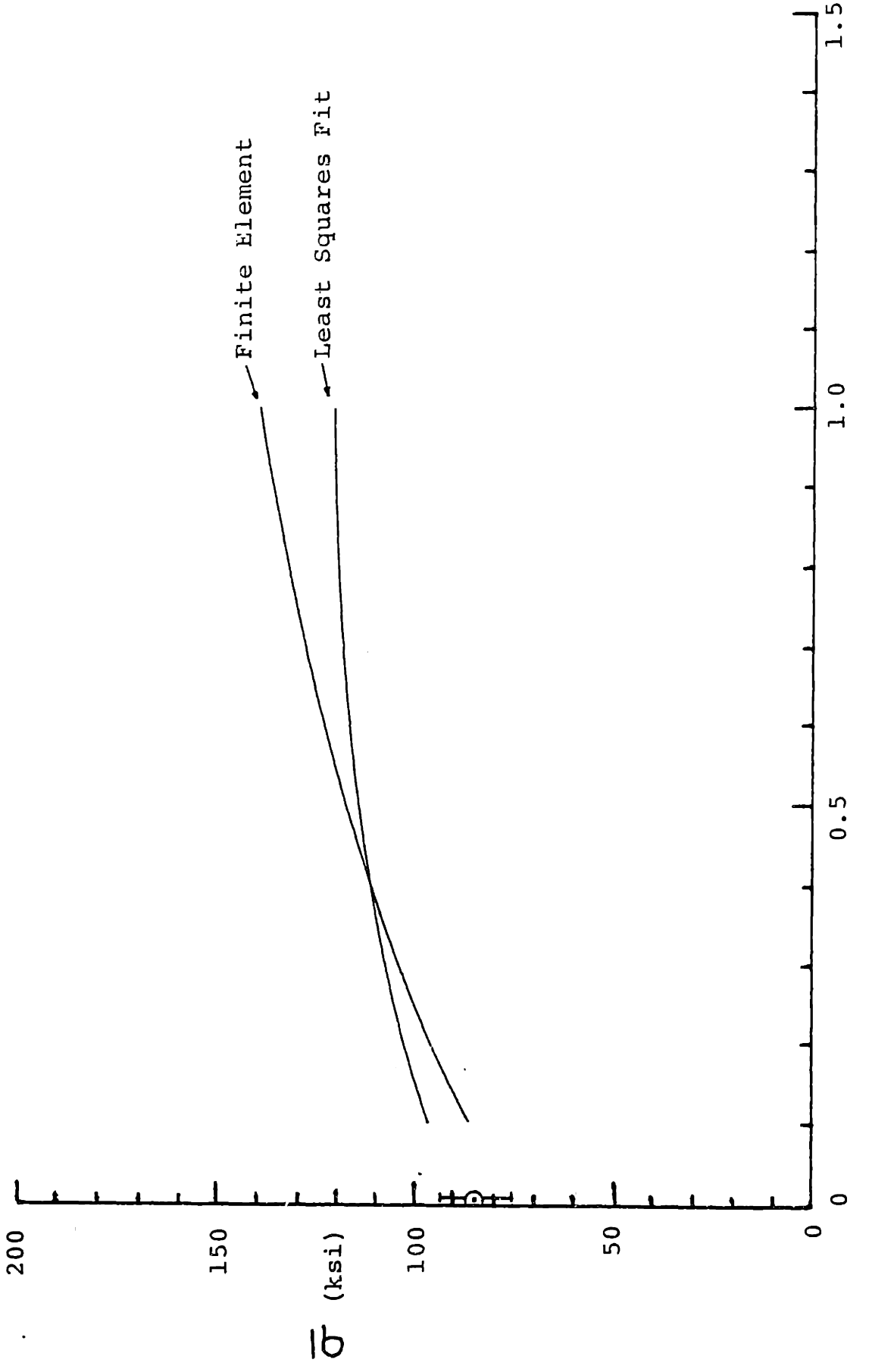

FIGURE 28 - LEAST SQUARES FIT OF MICRODEBONDING RESULTS AND PREDICTED BEHAVIOR BASED ON FINITE ELEMENT ANALYSIS FOR SP250 463.

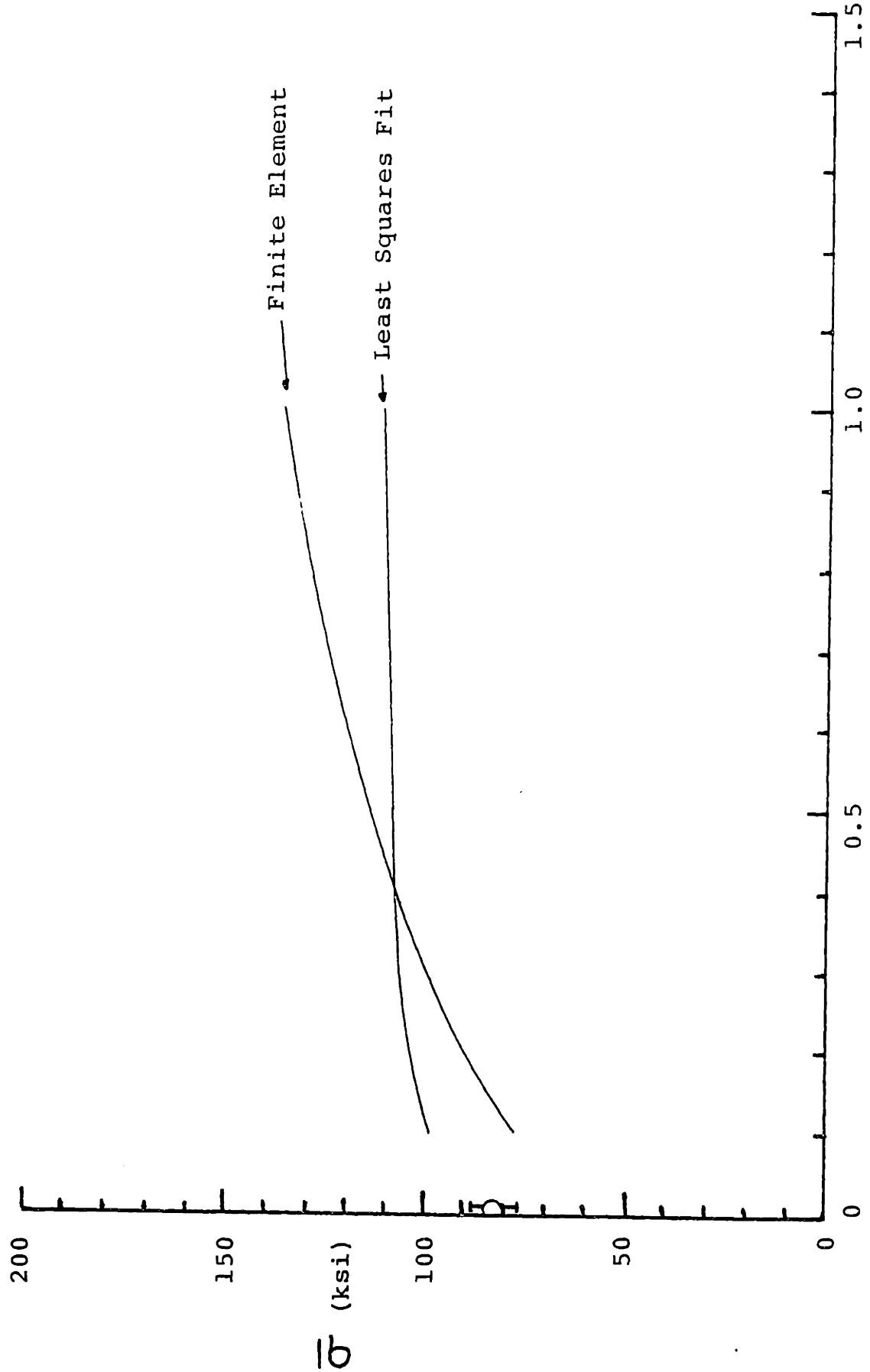

FIGURE 29 - LEAST SQUARES FIT OF MICRODEBONDING RESULTS AND PREDICTED BEHAVIOR BASED ON FINITE ELEMENT ANALYSIS FOR SP250 449.

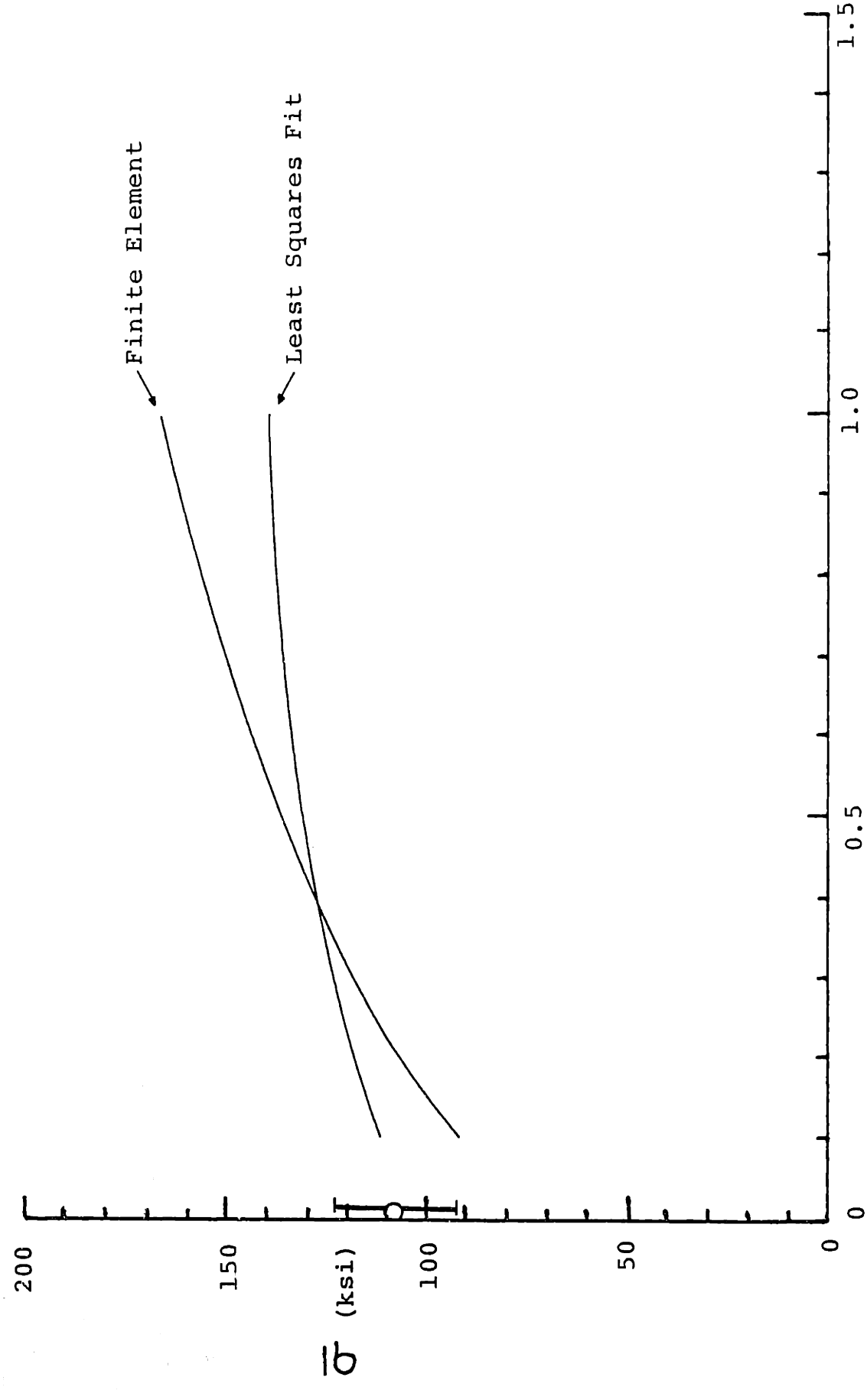

FIGURE 30 - LEAST SQUARES FIT OF MICRODEBONDING RESULTS AND PREDICTED BEHAVIOR BASED ON FINITE ELEMENT ANALYSIS FOR C-CK-U.

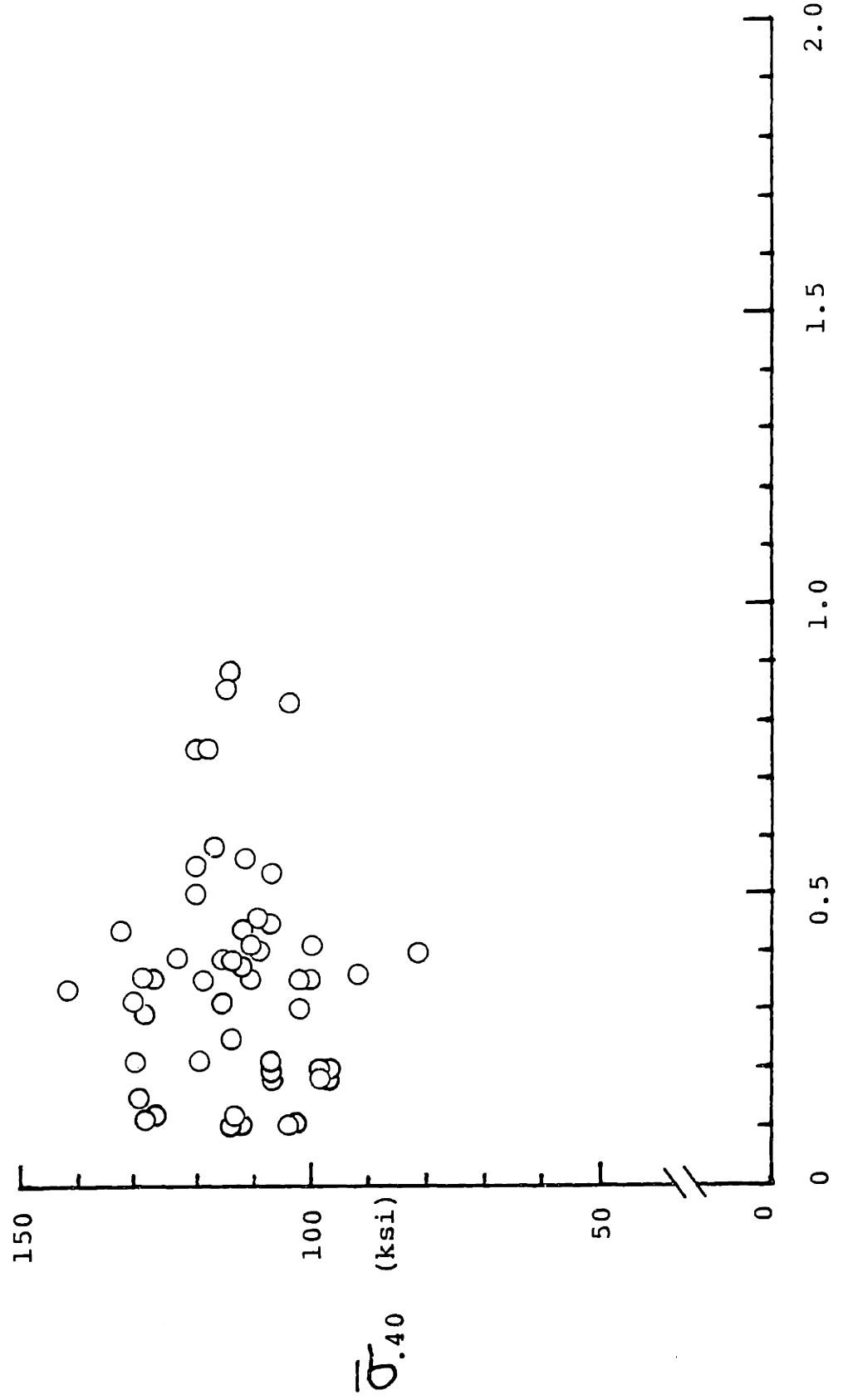

FIGURE 31 - VALUES OF $\bar{\sigma}_{.40}$, OBTAINED BY SHIFTING EXPERIMENTAL DATA, vs. T_m/D_f FOR SPECIMEN SP250 463.

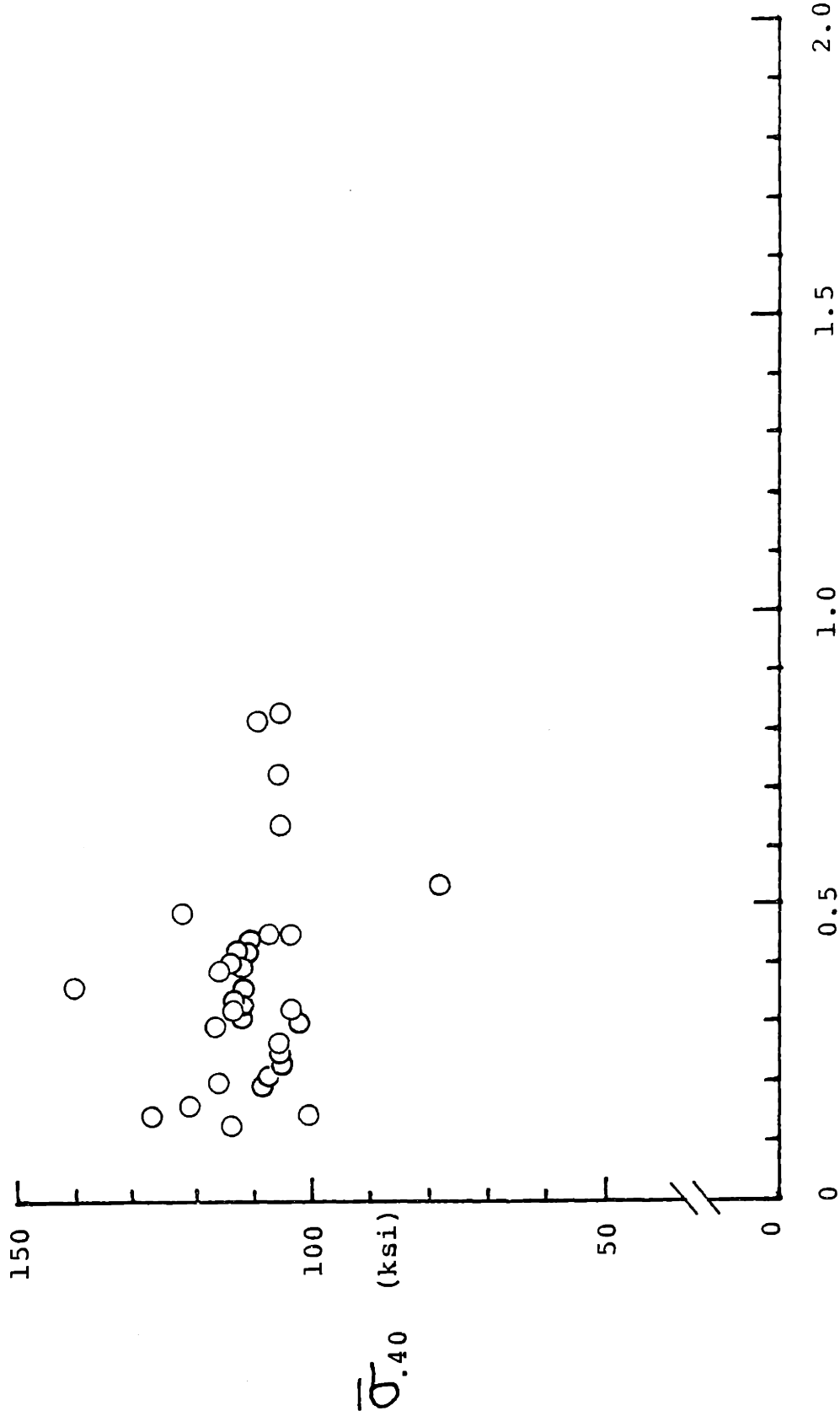

FIGURE 32 - VALUES OF $\bar{\sigma}_{.40}$, OBTAINED BY SHIFTING EXPERIMENTAL DATA, vs. T_m/D_f FOR SPECIMEN SP250 449.

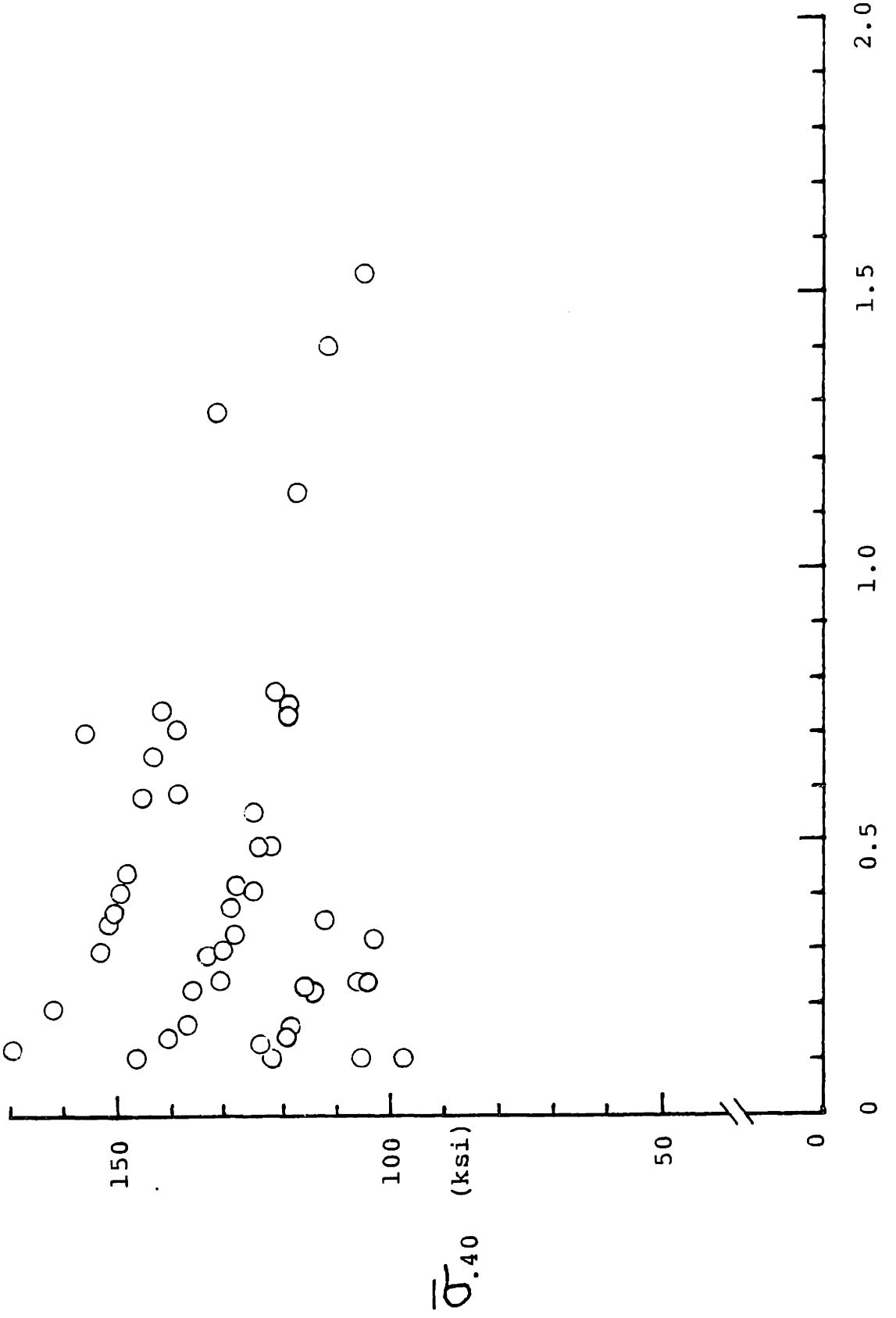

FIGURE 33 - VALUES OF $\bar{\sigma}_{.40}$, OBTAINED BY SHIFTING EXPERIMENTAL DATA, vs. T_m/D_f FOR SPECIMEN C-CK-U.

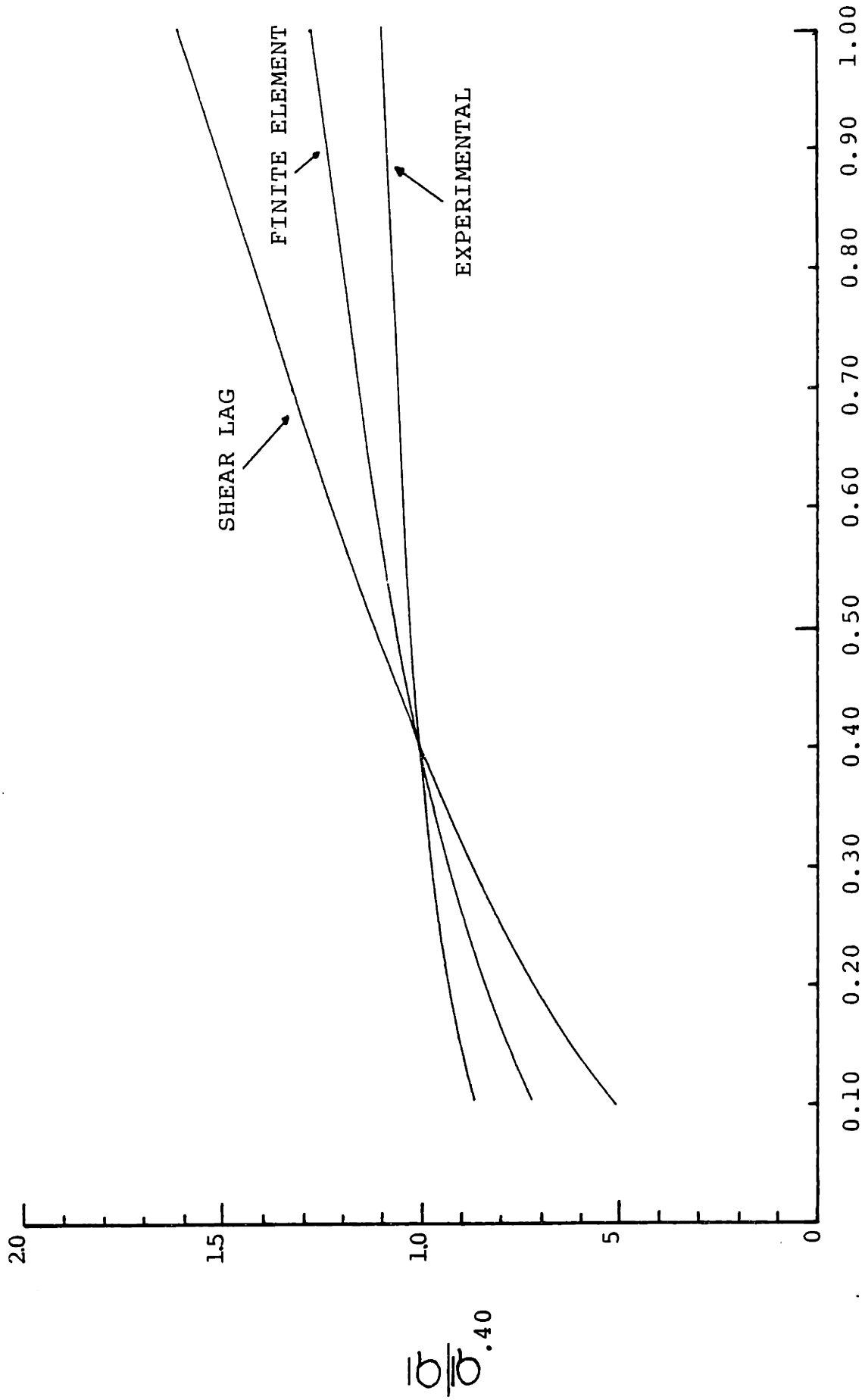

FIGURE 34 - VARIATION OF $\bar{\sigma}$ vs. T_m/D_f AS PREDICTED BY FINITE ELEMENT ANALYSIS, SHEAR LAG ANALYSIS AND FOR TYPICAL EXPERIMENTAL RESULT, ALL RESULTS NORMALIZED BY $\bar{\sigma}_{.40}$.

APPENDIX

TABULATED DATA FROM MICRODEBONDING TEST

Specimen: SP 250 S2 463
Fiber : S-Glass $E_f = 12.5 \times 10^6$
Matrix : Epoxy $G_m = 1.538 \times 10^5$

$(G_m/E_f)^{1/2} = 0.1109$

Test Date: 1/11/82

Run#	T_m (μm)	D_f (μm)	T_m/D_f	P (grams)	$\bar{\sigma}_A$ (psi)	$\bar{\sigma}_{.40}$ (psi)
1	1.0	9.5	0.11	4.5	90,299	102,742
2	2.0	10.0	0.20	5.5	99,604	106,753
3	1.5	10.0	0.15	6.5	117,714	129,845
4	2.0	10.0	0.20	5.5	99,604	106,753
5	2.5	10.0	0.25	6.0	108,659	113,888
6	1.0	9.0	0.11	4.5	112,795	128,338
7	1.0	10.0	0.10	5.0	90,549	104,013
8	1.0	10.0	0.10	5.5	99,604	114,415
9	2.0	11.0	0.32	7.5	112,251	114,784
10	3.5	10.5	0.33	8.5	139,623	142,335
11	2.0	11.0	0.18	6.0	89,801	97,266
12	1.0	8.5	0.12	4.0	100,262	113,090
13		Bad	Load			
14	3.0	8.5	0.35	5.0	125,328	127,013
15	2.5	8.5	0.29	5.0	125,328	129,424
16	2.0	9.0	0.22	5.5	122,969	130,545
17		Bad	Load			
18	8.0	9.0	0.89	5.5	122,969	113,517
19	3.5	11.0	0.32	8.5	127,218	130,089
20	4.0	9.0	0.44	6.0	134,148	132,876
21	7.5	10.0	0.75	7.0	126,769	119,045
22	4.0	10.0	0.40	6.0	108,659	108,659
23	3.5	10.0	0.35	6.0	108,659	110,120
24		Bad	Load			
25	4.5	9.0	0.50	5.5	122,969	120,255
26	4.0	10.5	0.50	5.5	114,983	115,574
27	7.5	10.0	0.75	5.5	126,769	119,045
28	9.0	10.5	0.86	7.5	123,197	114,119
29	9.0	11.5	0.35	8.5	116,393	117,958
30	3.5	10.0	0.35	7.0	126,769	128,473

Specimen: SP 250 S2 463
Fiber : S-Glass $E_f = 12.5 \times 10^6$
Matrix : Epoxy $G_m = 1.538 \times 10^5$

$(G_m/E_f)^{1/2} = 0.1109$

Test Date: 1/12/82

Run#	T_m (μm)	D_f (μm)	T_m/D_f	P (grams)	$\bar{\sigma}_A$ (psi)	$\bar{\sigma}_{.40}$ (psi)
1		Large	Scratch	Hitting	Interface	
2	2.0	10.5	0.19	5.5	90,344	97,326
3	2.0	10.0	0.20	5.0	90,549	97,048
4			Oval	Fiber		
5	3.0	8.0	0.38	4.0	113,187	113,769
6			Bad	Photo		
7	1.0	8.5	0.12	4.5	112,795	127,227
8			Bad	Loading		

Specimen: SP 250 S2 463
Fiber : S-glass $E_f = 12.5 \times 10^6$
Matrix : Epoxy $G_m = 1.538 \times 10^5$

$(G_m/E_f)^{1/2} = 0.1109$

Test Date: 1/13/82

Run#	T_m (μm)	D_f (μm)	T_m/D_f	P (grams)	$\bar{\sigma}_A$ (psi)	$\bar{\sigma}_{.40}$ (psi)
1	2.0	9.0	0.22	5.0	111,790	118,677
2	2.0	10.5	0.18	6.0	98,557	106,750
3	~0	9.5	~0	4.5	90,299	———
4			Bad	Load		
5			"	"		
6			"	"		
7	~0	9.5	~0	4.0	80,265	———
8	4.0	10.0	0.40	4.5	81,495	81,495
9	3.5	9.0	0.39	5.5	122,969	123,281
10	4.5	9.5	0.47	5.5	110,365	108,599
11	~0	9.5	~0	4.0	80,265	———
12	~0	9.0	~0	3.5	78,253	———
13	~0	7.5	~0	3.0	96,586	———
14	~0	10.0	~0	4.0	72,440	———
15	~0	9.5	~0	4.0	80,265	———
16	~0	8.0	~0	3.0	84,890	———
17			Bad	Load		
18			"	"		
19	4.5	10.0	0.45	6.0	108,659	107,387
20	3.0	10.0	0.30	5.5	99,604	102,511

Specimen: SP 250 S2 463
Fiber : S-glass $E_f = 12.5 \times 10^6$
Matrix : Epoxy $G_m = 1.538 \times 10^5$

$(G_m/E_f)^{1/2} = 0.1109$

Test Date: 2/23/82

Run#	T_m (μm)	D_f (μm)	T_m/D_f	P (grams)	$\bar{\sigma}_A$ (psi)	$\bar{\sigma}_{.40}$ (psi)
1	3.5	9.5	0.37	4.5	90,299	91,006
2			Bad	Load		
3			"	"		
4			"	"		
5			"	"		
6			"	"		
7			"	"		
8	4.0	9.5	0.42	5.0	100,332	99,844
9	6.0	10.5	0.57	7.0	114,983	110,982
10	3.5	9.5	0.37	5.5	110,365	111,229
11		Located Next		to	Cross Ply	
12			Bad	Load		
13			"	"		
14			"	"		
15	5.5	9.5	0.58	6.0	120,398	116,007
16			Bad	Load		
17	3.5	10.0	0.35	5.5	99,604	100,943
18	4.0	9.5	0.42	5.5	110,366	109,829
19	5.0	9.0	0.55	5.5	122,969	119,115
20			Bad	Load		
21			"	"		
22			"	"		

Specimen: SP 250 S2 463
Fiber : S-glass $E_f = 12.5 \times 10^6$
Matrix : Epoxy $G_m = 1.538 \times 10^5$

$(G_m/E_f)^{1/2} = 0.1109$

Test Date: 3/25/82

Run#	T_m (μm)	D_f (μm)	T_m/D_f	P (grams)	$\bar{\sigma}_A$ (psi)	$\bar{\sigma}_{.40}$ (psi)
1	3.5	10.0	0.35	5.5	99,604	100,943
2	1.0	10.0	0.10	5.5	99,604	114,415
3			Bad	Loading		
4			"	"		
5	2.0	10.5	0.19	5.5	90,344	97,326
6	~0	8.5	~0	4.0	100,262	———
7			Bad	Load		
8			Next to	Cross	Ply	
9	5.0	9.5	0.53	5.5	110,365	107,302
10	3.5	8.0	0.44	4.0	113,187	112,113
11			Bad	Loading		
12	7.5	9.0	0.83	5.0	111,790	103,920
13			Bad	Loading		

Specimen: SP 250 S2 449
Fiber : S-Glass $E_f = 12.5 \times 10^6$
Matrix : Epoxy $G_m = 1.538 \times 10^5$

$(G_m/E_f)^{1/2} = 0.1109$

Test Date: 2/8/82

Run#	T_m (μm)	D_f (μm)	T_m/D_f	P (grams)	$\bar{\sigma}_A$ (psi)	$\bar{\sigma}_{.40}$ (psi)
1		Probe	Sliding			
2		"	"			
3		"	"			
4		Oval	Fiber	Cross	Section	
5		Probe	Sliding			
6	2.0	8.5	0.24	4.0	100,263	105,518
7		Probe	Sliding			
8	3.0	9.5	0.32	5.5	110,366	112,856
9	3.0	9.5	0.32	5.5	110,366	112,856
10	~0	9.0	~0	4.0	89,432	———
11		Probe	Sliding			
12	~0	9.5	~0	4.0	80,266	———
13	1.5	10.5	0.14	5.5	90,345	100,395
14		Probe	Sliding			
15	2.0	11.0	0.18	6.5	97,285	105,372
16		Probe	Sliding			
17		"	"			
18		"	"			
19		"	"			
20	~0	10.0	~0	4.5	81,495	
21		Bad	Loading			
22	~0	10.0	~0	4.5	81,495	———
23	5.0	10.5	0.48	7.5	123,197	120,971
24	~0	9.5	~0	4.5	90,299	———
25	4.0	10.5	0.38	7.0	114,984	115,575
26	3.0	10.0	0.30	6.0	108,660	111,831
27		Bad	Loading			
28	~0	9.0	~0	4.0	89,432	———
29		Bad	Loading			
30		"	"			
31		"	"			
32	~0	9.0	~0	4.0	89,432	———
33	~0	9.5	~0	4.0	80,266	———
34		Next	to	Cross	Pl	
35		"	"	"	"	
36		Bad	Loading			
37		"	"			
38		"	"			
39		"	"			
40		"	"			
41		"	"			

Specimen: SP 250 S2 449
Fiber : S-Glass $E_f = 12.5 \times 10^6$
Matrix : Epoxy $G_m = 1.538 \times 10^5$

$(G_m/E_f)^{1/2} = 0.1109$

Test Date: 2/8/82

Run#	T_m (μm)	D_f (μm)	T_m/D_f	P (grams)	$\bar{\sigma}_A$ (psi)	$\bar{\sigma}_{.40}$ (psi)
42		Bad	Loading			
43		"	"			
44		"	"			
45		"	"			
46	~0	10.5	~0	5.5	90,345	———
47	5.0	11.0	0.45	7.0	104,769	103,542
48	2.0	10.5	0.19	4.0	106,771	115,023
49	~0	9.5	~0	4.0	80,266	———
50	~0	9.5	~0	4.5	90,299	———
51	2.5	9.5	0.26	5.0	100,332	104,749
52	4.0	9.5	0.42	5.5	110,366	109,829
53	3.0	9.5	0.32	5.0	100,332	102,596

Specimen: SP 250 S2 449
Fiber : S-Glass $E_f = 12.5 \times 10^6$
Matrix : Epoxy $G_m = 1.538 \times 10^5$

$(G_m/E_f)^{1/2} = 0.1109$

Test Date: 2/22/82

Run#	T_m (μm)	D_f (μm)	T_m/D_f	P (grams)	$\bar{\sigma}_A$ (psi)	$\bar{\sigma}_{.40}$ (psi)
1		Bad	Loading			
2		"	"			
3		"	"			
4		"	"			
5	——	10.0	~0	4.0	72,440	——
6		Bad	Loading			
7	——	11.5	~0	5.5	75,316	——
8	1.0	8.0	0.13	4.0	113,118	126,652
9	1.0	8.5	0.12	4.0	110,263	113,091
10	9.0	——	~0	3.5	78,253	——
11						
12	10.0	3.0	0.30	5.5	99,605	102,512
13		Bad	Loading			
14	8.5	3.5	0.41	4.5	112,796	112,518
15		Bad	Loading			
16	——	9.0	~0	3.5	78,253	——
17	9.0	2.5	0.28	5.0	111,790	115,849
18	1.5	10.0	0.15	6.0	108,660	119,858
19	3.0	8.5	0.35	5.5	137,862	139,715
20	3.5	9.5	0.37	5.5	110,366	111,230
21		Bad				

Specimen: SP 250 S2 449
Fiber : S-Glass $E_f = 12.5 \times 10^6$
Matrix : Epoxy $G_m = 1.538 \times 10^5$

$(G_m/E_f)^{1/2} = 0.1109$

Test Date: 3/25/82

Run#	T_m (μm)	D_f (μm)	T_m/D_f	P (grams)	$\bar{\sigma}_A$ (psi)	$\bar{\sigma}_{.40}$ (psi)
14	6.0	9.5	0.63	5.5	110,366	105,465
15		Bad	Loading			
16	——	9.5	0	4.0	80,266	——
17		Bad	Loading			
18	2.0	8.5	0.24	4.0	100,263	105,518
19	4.5	10.0	0.45	6.0	108,660	107,388
20	3.5	9.0	0.39	5.0	111,790	112,073
21	2.0	10.0	0.20	5.5	99,605	106,754
22	3.0	9.5	0.32	5.5	110,366	112,856
23		Bad	Loading			
24	——	9.0	0	3.5	78,253	——

Specimen: SP 250 S2 449
Fiber : S-Glass $E_f = 12.5 \times 10^6$
Matrix : Epoxy $G_m = 1.538 \times 10^5$

$(G_m/E_f)^{1/2} = 0.1109$

Test Date: 3/26/82

Run#	T_m (μm)	D_f (μm)	T_m/D_f	P (grams)	$\bar{\sigma}_A$ (psi)	$\bar{\sigma}_{.40}$ (psi)
1	7.0	8.5	0.82	4.5	112,796	104,983
2		Bad	Loading			
3		"	"			
4		"	"			
5	8.0	10.0	0.80	6.5	117,715	109,832
6		Bad	Loading			
7		"	"			
8	5.0	9.5	0.53	4.0	80,266	78,039
9		Bad	Loading			
10	6.0	8.5	0.71	4.5	112,796	106,506
11		Located	Next to	Crossply		
12		Located	Next to	Crossply		
13		Bad	Loading			
14		Located	Next to	Crossply		
15		"	" "	"		
16	3.5	8.5	0.41	4.5	112,796	112,518
17	4.0	9.5	0.42	5.5	110,366	109,829
18		Bad	Loading			
19		Bad	Loading			

Specimen: C-CK-U Celanese System F-Unsized
Fiber : Graphite $E_f = 35 \times 10^6$ psi
Matrix : Epoxy $G_m = 1.75 \times 10^5$ psi

$(G_m/E_f)^{1/2} = 0.071$

Test Date: 1/28/82

Run#	T_m (μm)	D_f (μm)	T_m/D_f	P (grams)	$\bar{\sigma}_A$ (psi)	$\bar{\sigma}_{.40}$ (psi)
1	9.00	7.0	1.29	4.0	147,837	131,501
2	0.75	6.0	0.125	3.0	150,917	169,533
3	4.00	7.0	0.57	3.5	129,357	124,856
4	2.00	6.0	0.33	2.5	125,764	128,207
5	5.00	7.0	0.71	4.0	147,837	139,593
6	0.75	7.0	0.11	3.5	129,357	147,183
7	1.00	6.5	0.15	0.15	107,160	118,203
8	2.00	7.0	0.29	3.0	110,878	114,502
9	1.25	6.0	0.20	3.0	150,917	161,749
10	1.50	6.5	0.23	3.0	128,592	135,909
11	0.75	8.0	0.09	4.0	113,188	131,396
12	1.00	7.0	0.13	3.0	110,878	124,067
13	0.75	6.5	1.15	3.0	128,592	115,704
14	2.00	8.0	0.25	3.5	99,039	103,805
15	2.00	7.0	0.29	3.5	129,357	133,585
16	5.50	7.0	0.78	3.5	129,357	121,000
17	12.00	5.5	2.20	2.5	149,669	126,211
18	5.00	7.0	0.71	4.5	166,316	157,041
19	2.00	5.5	0.36	2.5	149,669	151,254
20	2.00	6.5	0.31	3.0	128,592	131,812
21	1.50	6.5	0.23	2.5	107,160	113,257

Specimen: C-CK-U Celanese System F-Unsized
Fiber : Graphite $E_f = 35 \times 10^6$ psi
Matrix : Epoxy $G_m = 1.75 \times 10^5$ psi

$(G_m/E_f)^{1/2} = 0.071$

Test Date: 1/29/82

Run#	T_m (μm)	D_f (μm)	T_m/D_f	P (grams)	$\bar{\sigma}_A$ (psi)	$\bar{\sigma}_{.40}$ (psi)
1	1.0	6.5	0.15	3.0	128,592	141,844
2	~0	7.0	~0	3.0	110,878	———
3	~0	6.5	~0	3.0	128,592	———
4	4.5	6.0	0.75	2.5	125,764	118,102
5	3.0	6.0	0.50	2.5	125,764	122,989

Specimen: C-CK-U Celanese System F-Unsized
Fiber : Graphite $E_f = 35 \times 10^6$ psi
Matrix : Epoxy $G_m = 1.75 \times 10^5$ psi

$(G_m/E_f)^{1/2} = 0.071$

Test Date: 2/6/82

Run#	T_m (μm)	D_f (μm)	T_m/D_f	P (grams)	$\bar{\sigma}_A$ (psi)	$\bar{\sigma}_{.40}$ (psi)
1	2.5	6.5	0.38	3.0	128,592	129,253
2	3.5	6.0	0.58	3.0	150,917	145,412
3	0.5	7.0	0.07	2.5	92,398	89,028
4	0.5	6.0	0.08	2.0	100,611	118,180
5	1.5	6.0	0.25	2.5	125,764	131,816
6	0.5	7.0	0.07	3.0	110,878	131,990
7	0.5	6.5	0.08	2.0	85,728	100,698
8		Bad	Load			
9	0.5	6.5	0.08	2.5	107,160	125,872
10	~0	6.5	~0	2.0	85,728	———
11	~0	6.5	~0	2.0	85,728	———

Specimen: C-CK-U Celanese System F-Unsized
Fiber : Graphite $E_f = 35 \times 10^6$ psi
Matrix : Epoxy $G_m = 1.75 \times 10^5$ psi

$(G_m/E_f)^{1/2} = 0.071$

Test Date: 2/7/82

Run#	T_m (μm)	D_f (μm)	T_m/D_f	P (grams)	$\bar{\sigma}_A$ (psi)	$\bar{\sigma}_{.40}$ (psi)
1	1.0	6.0	0.17	2.5	125,764	136,999
2	~0	7.0	~0	3.0	110,878	———
3	0.75	6.5	0.12	2.5	107,760	120,871
4	~0	6.5	~0	2.5	107,760	———
5	0.5	7.0	0.07	3.0	110,878	131,990
6		Bad	Load			
7	0.5	6.5	0.08	2.0	85,728	100,698
8	0.75	7.0	0.11	2.5	92,398	105,131
9	0.75	6.5	0.12	2.0	85,728	96,697
10	0.5	7.0	0.07	3.0	110,878	131,990
11	4.0	6.0	0.67	3.0	150,917	143,330
12	2.5	6.0	0.42	3.0	150,917	150,182
13	3.0	5.0	0.60	2.0	144,880	139,123
14	8.5	6.0	1.42	2.5	125,764	110,798
15	8.5	5.5	1.55	2.0	119,736	104,568
16		Bad	Load			
17	3.0	6.0	0.50	2.5	125,764	122,989
18		Bad	Load			
19	2.0	5.5	0.36	2.5	149,669	151,254
20	4.5	6.0	0.75	3.0	150,917	141,722
21	0.5	6.5	0.08	2.5	107,160	125,872
22	2.5	7.0	0.36	3.0	110,878	112,052
23	2.0	6.0	0.33	2.0	100,611	102,565
24	4.5	6.0	0.75	2.5	125,764	118,102
25	1.5	6.0	0.25	2.0	100,611	105,453
26	~0	6.0	~0	2.0	100,611	———
27	2.5	5.5	0.45	2.5	149,669	147,916
28	~0	6.5	~0	2.0	85,728	———
29	2.5	6.0	0.42	2.5	125,764	125,152
30	0.5	6.5	0.08	2.5	107,160	125,872
31	2.0	6.5	0.31	3.5	150,024	153,897
32	3.0	7.0	0.43	3.5	129,357	128,425
33		Bad	Load			
34	0.5	6.5	0.08	2.5	107,160	125,872
35	1.0	6.5	0.15	2.5	107,160	118,203
36	~0	7.0	~0	2.5	92,398	———